UNIVERSITY OF CAMBRIDGE

Quantifying Passive Drug Transport Across Lipid Membranes

Jehangir Cama

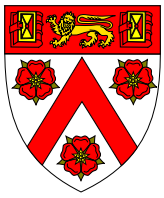

Trinity College

A Thesis submitted in June 2015, for the degree of Doctor of Philosophy

Declaration

I hereby declare that this Dissertation is the result of my own work and includes nothing which is the outcome of work done in collaboration except as specified in the text. It is not substantially the same as any I have submitted, or is being concurrently submitted for a Degree or Diploma or other qualification at the University of Cambridge or any other University or similar institution. I further state that no substantial part of my dissertation has already been submitted, or is being concurrently submitted for any such Degree, Diploma or other qualification at the University of Cambridge or any other University or similar institution. This Thesis does not exceed the prescribed word limit of 60,000 words.

Jehangir Cama
Cambridge
June 2015

Abstract

Quantifying Passive Drug Transport across Lipid Membranes

JEHANGIR CAMA

Biological and Soft Systems

Department of Physics, Cavendish Laboratory

Antibiotic resistance has emerged as one of the World's leading public health challenges. The inexorable emergence of drug resistant pathogens, combined with a steep decline in antibacterial drug discovery, has led to a major crisis. One of the most common drug resistance mechanisms involves bacteria adapting to reduce intracellular drug accumulation. To understand these resistance mechanisms, one needs quantitative information about the membrane permeability of drugs. In this Thesis, we develop a novel optofluidic permeability assay that allows us to quantify the permeability coefficient of drugs crossing lipid membranes. Lipid vesicles are used as model systems and drug molecules are tracked directly using their autofluorescence in the ultraviolet. The permeability coefficient of the drug is inferred by studying the increase in drug autofluorescence intensity within vesicles as they traverse a microfluidic network while exposed to the drug for well defined times. This provides a novel platform from which we can develop membrane models for understanding drug permeability.

We incorporate the *Escherichia coli* outer membrane protein OmpF in vesicles and quantify its role in the transport of fluoroquinolone antibiotics. We provide direct visualisation of OmpF mediated fluoroquinolone transport. We study the pH dependence of antibiotic transport both through pure phospholipid membranes and through OmpF, and present a physical mechanism to explain the pH dependence of *E. coli*

fluoroquinolone susceptibility. We also show the importance of lipid composition on drug permeability – changing the lipid composition of the membrane is shown to change antibiotic permeability by over an order of magnitude. Finally, we report on the discovery of a novel signalling mechanism in *E. coli* that relies on the transport of small drug-like molecules, and discuss the role it plays in stress response in the microbial community.

Acknowledgements

Most scientific research today is fuelled by collaboration, and the work presented in this Thesis is no exception. I have benefited enormously from interactions with my peers, who have helped shape my approach both to science and to life outside the scientific realm.

I would first like to thank my supervisor, Dr. Ulrich Keyser, for all his help and support throughout my PhD. Needless to say, none of this research would have been possible without his guidance, and I am truly grateful to have had the opportunity to work in his laboratory. The Keyser group is an enormously fun place to work in, and the people in it a close knit family which I am very fortunate to be part of.

I would also like to thank Dr. David Summers, my second supervisor, for all things indole and for his weekly meetings, which really served as a source of inspiration and motivation. His meetings symbolized all things good about doing science in Cambridge, and I truly appreciate being a part of his discussions. I also thank his students Hannah and Junyan for all their help with the indole experiments.

I thank Prof. Mathias Winterhalter for providing us with samples of OmpF for use in our experiments, and his student Harsha Bajaj for all her help and measurements which were critical to the success of the work.

It is to Catalin that I owe the most at the beginning of my research, for showing me how to negotiate the various pitfalls of day-to-day experimental science. Our trip to Romania for his wedding was also one of the most epic road-trips I have undertaken; the word 'Transfagarasan' is now suitably embossed on the collective memory of the group! I am also very grateful to Stefano for patiently teaching me all that I know

about microfluidics, the Italian way of life and most importantly, how not to drink river water.

Nadanai, Vivek and I formed the Trinity trinity in the Keyser group. I thank Nadanai for our long discussions on music, philosophy and life, and Vivek for keeping the Indian flag flying in the Keyser lab, and for his Dhansak preparation skills which would suitably endear him to the most traditional of Parsi households! Nick Bell was the only golfing partner I found anywhere near the Cavendish, and I value his direct, no-nonsense approach to research in particular and life in general. To Nick and Vivek go credits for proofreading this Thesis.

Theresa helped me collect data for the OmpF measurements, and has tirelessly worked towards adapting our setup for studying ion transport. I am extremely grateful to her for her efforts in this regard. Karolis and Oliver made great table-football sparring partners. I have also enjoyed philosophical discussions on various things scientific with Karolis. I thank Silvia for a proper Spanish introduction to Spain, and for all her guidance during the course of my PhD. Kerstin, Elisa, Madhavi, Anna M., Thomas, Alex, Irene and Jinglin make up the formidable Team Origami; I thank them all for their support around the lab, Elisa for introducing me to raclette and Kerstin and Thomas for feuerzangenbowle. Christian, Simon, Yizhou and Michael are all great companions, and I thank Michael in particular for his suggestions with various software issues over the years. I'd also like to mention Oliver Otto and Lorenz Steinbock, who made me feel very welcome when I first joined the group.

I'd like to thank Nicholas Thomson for showing me how to handle bacterial cultures and temperamental centrifuges. Avelino Javer helped enormously with the MATLAB scripts that we use, for which I am extremely grateful. I'd also like to thank Anna Heufner and Cynthia Fisher for teaching me eukaryotic cell culture protocols. Dr. Tuomas Knowles kindly let us use his photolithography facilities; I thank him for the use of his laboratory and Thomas Muller for teaching me photolithography. I offer my sincere thanks to Sarah Gallagher, who directed me to the Knowles group when I needed to construct my microfluidic devices. I am grateful to Ralf Seidel and his students Hergen and Friederich for the hospitality they showed me in Dresden when I visited their laboratory.

The Biological and Soft Systems sector at the Cavendish is a vibrant community to be part of, and I would particularly like to thank Pete, Suresh, Will, Owen, Kim and Daniel for all their efforts in keeping everything running as smoothly as possible.

Words can hardly do justice to the debt I owe my college, Trinity. Besides funding my PhD, it has provided me a home away from home, and has helped forge friendships that will stay with me through my life. It has been a privilege to be a member of this marvellous College, and I thank all the wonderful friends I have made there for their constant encouragement, banter and support.

I thank the Cambridge Philosophical Society for awarding me a Research Studentship in the final year of my degree.

I must thank my piano teacher, Prof. Peter Uppard, for his wonderful lessons, which have been one of the highlights of my time in Cambridge. I'd also like to thank Joy Seddon, who has been like a grandmother to me in Cambridge, for all her kindness (and cakes!) over the years.

I would never have reached Cambridge without the support of my family and friends back home, and it is to them that I owe my greatest thanks. My mother Shernaz in particular has always been my strongest supporter, and I thank her for all she has done for me over the years.

My grandfather, the late Lt. Gen. Adi Sethna, was a guiding influence throughout my childhood, and remains a role model to me. It is to his memory that I dedicate this Thesis.

Contents

Abstract v

Acknowledgements vii

List of Figures xv

List of Symbols and Abbreviations xix

1 Introduction 1

2 Experimental Design 7

2.1 Introduction 7

2.1.1 The need for technological development 8

2.1.2 UV autofluorescence and Label-Free tracking 10

2.1.3 Norfloxacin as a model antibiotic 11

2.1.4 Giant Unilamellar Vesicles as Model Lipid Systems 14

2.1.5 Overton's Rule 16

2.2 Microfluidics 18

2.2.1 Microfabrication Techniques 19

2.2.2 Vesicle based microfluidics 21

2.3 The Optofluidic Permeability Assay 22

2.3.1 Optical Setup . . . 22
2.3.2 Microfluidic Chip Design and Fabrication . . . 23
2.3.3 Vesicle electroformation protocol . . . 26
2.3.4 Microfluidic flow control . . . 27
2.3.5 Diffusion model for calculating drug permeability . . . 28
2.3.6 Data Analysis . . . 33
2.4 Conclusions . . . 35

3 Transport Across Pure Phospholipid Membranes 37
3.1 Introduction . . . 37
3.1.1 Phospholipid Bilayers . . . 38
3.1.2 Phosphatidylcholine lipids . . . 39
3.2 pH dependence of norfloxacin transport . . . 40
3.2.1 Norfloxacin charge dependence on pH . . . 40
3.2.2 Calibrating the autofluorescence on our microscope . . . 41
3.2.3 Results of the optofluidic assay . . . 42
3.3 Changing the lipid composition affects norfloxacin permeability . . . 49
3.3.1 Norfloxacin transport through DOPC lipids . . . 49
3.3.2 Why is permeation through DOPC faster? . . . 51
3.4 Tetracycline transport . . . 54
3.4.1 Tetracycline . . . 54
3.4.2 Tetracycline transport across DPhPC bilayers . . . 55
3.5 Interaction of Quantum Dots with lipid membranes . . . 57
3.5.1 Quantum Dots in Biology . . . 57
3.5.2 Quantum Dot Cytotoxicity . . . 59
3.5.3 Interactions with Vesicle membranes . . . 60
3.6 Conclusions . . . 62

4 Exploring the role of Nanopores in Membrane Transport **65**

4.1 Introduction 65

4.1.1 The Outer Membrane of the Gram-negative Cell Wall 66

4.1.2 Traditional Experimental Techniques used in Porin transport . 71

4.2 Experimental Techniques and Materials 75

4.2.1 Optofluidic Permeability Assay 75

4.2.2 Vesicle formation and OmpF incubation 77

4.2.3 OmpF insertions counted using ionic current sensing 78

4.2.4 Flux calculations 79

4.2.5 Data Analysis 80

4.3 Results 81

4.3.1 Optofluidic assay reveals norfloxacin uptake through OmpF . . 81

4.3.2 Single OmpF Channel Electrophysiology measurements 85

4.4 Discussion 86

4.5 Conclusions 88

5 Indole signalling in *Escherichia coli* **89**

5.1 Introduction 89

5.1.1 Indole 90

5.2 Measuring Cell Associated Indole 92

5.2.1 UV Absorbance Assay 92

5.2.2 Experimental details 92

5.2.3 Calculation of Cell Associated Indole 95

5.2.4 Results 96

5.2.5 Results on cell associated indole using the Kovacs assay 97

5.3 Discovery of the Indole Pulse 99

5.4 Indole and Bacterial Stress Response 100
5.4.1 Indole response under antibiotic stress 100
5.4.2 Lipid permeability of norfloxacin is indole independent 101
5.5 Conclusions 102

6 Outlook **105**
6.1 Vesicle based permeability measurements 105
6.1.1 Antibiotic transport studies 107
6.1.2 Ion flux measurements 108
6.2 Transport measurements on the single cell level 110
6.3 Future measurements on indole signalling 112

7 Concluding Remarks **115**

A Protocol for the Optofluidic Permeability Assay **117**

B Microfluidic Chip Designs **125**

C Theoretical basis for the linear relationship of $\Delta I(0)$ vs R **129**

D List of Publications **133**

Bibliography **135**

List of Figures

2.1 PAMPA assay. 9

2.2 Norfloxacin molecule. Source: www.wikipedia.org 12

2.3 UV absorbance characteristics of norfloxacin. 12

2.4 Norfloxacin autofluorescence profile. 13

2.5 Electroformation of Giant Unilamellar Vesicles. 15

2.6 A typical microfluidic chip. 18

2.7 Schematic of microfabrication protocol. 20

2.8 Schematic of Optical Setup. 22

2.9 Schematic of microfluidic network. 24

2.10 Typical GUVs obtained after electroformation. 26

2.11 10× fluorescence image of microfluidic device showing norfloxacin diffusion in the channel. 27

2.12 Schematic of a Giant Unilamellar Vesicle. 28

2.13 Typical calibration plot of $\Delta I(0)$ *vs* R. 35

3.1 The Phospholipid Bilayer. 38

3.2 pH dependence of norfloxacin charge. 40

3.3 Autofluorescence intensity of norfloxacin at 340 nm excitation. 41

3.4 Preliminary analysis of norfloxacin uptake in individual vesicles. . . . 43

3.5 Norfloxacin uptake into vesicles increases as the length travelled in the chip increases. 44
3.6 Measurements of the permeability coefficient (P) of norfloxacin across DPhPC lipid membranes. 45
3.7 Plot of permeability coefficient (P) against vesicle velocity. 48
3.8 Norfloxacin transport through DOPC vesicles at pH 7. 50
3.9 Chemical structures of DPhPC and DOPC lipids. 52
3.10 Tetracycline chemical structure. Source: www.wikipedia.org 54
3.11 Tetracycline transport through DPhPC vesicles at pH 7. 56
3.12 Dependence of the emission wavelength of CdSe QDs on their diameter. 58
3.13 Fluorescence micrograph of CdSe-ZnS QD labelled beads emitting at different wavelengths. 60
3.14 Scatter plot for CdSe QD permeability experiment. 62

4.1 Schematic of the *E. coli* cell envelope. 66
4.2 The OmpF porin. 68
4.3 Liposome swelling assays. 72
4.4 Single channel electrophysiology. 74
4.5 Schematic of the OmpF optofluidic permeability assay. 76
4.6 Port-a-Patch calibration measurement. 79
4.7 Optofluidic permeability assay shows the rapid uptake of norfloxacin in OmpF embedded proteoliposomes. 82
4.8 Norfloxacin uptake measurements in OmpF-embedded proteoliposomes using different vesicle batches. 83
4.9 Permeability histograms showing the enhanced permeability of proteoliposomes containing OmpF at both pH 5 and pH 7. 84

5.1 The indole molecule. Source: www.wikipedia.org 90

5.2 UV absorbance assay to determine the amount of indole absorption by cells. 93

5.3 UV absorbance curves for the supernatant when an indole concentration of 1.5 mM was added externally to control/bacterial solutions. . . 95

5.4 Results of the UV absorbance assay. 96

5.5 Results of the Kovacs assay. 98

5.6 The Indole Pulse. 99

5.7 Indole does not affect the permeability of DPhPC membranes to norfloxacin at pH 7. 101

6.1 Microfluidic vesicle formation. 106

6.2 Fura-2 pentasodium salt (Life Technologies) fluorescence characteristics. 109

6.3 Schematic of a proposed microfluidic system that sorts bacterial cells on the basis of antibiotic uptake. 111

B.1 'Long' chip design. 126

B.2 'Medium' chip design. 127

B.3 'Short' chip design. 128

C.1 Schematic depicting a vesicle of radius r in a microfluidic channel of height h. 130

List of Symbols and Abbreviations

$\Delta\psi$	Cytoplasmic membrane potential
ΔI	Normalised fluorescence intensity difference between the interior and exterior of a vesicle
c	Concentration
D	Diffusion Coefficient
d	Thickness of lipid bilayer
DOPC	1,2-dioleoyl-sn-glycero-3-phosphocholine
DPhPC	1,2-diphytanoyl-sn-glycero-3-phosphocholine
fps	Frames per second
GUV	Giant Unilamellar Vesicle
I	Fluorescence intensity
IM	Inner Membrane
IMPs	Integral Membrane Proteins
ITO	Indium Tin Oxide
J	Flux of molecules
K	Partition Coefficient

LPS	Lipopolysaccharide
MD	Molecular Dynamics
MDO	Membrane Derived Oligosaccharide
MIC	Minimum Inhibitory Concentration
OD	Optical Density
OM	Outer Membrane
OmpF	Outer Membrane Protein F
P	Permeability Coefficient
PAMPA	Parallel artificial membrane permeability assay
PC	Phosphatidylcholine
PDMS	Polydimethylsiloxane
PMF	Proton Motive Force
PMPs	Peripheral Membrane Proteins
R	Radius of vesicle
r.p.m	Revolutions per minute
Re	Reynolds Number
s.d	Standard deviation
s.e	Standard error
UV	Ultraviolet
WHO	World Health Organization

Chapter 1

Introduction

> "There are more things in heaven and earth, Horatio, than are dreamt of in your philosophy."
>
> Hamlet (*The Tragedy of Hamlet, Prince of Denmark*)

"Chance favours the prepared mind." So pronounced Louis Pasteur, doyen of 19th century microbiology and inventor of sterilization protocols still in use today. What irony then that, just two years after Pasteur's death, at the institute named in his honour, a remarkable discovery by one Ernest Duchesne went unheeded. Duchesne, in the course of his graduate studies, had observed that fungi from the genus *Penicillium* were capable of destroying pathogenic bacteria both in laboratory cultures and when injected into guinea pigs [1]. His proposal of exploiting this bacteriostatic property of the mould for therapeutic purposes fell on deaf ears, and one of medicine's greatest ever discoveries fell, temporarily, by the wayside.

Exactly 33 years to the day after Pasteur's death, on the 28th of September 1928, the Scottish biologist Alexander Fleming noticed that one of his culture plates of *Staphyloccocus* bacteria was contaminated with mould. Remarkably, the bacterial colonies around the mould were transparent, suggesting that the bacteria were undergoing lysis [2]. On investigating, he found that the mould belonged to the genus *Penicillium*; he had in essence rediscovered Duchesne's observations. However, unlike Duchesne and his superiors at the Pasteur Institute, Fleming recognized the significance of his

discovery and isolated the antibacterial chemical, which he named penicillin, that was produced by the mould. As he remarked in his Nobel lecture [3]:

> "....penicillin started as a chance observation. My only merit is that I did not neglect the observation and that I pursued the subject as a bacteriologist."

Chance did indeed favour the prepared mind, then.

The rest, as they say, is history. Penicillin was amongst the first of many antibiotics to be discovered and synthesized, and completely changed the face of the medical and pharmaceutical industries. Surgical procedures became much safer, typhoid, plague, tuberculosis and other dreaded diseases no longer carried death sentences, and average life expectancy rates climbed steadily higher. According to Ms. Zsuzsanna Jakab, Regional Director for Europe, World Health Organization, "The use of antibiotics – and vaccines – has lengthened our life-spans by 20 years on average". Antibiotics form the bedrock of all modern medicine. The discovery of penicillin can rightfully claim to be amongst the most influential in the history of humanity.

However, bacteria have not survived on Earth for billions of years without an extraordinary amount of resilience. Their rapid growth rate allows for the prompt selection of mutant organisms capable of resisting external stress. Fleming acknowledged this danger in his Nobel speech, saying [3]:

> "It is not difficult to make microbes resistant to penicillin in the laboratory by exposing them to concentrations not sufficient to kill them, and the same thing has occasionally happened in the body.....there is danger that the ignorant man may easily underdose himself and by exposing his microbes to non-lethal quantities of the drug, make them resistant."

Inevitably, resistance began appearing almost immediately after the introduction of antimicrobials in the clinic. Sulfonamides, introduced in 1937, saw resistance develop just a couple of years after their introduction – the same sulfonamide resistance mechanisms operate today [4]. The cause of resistance was not limited to antibiotic underexposure. Before penicillin was even introduced therapeutically, members of the penicillin discovery team found a bacterial enzyme that was capable of destroying the drug

[5]. This is due to the fact that a number of antibiotic resistance genes are found naturally in microbial populations [4, 6]. The use of penicillin led to the spread of genes encoding β-lactamases, the enzymes capable of cleaving penicillin, and synthetic studies had to be undertaken to chemically modify penicillin to protect against degradation by these enzymes [4].

By the 1950s, resistance to multiple antimicrobials was being reported in Japan – *Shigella dysenteriae* strains resistant to upto four different antibiotics were isolated [7]. Even more worryingly, it was found that the multiple antibiotic resistance characteristics of *S. dysenteriae* could be transferred to other *Enterobacteriaceae* by simply mixing liquid cultures of sensitive and resistant bacteria and plating them out on solid media [7]. It turned out that resistance genes were being transferred via plasmid exchange between bacteria, and that this exchange was carried out by cell-to-cell contact [7, 8]. Multidrug resistance, thus, is an example of infective heredity in bacteria [8, 9].

However, a common trait emerged from these initial studies – investigations into the biochemical mechanisms of resistance revealed that multidrug resistance was caused by a decrease in the cell permeability of drugs [8]. Understanding drug permeability therefore became a critical issue in the study of antibiotic resistance. It is to the study of drug transport that the majority of this Thesis is devoted.

In hindsight, it should have come as no surprise that reduced cell permeability was the route of choice for the development of multidrug resistance. The cell membrane provides all cells with their first line of defence against external stress. Most antibiotic targets are found in the cytoplasm [10], and hence preventing drugs from reaching their targets seems one of the obvious things to do, from the perspective of the cell. The reduced influx (or increased efflux) of drug molecules confers protection against *all* drugs with intracellular targets; the bacterial equivalent of killing many birds with one stone, as it were.

In order to elucidate the mechanisms by which bacteria can adapt their cell membranes to make them less permeable, we need to understand how drugs interact with the various components of the membrane. Cell membranes typically consist of lipid bilayers which contain a number of proteins embedded in them. The number of membranes can vary – Gram-positive bacteria have a single membrane, whereas Gram-negative bacteria have a double membrane cell wall. The lipid bilayers present in these

membranes contain non-polar, hydrophobic cores, and hence pose a significant barrier for polar molecules and ions attempting entry into the cell. The cellular entry of such moieties is controlled by a variety of membrane protein channels, that provide a pathway for these molecules and ions across the lipid barrier.

To understand drug permeability, then, one has to understand how drugs translocate across **both** the lipid barrier as well as across these membrane protein channels. This is of fundamental importance in drug design and development. However, such measurements pose significant challenges – attempting measurements on live bacteria is difficult due to their small size. Furthermore, traditional microbiology involves bulk experiments, where populations of cells are sampled. Bulk experiments are not very conducive to the quantitative study of membrane transport processes. Additionally, with whole cell experiments, it is very challenging to quantify transport through different permeation pathways since there is little control over the system. New techniques are thus required to tackle the membrane transport problem quantitatively, with an emphasis on control over the experimental system under investigation.

From a physicist's perspective, the obvious way to tackle such a complicated problem was by removing as many complications as possible. Biologists tend to take the opposite approach. To understand transport, they would knock out, one by one, various proteins implicated in transport and measure the response. However, one can never be sure of the side effects of removing particular proteins on the overall physiology of the cell, and we therefore settled on a bottom-up approach to the problem. If the major constituent of cell membranes is the lipid bilayer, why not first understand the role that the lipid bilayer alone has to play in drug transport? Once the baseline level of passive, diffusive transport across the lipid bilayer is quantified, one can start incorporating protein channels into the lipid membrane and quantify the effect of each individual type of membrane protein on transport in a completely unambiguous manner. Of course, we cannot replicate the conditions existing in a living cell, but for studying passive diffusion, which is one of the most important modes of drug transport [11, 12], this approach yields quantitative and comprehensive results.

In this Thesis, we develop a new microfluidic approach to quantify drug permeability across pure lipid membranes. We use Giant Unilamellar Vesicles (GUVs) as our model lipid systems, and study drug accumulation within the vesicles as they traverse a mi-

crofluidic channel network while exposed to the drug. We exploit the ultraviolet (UV) autofluorescence properties of various antibiotics to track their molecules in a label-free manner, thus directly measuring the membrane permeation of the drug. After measuring the baseline permeability of the lipid membrane, we incorporate the *Escherichia coli* outer membrane protein pore OmpF in our vesicle membranes and study the effect of these pores on drug uptake. Our approach enabled the direct visualisation of OmpF-mediated antibiotic uptake in a manner not previously possible. Combining our measurements on lipid and OmpF-mediated transport allowed us to present a physical mechanism explaining the pH dependence of fluoroquinolone antibiotic susceptibility in *E. coli*.

In addition to our studies on drug permeability, we report on the discovery of a novel signalling mechanism in *E. coli*. This signalling mechanism relies on the ability of indole, a small drug-like molecule, to diffuse passively across bacterial membranes – membrane transport is thus fundamental to bacterial signalling as well. Understanding bacterial communication and signalling in response to stress is vital in the battle against antibiotic resistance, and we propose that the indole pulse signalling mechanism that we discovered is part of a widespread stress response in *E. coli*. This further extends the scope of our permeability technique, since we can also examine the effect of indole and other signalling molecules on drug permeability.

The Thesis is structured thus:

Chapter 2 introduces our new microfluidic technique. We discuss the need for technological development in the field, explain our model systems and optical setup, and lay the experimental and theoretical foundations for the optofluidic permeability assay that we developed.

Chapter 3 describes the results that we obtained on studying transport across pure phospholipid membranes. We validate theoretical predictions for the pH dependence of the transport of norfloxacin, a fluoroquinolone antibiotic, across lipid membranes and measure its permeability coefficient. We show the importance of studying transport in the lipid system of interest – changing the lipid molecule leads to an order of magnitude change in the norfloxacin permeability. We further report measurements on the permeability of tetracycline, a different class of antibiotic. We conclude the

chapter with a measurement of the permeability of Quantum Dots, in order to show the versatility of our technique in studying a variety of systems.

Chapter 4 deals with the results of transport through the OmpF pore. Reconstituting OmpF in the vesicle membranes makes them much more permeable to norfloxacin, and we quantify the flux through these pores. Our technique allows us to quantify, independently, transport through the pores and transport through the lipids, a measurement that was not feasible in the past.

Chapter 5 reports on the measurements that we undertook in order to elucidate the indole pulse signalling mechanism. This work was carried out in collaboration with the group of Dr. David Summers (Dept. of Genetics, Cambridge), and we shall explain the assay that we used to measure cell associated indole concentrations. This measurement was required in order to quantify the concentrations of indole achieved within cells during the pulse signal.

Chapter 6 details the outlook for our permeability assay. We discuss ways to improve on the technique and describe other uses that the assay is being put to, such as the study of ion transport through nanopores. We also discuss future developments that would enable us to modify our assay for single cell analysis, providing a tool to distinguish resistant cells from normal cells in a clinical setting. A discussion on future directions for indole signalling research is also provided.

Chapter 7 contains some brief concluding remarks.

Antibiotic resistance is too important a problem for the wider non-biology community to ignore. It is a challenge that must involve the collective scientific might of humanity, encompassing biologists, physicists, mathematicians, chemists, programmers, engineers and others. This work is a small example of how research in a physics laboratory can be applied to a pressing medical problem, and one hopes that the reader will be left with a better understanding of drug-membrane interactions by the conclusion of this Thesis.

We shall now commence our discussion on the experimental and theoretical design of the new permeability assay.

Chapter 2

Experimental Design

> "Try not! Do, or do not, there is no try."
>
> Yoda (*The Empire Strikes Back*)

2.1 Introduction[1]

We begin our discussion of membrane transport by outlining the basic technical problems that experimentalists encounter when studying drug permeation across biological membranes. We shall introduce the concept of autofluorescence and describe how we exploit this property of drug molecules to track them in a label-free manner, thus circumventing a whole host of problems in the field. Our interests lie mainly in the study of antibiotic transport, and thus our emphasis and techniques will be tailored to the study of these drugs. However, the techniques developed can easily be adapted to study the membrane permeability of other molecules of interest.

The rest of this chapter will be dedicated to describing a new microfluidic assay to measure the permeability of drugs across lipid membranes.

[1] We published most of the work presented in this chapter and part of the following chapter in reference [13].

2.1.1 The need for technological development

Consider the following scenario: you are working in the pharmaceutical industry, on the development of a promising new drug. *In vitro* screens have shown that the molecule binds well to its intended target within the cell. But tests on actual living cells are failing to show desired results. What could possibly be wrong?

The obvious next step would be to check whether the drug is actually accumulating inside the cell. One would imagine that such an important process in drug development had been optimised years ago, taking into account the tremendous biochemical variety of cellular membranes and having specific assays to test drugs against particular cell types.

The reality couldn't be more different.

The cell permeation capabilities of drug molecules are typically estimated in the pharmaceutical industry by the measurement of their partition coefficients (K) in completely artificial aqueous:organic phase systems [14]. The solvents generally used for the purpose are water and octanol. The premise is that octanol, being hydrophobic, is a good approximation for the non-polar, hydrophobic core of lipid bilayers that form the main barrier preventing drug molecules from entering the cell. The partition coefficient measurement involves mixing water and octanol with the drug under investigation, and measuring how the drug preferentially partitions into the two solvents. The result is generally reported in terms of a log scale:

$$\log K_{oct/water} = \log \left(\frac{[solute]_{octanol}}{[solute]_{water}} \right) \tag{2.1}$$

Actual drug permeability and flux across lipid membranes is not measured directly; it is inferred from a knowledge of the partition coefficient and the diffusion coefficient of the drug in a generic non-polar phase [15]. This technique, although suitable for a qualitative understanding of drug lipophilicity, completely disregards the tremendous variety in membrane compositions found in cells. The lipid composition of the membrane can vary significantly, not just between species, but even in the same cell under different environmental conditions [16, 17]. An ability to directly measure drug per-

meability across lipid membranes would therefore represent a significant improvement over this method.

Another industry standard for estimating drug absorption in the human intestine involves the use of a culture of Caco-2 cells. The Caco-2 cell line consists of heterogeneous human epithelial colorectal adenocarcinoma cells, and hence a confluent layer of these cells is considered to be a good *in vitro* model for testing the absorption of drugs in the human gut. However, the inherent heterogeneity in the cell line combined with different culture conditions in labs across the world has led to a divergence in the properties of some of the cell lines, making results from different laboratories difficult to compare [18]. Further, this technique only provides information about drug absorption into the human bloodstream; the membrane barrier of the target cell is not considered here. This technique also cannot differentiate between active and passive transport and is therefore not suitable for studying the finer details of drug permeation [19].

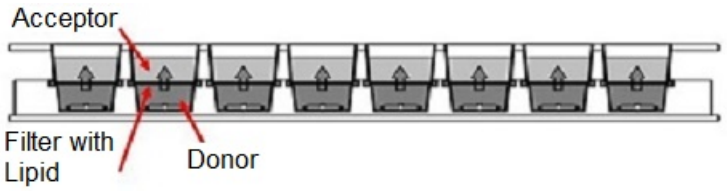

Figure 2.1 – Cross section of the PAMPA Explorer™ sandwich plate sold by BioTek Instruments, Inc. (www.biotek.com). The flux of molecules across a filter supporting a lipid bilayer is measured using UV spectroscopy.

PAMPA (parallel artificial membrane permeability assay) is yet another commonly used technique that measures the flux of a drug crossing an artificial membrane [20]. It involves using microtiter plates where artificial lipid bilayers are formed on a hydrophobic filter material. The solute of interest is added to one side of the bilayer, and its transport across is measured using UV spectroscopy (Figure 2.1). The flux values are calculated by comparing the UV absorption of the sample against a reference well in the plate devoid of a lipid bilayer [20]. It is believed, however, that residual solvents in the membrane affect permeation kinetics studied using this technique [19]. Furthermore, the use of PAMPA in measuring absorption due to transporter-mediated processes is not advisable [21]. An investigation into the technique by industry scientists concluded:

"Upon examination of the quality of data and quantity of time, the PAMPA assay may be a very limited asset to a drug discovery effort" [22].

From a drug development point of view, there is thus an obvious incentive for inventing new techniques capable of studying drug transport across lipid membranes in a direct, quantitative manner, and where the model lipid system can be tuned to imitate the lipid composition of target cells as closely as possible.

However, another major motivation for the development of new drug permeation assays is for the better understanding of antibiotic resistance in bacteria. A majority of antibacterials work by targeting processes occurring in the bacterial cytoplasm; thus, one of the major forms of antibiotic resistance involves bacteria adapting to decrease intracellular drug accumulation by mutations in transport pathways, lipid compositions or by switching on efflux pumps [23].

Studying drug accumulation in bacteria is a complicated process, and various different approaches have been tried. Experiments involving tracking radiolabelled quinolone antibacterial agents [24], bioassays [25] and fluorescence based measurements [26, 27] have been used to study the uptake of antibiotics in bacterial cells in a range of environmental conditions. However, the use of different experimental conditions and antibiotics has complicated the comparison of results from these various techniques [28]; no one method has been standardized and used across species and drugs. A better understanding of drug-lipid interactions and a more reliable, quantitative assay for determining drug permeability is therefore required.

2.1.2 UV autofluorescence and Label-Free tracking

A major obstacle in studying the transport of small molecules in biological systems is the fact that they generally need to be tagged to track their movement and accumulation. This can be done via radiolabelling or by attaching a fluorophore to the molecule being studied. Radiolabelling is generally a tedious process, which can also change the biological activity of the molecule being studied [27]. Attaching a fluorescent tag to a drug molecule is likely to change its transport properties and kinetics, since the size of the fluorophore is generally either comparable or (in many cases) much larger than the molecule being tagged. Furthermore, with fluorescent tags one has to always worry

about chemical properties such as the binding constants of the molecule and its tag, an understanding of which is critical for the correct interpretation of concentrations from intensity measurements.

However, a large proportion of biomolecules and drugs have aromatic rings that absorb strongly in the ultraviolet region of the spectrum. When the molecule relaxes to its ground state, it emits light (fluorescence) at a wavelength higher than that absorbed. This fluorescence is intrinsic to the molecule, and is therefore termed 'autofluorescence'.

While UV absorption has been used in the past for studying drug transport [26], the use of UV autofluorescence microscopy is rather more recent [27]. In fact, autofluorescence is normally considered a problem in biological applications, since it can interfere with conventional fluorescence microscopy techniques. Removing autofluorescence is a considerable technical challenge [29]. The use of UV imaging in cells always requires a delicate balance with regards to the illumination intensity – too little and the poor signal to noise ratio (SNR) of the image will render it useless, too much and one risks damaging the cell and changing its biological activity.

However, if one uses model systems rather than cells, a drug's UV autofluorescence offers a very direct, easy to use platform for tracking drug accumulation and transport. Drug concentrations can be directly correlated with the autofluorescence intensity enabling the direct visualisation of drug transport across lipid barriers. Fortunately for us, a number of antibiotics are indeed autofluorescent in the UV, and we develop our assay using the fluoroquinolone antibiotic, norfloxacin, described below.

2.1.3 Norfloxacin as a model antibiotic

Norfloxacin (Figure 2.2) is part of the fluoroquinolone family of antibiotics. These molecules target the complexes formed between bacterial DNA and topoisomerases. Topoisomerases are the enzymes that control the supercoiling of DNA within the cell. The disruption of such complexes inhibits DNA synthesis thus causing cell death [30–32]. In particular, quinolones target the enzymes DNA gyrase and topoisomerase IV; it is generally accepted that the Gram-negative activity of quinolones is linked to gyrase inhibition and the Gram-positive activity to topoisomerase IV inhibition [32].

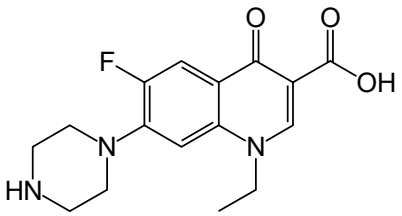

Figure 2.2 – Norfloxacin molecule. Source: www.wikipedia.org

Since the targets are intracellular, quinolone accumulation within the cell becomes critical to their efficacy. Understanding the membrane permeability of quinolones is thus crucial. Norfloxacin (and other fluoroquinolones) are ideal candidates for developing permeability assays, since their autofluorescence allows us to develop microscopy techniques that can directly track the molecules as they cross membrane barriers.

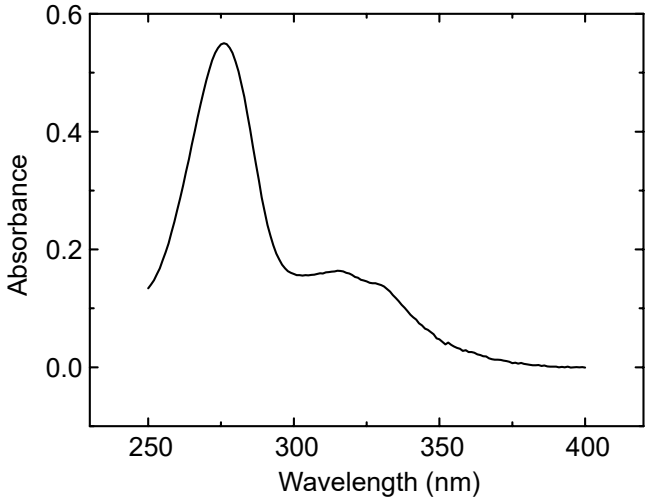

Figure 2.3 – UV absorbance characteristics of a 12.5 μM solution of norfloxacin prepared in 200 mM sucrose. Measured using a Cary 300 Bio UV VIS spectrophotometer.

The UV absorbance characteristics of norfloxacin are presented in Figure 2.3. There is a well defined peak in the deep UV, with maximum absorbance at 276 nm, and a broader secondary peak at around 325 nm. In order to best exploit an autofluorescence assay, then, one would like to be able to work in the deep UV, at excitation wavelengths around 280 nm.

However, setting up the optics required for deep UV epifluorescence proves to be surprisingly difficult. Standard borosilicate glass is opaque to wavelengths below 300 nm, and absorbs strongly in the 300-350 nm range as well. Therefore, for all deep UV fluorescence microscopes, the optical components require special UV-grade fused silica (or quartz) glass. Most importantly, the objective through which the excitation beam passes must transmit in the deep UV, and thus should be made of quartz. High quality quartz objectives, it turns out, are notoriously difficult to obtain and most of the high numerical aperture UV objectives in use today have sufficient transmission only down to about 330 nm.

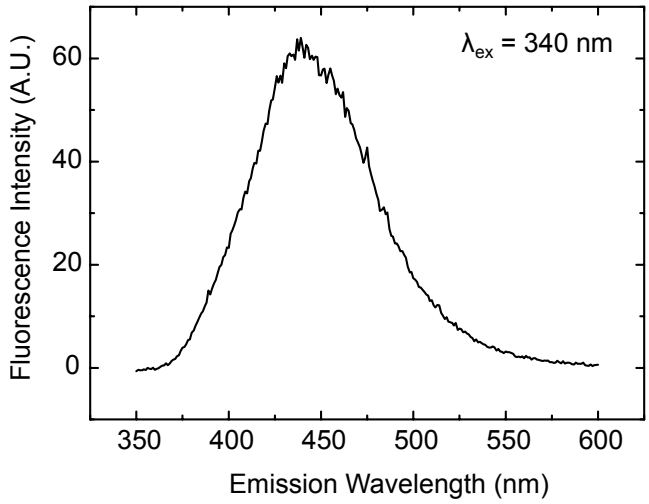

Figure 2.4 – Autofluorescence intensity profile (λ_{ex} = 340 nm) of a 12.5 μM solution of norfloxacin prepared in 200 mM sucrose. Measured using a Cary Eclipse Fluorimeter.

We therefore decided to use the secondary excitation peak of norfloxacin for our fluorescence assay, with an excitation wavelength of 340 nm (Figure 2.4). The emitted light peaks at a wavelength around 440 nm, well into the visible region of the spectrum, which is easy to detect with standard cameras and detection systems. Norfloxacin was thus a suitable candidate antibiotic for setting up our permeability assay. As we shall see in the following chapters, the technique can be extended to other drug molecules and nanoparticles as well. We must now turn our attention to choosing a suitable lipid system for the assay.

2.1.4 Giant Unilamellar Vesicles as Model Lipid Systems

Passive diffusion across the membrane is thought to account for the absorption of 80-95% of commercial drugs [11, 12]. Lipid model systems for studying passive diffusion thus play an important role in the study of drug uptake.

The first model lipid systems involving reconstituted cell membranes were created by Mueller and his coworkers in 1962 [33]. This led to the development of lipid electrophysiology, traditionally involving the preparation of "black" lipid membranes (so called because under reflected light, destructive interference between light reflected off the two layers of the membrane bilayer makes the structure appear dark) across apertures in a teflon film separating two reservoirs [34]. However, these techniques are not easily integrated with microscopy, and generally involve the application of electric fields; diffusion is therefore not necessarily passive.

An alternative approach was the use of lipid vesicles as model systems. A lipid vesicle (also known as a 'liposome') consists of a lipid membrane that encapsulates a fluid. They form due to the amphipathic character of phospholipid molecules. Phospholipid molecules typically contain a polar headgroup followed by a non-polar hydrocarbon chain. In aqueous solutions, these molecules tend to form bilayers which maximise the interaction of the polar headgroups with water while minimising the interaction of the hydrophobic hydrocarbon chain with water. Energetically, the formation of closed, spherical vesicles is favoured, and thus simply shaking a lipid film in an aqueous solution gives rise to vesicles. However, such a process offers very little control over vesicle size, and also tends to favour the production of multilamellar vesicles with multiple phospholipid layers.

A popular early method for vesicle production was by extrusion; a lipid suspension in an aqueous medium is "extruded" (pushed) through pores with diameters ranging from tens to hundreds of nm. This provides a monodisperse population of unilamellar vesicles, with a relatively narrow size distribution [35]. However, this technique fails to produce vesicles with diameters exceeding 1 μm and thus is not easily compatible with microscopy studies. We require giant unilamellar vesicles (GUVs), whose diameters can be in the tens of microns; these are traditionally created by a process known as **electroformation** [36]. This involves depositing a thin lipid film on a conducting

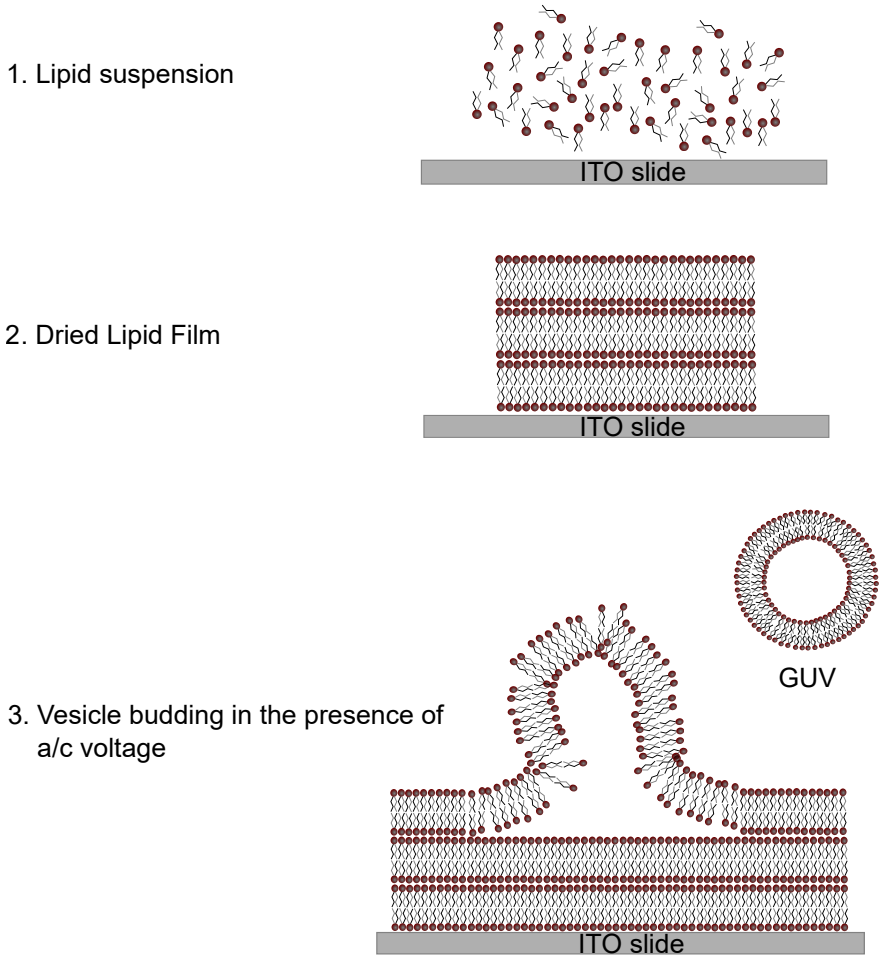

Figure 2.5 – Schematic representing the electroformation of GUVs. The lipid solution is spread on an ITO slide and left in a vacuum dessicator to evaporate the organic solvent – this produces a multilamellar lipid film on the ITO slide. The lipid film is then hydrated with a suitable aqueous buffer. The application of an alternating electric field causes the lipid film to bud off the ITO surface, encapsulating the solution thus forming vesicles.

surface, typically an Indium Tin Oxide (ITO) slide. A sandwich of two ITO slides is made, with the conducting surfaces facing each other, and a desired solution filling the gap between the slides. The application of an a/c voltage across the two conducting surfaces causes the lipid film to bud off, encapsulating the solution thus forming vesicles (Figure 2.5).

Electroformation has been the method of choice for GUV formation since its introduction by Angelova and Dimitrov [36], and we therefore settled on it for the purposes of our work. Besides their ease of observation, they are formed quickly (within 2-3 hours) and the vesicles formed are mostly unilamellar, and of good quality [37]. Indeed, such is the popularity of electroformation that it has even spawned the production of a commercial bench-top setup, the Nanion Vesicle Prep Pro (Nanion Technologies GmbH, Germany), that simplifies the experimental protocols involved. However, it must be noted that the actual process of electroformation is not well understood, and optimising the experimental protocol can prove challenging. This lack of understanding means that we have little control over the size range of the vesicles produced, which we need to correct for in our analysis. Moreover, electroformation in the presence of physiological salt concentrations is difficult [38], which limits the range of solutions that can be studied. However, notwithstanding these limitations, electroformation provided us with vesicles that were suitable for use in our assay and was the method employed by us for all the relevant experiments in this Thesis.

2.1.5 Overton's Rule

Theoretical studies of the permeability of cell membranes date back to the end of the 19th century. In 1899, the physiologist and biologist Charles Ernest Overton published a beautifully simple model predicting the permeability of biological membranes to a range of molecules [39]. He concluded that the entry of molecules into cells was governed by their "selective solubility" in the cell boundary [39]. Even more importantly, he predicted that the permeability of a molecule is a function of how soluble it is in lipids – the greater the lipid solubility, the higher the permeability. This concept has since been termed 'Overton's Rule' [39]. Remarkably, over a century of experimental investigations into lipid permeability have confirmed that Overton's Rule still rules [39, 40].

The rule stipulates that the transmembrane flux density (J) of a membrane-permeating molecule can be predicted if one knows its partition coefficient (K) from an aqueous into an organic phase [40]. Fick's law of diffusion can thus be rewritten as [15, 40]:

$$J = -D\frac{dc_m}{dx} = -D\left(\frac{c_{1m} - c_{2m}}{d}\right) = P(c_{2w} - c_{1w}) \tag{2.2}$$

where D is the diffusion coefficient of the molecule in the organic phase, c_{1m} and c_{2m} the concentration of the molecule at the two interfaces of the organic phase, c_{1w} and c_{2w} the corresponding molecule concentrations at the interfaces of the aqueous phase and d is the membrane thickness. $P \equiv KD/d$ is **defined** to be the permeability coefficient of the molecule across the membrane.

Over the past century, thousands of compounds have been tested, out of which only a tiny proportion show deviations from the rule [40]. The observed deviations are believed to be the result of transient defects in the membrane, with the proton being the most prominent example of substances belonging to this group [40]. It is important to clarify here that the rule only applies to simple lipid membranes – work over the past century has elucidated that true biological membranes have a range of protein pores in them, which facilitate membrane transport. In fact, Overton even predicted that ions would have to use a different pathway to enter cells, since the low dielectric constant of lipids prevented the solvation of charged particles [39].

However, the basic premise linking lipophilicity to membrane permeability still holds true, and is the foundation for the use of partition coefficients in the pharmaceutical industry. What we intend to do in this Thesis is develop a technique to measure the permeability of a molecule directly, without requiring knowledge of the partition coefficients, which can be difficult to measure in lipids. The intention is to directly measure the permeability of the molecule of interest across the lipid membrane of interest, rather than having to worry about which organic phase to use to model the lipid bilayer. We shall show how the use of specific lipids influences drug permeation, hence demonstrating why it is not advisable to use simple octanol partition coefficients to estimate drug permeability. Importantly, our technique will also enable us to study the influence of passive diffusion pores on drug permeation, and thus will provide a platform for investigating drug transport mechanisms in more detail than is typically the case.

2.2 Microfluidics

Microfluidics, as its name implies, refers to the technology of systems capable of manipulating small (10^{-9} – 10^{-18} litres) quantities of fluid using channels with dimensions of tens to hundreds of μm [41]. Besides offering precise control over fluid flow and mixing, all flows at such lengthscales are laminar, offering novel ways of controlling molecule concentrations in space and time [41]. The laminar flow patterns are a consequence of the low Reynolds number (*Re*) associated with microfluidic flows – *Re* is a dimensionless quantity that characterises the relative strength of inertial and viscous forces acting in a fluidic system. In microfluidic devices, viscosity dominates and laminar flows are the norm [41]. Fluid mixing is thus governed by diffusion, and depending on the flow velocities and the diffusion coefficient of the substances being mixed, one can predict the degree of mixing between flows at different points in a channel. In addition, small sample volumes, low cost, high-throughput capabilities and controlled microenvironments have made microfluidic technologies applicable across a wide range of fields [41–44].

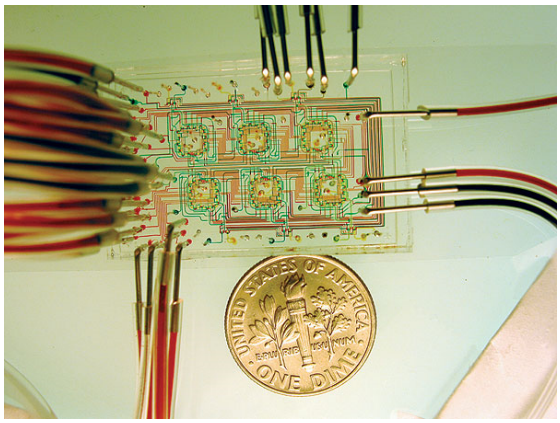

Figure 2.6 – A typical microfluidic device. This particular chip is used to study the growth of microbial populations. The channels are visualised here by passing dyes of different colours through the device. Pictured next to a 1 Dime coin (USA) for scale; the coin is 18 mm in diameter. Image taken from [45].

In medical diagnostics, for example, microfluidic devices are replacing conventional tests, enabling point-of-care diagnostics outside specialised laboratories. The Whitesides lab has pioneered the use of paper based microfluidic devices which are cheap, easy to

store and transport, and hence ideal for use in low-resource settings [46]. The use of low sample volumes is an added attraction – finger-pricks strike significantly less fear into people as compared to normal blood draws. Microfluidics allows one to perform many different diagnostic tests with just a few drops of blood, as opposed to the sometimes tens of millilitres required for conventional blood tests. Rapid colorimetric assays will also allow doctors to perform these tests during clinic visits, thus making the entire system more efficient.

In drug design and discovery, the use of small volumes allows for the testing of valuable chemicals that are not mass produced. *In vitro* assays to test the efficacy of drugs can be conducted on a single cell basis with high throughput, while still using low sample volumes.

In biomedical and molecular biology research, microfluidic devices are being used to perform studies on the single cell level, as opposed to bulk measurements that have for decades been the mainstay of the fields [47, 48]. Cellular heterogeneity is now finally open to detailed, microscopic investigation, and microfluidic assays are already revealing insights into a variety of biological processes [49–52].

2.2.1 Microfabrication Techniques

An important precursor to the development of microfluidics was the development of microfabrication techniques for constructing the devices with suitable spatial resolution. Photo- and soft lithography played a crucial role, and the polymer polydimethylsiloxane (PDMS) became the material of choice for testing and designing microfluidic chips [53]. PDMS is an optically transparent, silicone based polymer that is permeable to air, thus making it ideal for biological applications. It is easy to work with and relatively inexpensive; it is created by mixing an elastomeric component with a curing agent, which sets when baked. It is also capable of supporting useful components such as pneumatic valves, and has thus played a major role in the early development of microfluidic technologies [41].

The main steps in the creation of a typical microfluidic device are represented in Figure 2.7. In the photolithography step, the chip design is printed on a photo-emulsion film or a quartz mask; typically, the design is transparent on an otherwise opaque film.

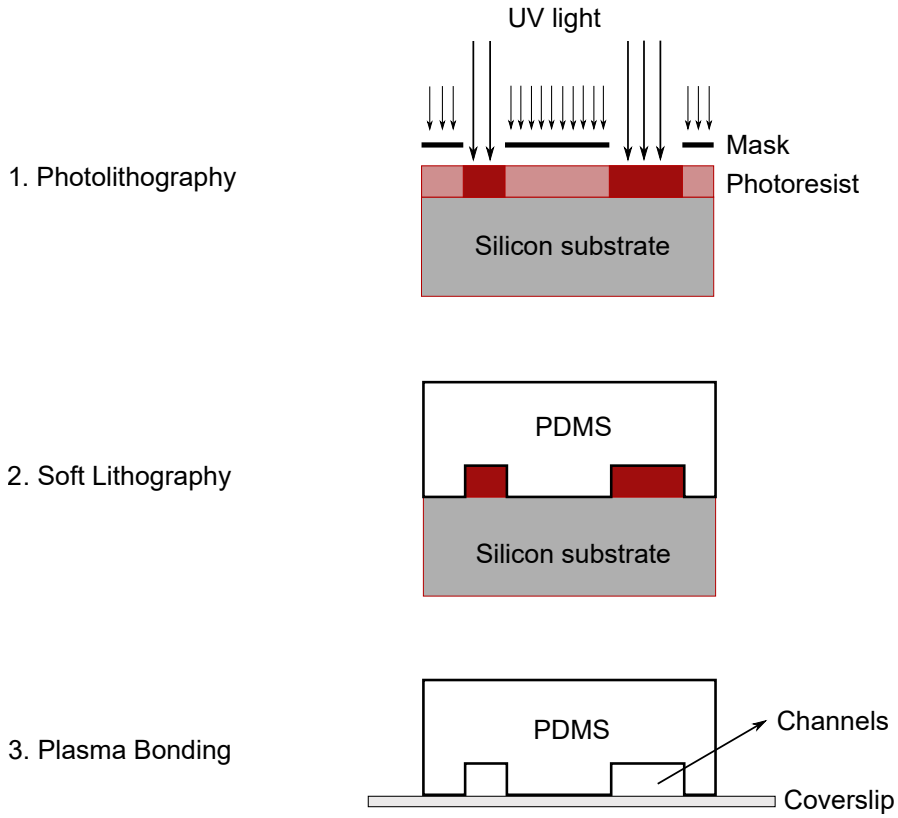

Figure 2.7 – Schematic of microfabrication protocol. In photolithography, the UV light selectively polymerises the photoresist that is exposed through the design mask (image adapted from Dr. Stefano Pagliara, with permission). After developing the mold, PDMS is poured onto the Si mold and baked. Once set, the PDMS chip is peeled off the Si mold and plasma bonded to a glass coverslip. The air gaps between the PDMS features and the coverslip form the desired microchannels.

A UV photoresist such as SU-8 is spin-coated on a silicon wafer, and then selectively exposed to UV light through the mask. The UV light polymerises the photoresist, and the remaining unpolymerised SU-8 is washed away by adding a chemical developer, which further strengthens the polymerised design. The resulting silicon mold is the negative replica of the final microfluidic chip, which is created by pouring a PDMS mixture on the mold and baking it in an oven.

Once set, the PDMS chip is simply peeled off the mold and bonded with a glass slide to create the microfluidic device; this is typically done by exposing both surfaces to an air plasma to facilitate bonding. The plasma leads to the formation of silanol (Si-

OH) groups in the PDMS at the expense of methyl groups. Since silanol groups are polar, they make the surface highly hydrophilic, thus facilitating the filling of the chip with aqueous solutions. When two such surfaces (either PDMS-PDMS or PDMS-glass) are brought in contact, the silanol groups condense yielding strong Si-O-Si bonds [54]. Although other bonding techniques have been developed [55], plasma bonding remains a very effective technique that provides a tight seal between the PDMS chip and glass. A strong seal is obviously crucial for any microfluidic device, in order to prevent fluids from leaking out of the microchannels, and we therefore used plasma bonding for creating all the microfluidic devices mentioned in this Thesis.

2.2.2 Vesicle based microfluidics

Transport studies involving vesicles in microfluidic devices have been performed recently in the group of Prof. Petra Dittrich in ETH Zurich. Her team has developed microfluidic platforms that immobilize vesicles using both physical [56] and chemical [19] trapping. The physical trapping technique used a PDMS chip with 60 chambers, in which GUVs were trapped hydrodynamically in between posts. The technique included the use of valves, which could isolate a trapped vesicle from the rest of the fluidic network. Solution exchange was possible without disrupting the vesicles, and GUVs remained stable over long periods (>12 hours) [56]. The technique was used to study the transport of the fluorescent dye calcein through the protein pore alpha hemolysin reconstituted in the vesicles.

For chemical trapping, small unilamellar vesicles (diameter $\sim$ 180 nm) were immobilized on a glass slide using avidin- and PEG(polyethylene glycol)-biotin bonds. The transport of the antibiotic tetracycline into these vesicles was observed by the formation of fluorescent complexes of the drug with salts enclosed in the vesicles [19].

Both these techniques involve the immobilization of vesicles in the chip, and this naturally limits the experimental throughput. Furthermore, fluorescent reporters were required to detect the uptake of tetracycline. However, these techniques show that it is possible to use vesicles for transport studies in microfluidic environments, and with this in mind, we went on to develop our own vesicle based microfluidic assay. The

experimental detail is provided in the next section, and the next two chapters of this Thesis will be devoted to some of the results we have obtained using this technique.

2.3 The Optofluidic Permeability Assay

2.3.1 Optical Setup

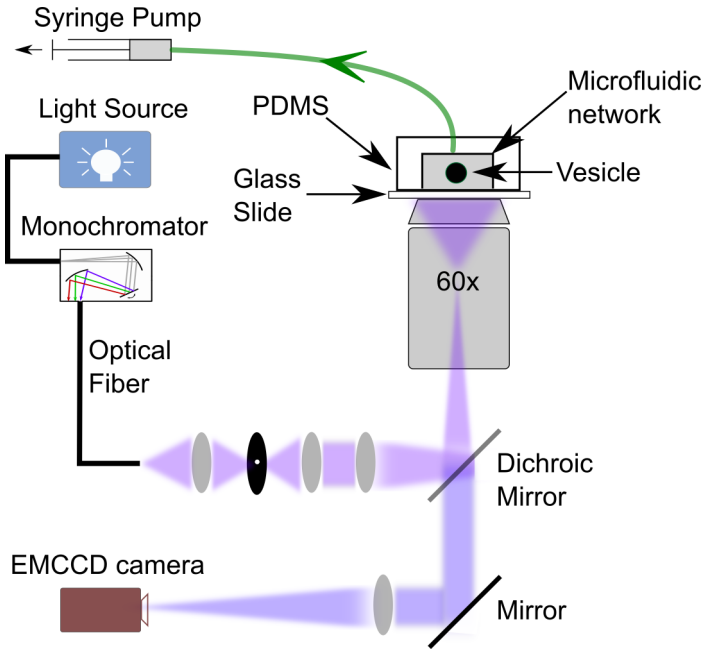

Figure 2.8 – Schematic of Optical Setup. Broadband white light is passed through a monochromator which selects the fluorescence excitation wavelength (340 nm). The excitation light is directed onto the microfluidic device and the emitted fluorescent radiation is focussed onto an EMCCD camera. Suction is applied at the outlet of the microfluidic network with a syringe pump.

The optical setup is a custom built UV epifluorescence microscope described schematically in Figure 2.8. The output from a broadband white light source (EQ99FC, Energetiq, USA) is passed to a monochromator (Monoscan 2000, OceanOptics, USA) which selects the desired excitation wavelength (340 nm) and directs it onto the microfluidic device via a Köhler illumination pathway and a suitable dichroic mirror (DLHS UV

351-355, Qi-Optiq, Germany). The objective used is a 60× water immersion UPLSAPO Olympus objective (NA 1.2). The emitted fluorescent light passes through the dichroic and is focussed onto the detector, an EMCCD camera (Electron Multiplying Charge Coupled Device Evolve 512, Photometrics – exposure time 2 ms, bin 2, EM gain 100, frame rate 65 fps) via a tube lens and a mirror. All lenses used (apart from the objective) are made from UV fused silica to optimise UV transmission and the optical fibers are UV grade (OceanOptics). The camera is controlled using the open-source software μManager 1.4 [57].

As we shall see later, it is possible for some of these experiments (with norfloxacin, for example) to be performed using commercial microscopes with suitable UV light sources and filter sets (for norfloxacin, a standard DAPI filter set works well). However, for applications which require deep UV transmission, it will be necessary to replace the optics in a commercial setup with quartz optics.

2.3.2 Microfluidic Chip Design and Fabrication

The microfluidic chips used in the assays were produced using standard photo- and soft lithography techniques [53, 58]. Three different chip designs were constructed, whose exact details can be found in appendix B. The channels are 40 μm wide. The basic principle of all three devices is the same, and is depicted in the schematic (Figure 2.9). A microfluidic T junction enables the mixing of two different solutions (the lipid vesicles and the drug) in a long channel. The main difference in the three chips is the length of this mixing channel – in the 'Long' design, the total length from the T junction to the outlet reservoir is about 380 mm. In the 'Medium' it is 127 mm and in the 'Short', just 28 mm. The different lengths were created to enable the study of membrane transport processes that occurred over different timescales. The 'Short' chip is designed for studying drug uptake which occurs in a matter of seconds – therefore here the initial viewpoint is almost immediately after the T junction. In the other devices, the initial viewpoint is about 15-20 seconds post flow mixing – this ensures that the drug/particle being studied has diffused across the entire width of the channel before the vesicles are imaged for the first time. Though not critical for the norfloxacin

measurements, this extra length is required when studying larger molecules/particles which have smaller diffusion coefficients.

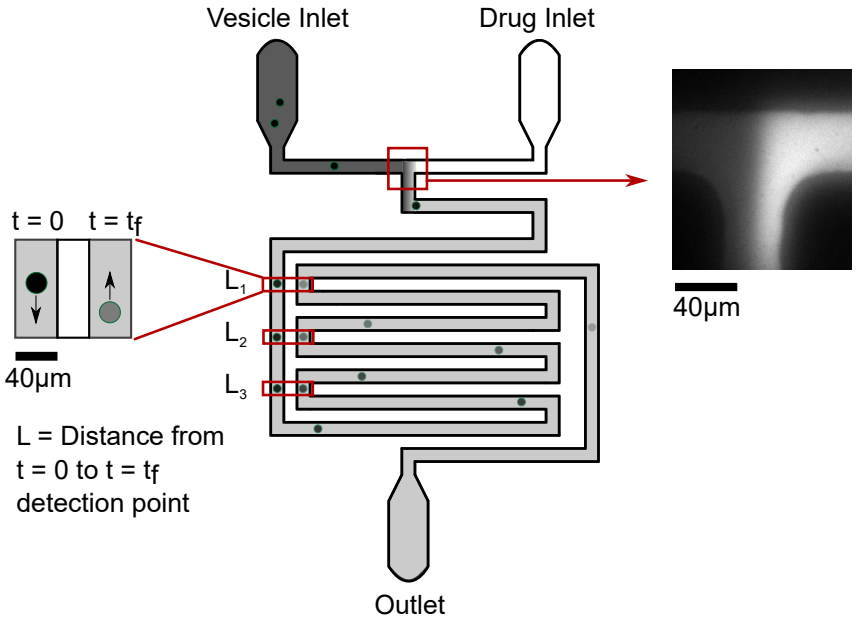

Figure 2.9 – Schematic of microfluidic network. The inset displays a typical flow pattern at the T junction in an experiment, illuminated in combined brightfield and fluorescence mode for clarity. Lipid vesicles are exposed to a uniform concentration of the drug along the network. The $t = 0$ point is chosen after the drug has equilibrated across the channel width. Vesicles at $t = 0$ and later time points are observed in the same field of view. The two observation points are a length L apart along the network. As vesicles progress along the network, if the drug is permeable, the fluorescence intensity inside the vesicles increases.

In all the designs, the channel is constructed such that it loops around multiple times (Figure 2.9). This allows the detection of vesicles at two distinct time points in the same field of view (at 60× magnification). By imaging vesicles at different positions in the chip, one can study the time dependence of drug uptake. We also included a network of pillars in the inlet reservoirs as filters to prevent large lipid aggregates from entering the microfluidic network and blocking the flow. There are two sets of pillars – a coarse filter with 75 μm gaps, and a fine filter with 40 μm gaps (appendix B).

Photolithography of the Si molds[2]

The masks were designed in AutoCAD and printed on emulsion film (JD Photo-Tools UK). SU-8 3050 (Chestech UK) photoresist was spin coated (SCS Spincoat G3P-8, 7s at 500 rpm followed by 30s at 3,000 rpm) onto a Si wafer (Microchemicals, Germany) and then baked on a hot plate (96 °C for 20 mins). After aligning the desired film mask on the wafer, it was exposed to UV (the UV lamp was an OAI system with an output power of 200 W) for 15 seconds, post-baked for about 6-7 mins at 96 °C and then developed in Propylene glycol monomethyl ether acetate (PGMEA) for approximately 10 mins. This was then rinsed with isopropanol and blow dried with N_2. The protocol led to the formation of channels with a height of 50 μm.

Soft Lithography for constructing the PDMS chip

A negative replica of the desired Si mold is obtained using Sylgard 184 Polydimethylsiloxane (PDMS – from Dow Corning); a 9:1 ratio of elastomer:curing agent PDMS mixture is poured onto the Si mold and cured for 55 mins at 60 °C in an oven. This is then carefully peeled off the Si mold and cut into a desired shape using a sharp blade. The inlet and outlet holes are punched using a 1.5 mm biopsy punch. It is important to clean the punched columns and the rest of the PDMS chip with 96% ethanol (it must then be dried gently with N_2). Finally, the PDMS chip is bonded to a glass coverslip (Type 1, Assistent, Germany) by exposing the surfaces being bonded to an air plasma (10 W plasma power, 10 s exposure, 25 sccm, plasma etcher from Diener Electronic GmbH & Co. KG, Germany) and then binding the two exposed surfaces together to create a sealed microfluidic device. This is placed in an oven at 60 °C for 10 mins to enhance the adhesion. The chip should be filled with the buffer/water within 10-15 mins after construction so that the channels wet easily – the plasma bonding makes the channels temporarily hydrophilic, and this property must be exploited. Once the chip is filled and checked to ensure there are no air bubbles, the device is ready for use.

[2]The 'Short' design Si mold was constructed by Dr. Stefano Pagliara, whose photolithography protocol differs slightly from mine. This additional protocol is provided in appendix B.

2.3.3 Vesicle electroformation protocol

GUVs are created by electroformation using a Nanion Vesicle Prep Pro setup. Figure 2.10 depicts some typical GUVs obtained with this protocol.

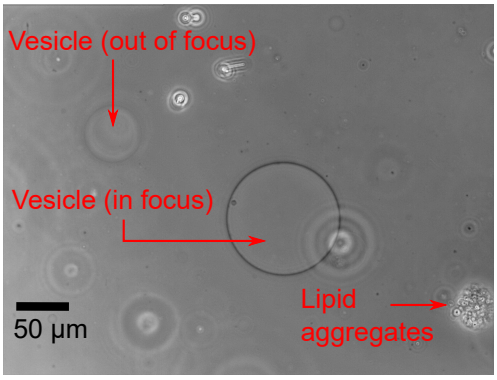

Figure 2.10 – Typical GUVs obtained after electroformation. Imaged under brightfield with 20x magnification. The heterogeneity of results obtained via electroformation is seen. Since there is no difference in solutions between the interior and exterior of the GUVs, they can float in solution; therefore the two GUVs seen here are not in the same focal plane. We also observe lipid aggregates after electroformation, and have built in safeguards in our analysis to separate these from vesicle detections.

60 µl of 5 mg/ml 1,2-diphytanoyl-*sn*-glycero-3-phosphocholine (DPhPC) lipid (Avanti Polar Lipids) in chloroform is spread on the conducting surface of an ITO coated glass slide (Nanion/Visiontek) within a rubber O-ring. The chloroform is evaporated for 10 mins in a desiccator following which 600 µl of the appropriate buffer (200 mM sucrose in a 5 mM phosphate buffer for pH 7 or 200 mM sucrose in a 5 mM acetic acid buffer for pH 5) is deposited within the O-ring and a sandwich made with another ITO coated slide (conducting surfaces facing each other). This is placed in the Nanion Vesicle Prep Pro whereupon electroformation proceeds in 3 steps: (i) The a/c voltage increases linearly from 0 to 3 V peak to peak (p-p) at 5 Hz in 5 mins. (ii) The voltage stays at 3 V p-p and 5 Hz for 2 hrs. (iii) The voltage decreases linearly to 0 V at 5 Hz in 5 mins. The electroformation was carried out at 37.5 °C. The vesicles were stored at 4 °C and used within a week. This formation protocol was used for all the vesicle experiments in this Thesis.

2.3.4 Microfluidic flow control

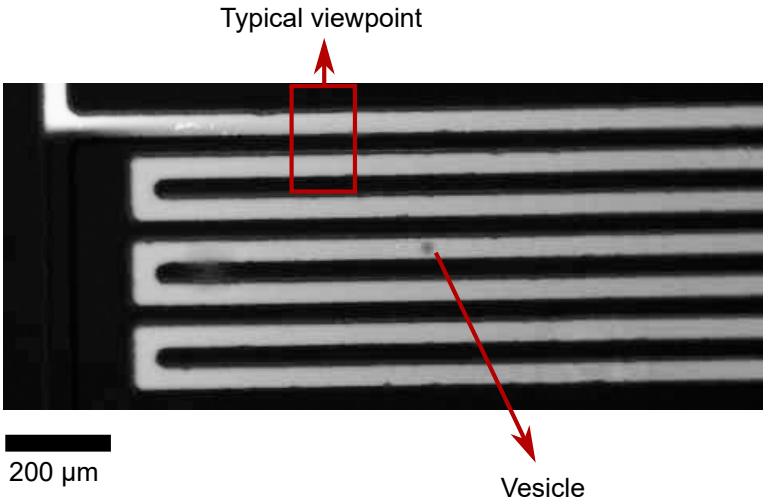

Figure 2.11 – Snapshot at the T junction of the 'Short' microfluidic chip in action, using a 10× objective on a commercial Olympus IX73 microscope. Norfloxacin fluorescence is excited using an arc lamp and a DAPI filter set. For data collection, as mentioned earlier, 60× objectives are used.

The microfluidic flows are controlled by applying suction at the outlet reservoir using a neMESYS syringe pump system. In early experiments, a 1 ml Duran Borosilicate glass syringe (ILS, Germany) was used. However, it was observed that syringes with lower volumes provided better flow control, and were less susceptible to air bubbles. The optimum syringe volume for our experiments was found to be 250 µl, and hence most experiments were carried out with a 250 µl Duran Borosilicate glass syringe (ILS, Germany). The volume of the syringe should be chosen such that it exceeds the volume of the tubing used to connect the syringe to the microfluidic chip; this helps in removing air bubbles when filling the syringe and tubing with solutions before starting the experiment. The tubing used was Upchurch 1520G (0.03 inch inner diameter). At the inlets, pipette tips with 50 µl of vesicle stock solution and 50 µl of 2 mM norfloxacin solution respectively were input into the two reservoirs, using a previously described technique [59]. Initially, to ensure a uniform distribution of norfloxacin throughout the network, a fast flow (30-100 µl/hr) was applied. Once the fluorescence intensities were observed to be uniform in the detection regions, the flow rate was decreased to about 3 µl/hr. Data collection was started once the flows settled and individual vesicles

were slow enough (∼1 mm/s) to be tracked in the field of view for about 5-10 frames to ensure a reliable statistical analysis of the relevant measured quantities. It is important to note that we study individual vesicles as they pass through the network – this is not a bulk experiment – with a throughput up to 100 vesicles per hour.

A detailed experimental protocol for this assay is provided in appendix A. A typical snapshot (zoomed out) of the experiment in progress is depicted in Figure 2.11.

2.3.5 Diffusion model for calculating drug permeability

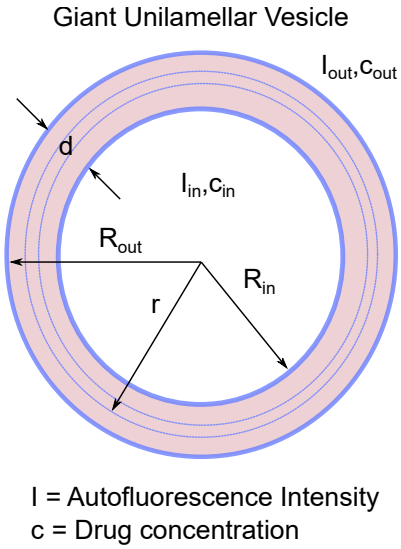

Figure 2.12 – Schematic of a Giant Unilamellar Vesicle.

A giant unilamellar vesicle created by electroformation is shown schematically in Figure 2.12. A lipid bilayer separates the interior from the exterior of the vesicle. Autofluorescence intensities within the vesicle I_{in} are related to the concentration of the drug inside the vesicle c_{in}.

Preliminary confocal measurements on vesicles suspended in a bath of norfloxacin proved that although the concentration of norfloxacin that is diffusing into the vesicles (c_{in}) is dependent on time, its spatial concentration within the vesicle is uniform [13, 60]. The norfloxacin diffuses almost instantaneously (within a second) across the volume of the vesicle.

Thus the rate limiting step in the diffusion process is membrane permeation. The flux of norfloxacin molecules passing through the membrane at a given time t is thus given by [13]:

$$\frac{J(t)}{4\pi r^2} = -KD\frac{dc}{dr} \tag{2.3}$$

which on integration gives:

$$J(t) = 4\pi R_{in}R_{out}\frac{KD}{d}(c_{out} - c_{in}(t)) \tag{2.4}$$

where D is the diffusion coefficient and K the partition coefficient. The drug concentration outside the vesicle c_{out} stays constant over time. Since the thickness (d) of the bilayer ($\sim$ 5 nm [61]) is 3-4 orders of magnitude less than the radius (R) of the vesicles being considered, we may assume that the inner and outer radii are the same, i.e, $R_{in} \sim R_{out} = R$.

The flux of particles passing through the membrane per unit time also equals the variation in the number of particles trapped inside the vesicle. Since within the vesicle the norfloxacin concentration is homogeneous, we can write:

$$J(t) = \frac{dc_{in}(t)}{dt}\left(\frac{4\pi R^3}{3}\right) \tag{2.5}$$

Equating the two equations gives:

$$\frac{dc_{in}(t)}{dt} = \frac{3KD}{Rd}(c_{out} - c_{in}(t)) \tag{2.6}$$

Solving this with boundary conditions:

- $c_{in}(t = 0) = 0$
- $c_{in}(t = t_f) = c_{in}(t_f)$

and using our definition of the permeability coefficient $P \equiv KD/d$, we obtain the solution:

$$P = -\left(\frac{R}{3t}\right) \ln\left(\frac{c_{out} - c_{in}(t)}{c_{out}}\right) \tag{2.7}$$

We thus have an equation for the permeability coefficient *P*, our quantity of interest. However, we need to adapt this equation based on our experimentally measured parameters. In our experiment, we measure the autofluorescence intensities within the vesicles (I_{in}) at different time points, the background autofluorescence intensity of the drug (I_{out}), the radius of the vesicle (R) and, indirectly (by measuring vesicle velocity), the time (t) taken for the vesicle to move between detection positions.

Let us examine our equation for *P* in a little more detail before proceeding. We detect the vesicles at different points, and use the flux of drug molecules into the vesicle in the intervening time to determine *P*. Hence, it should be obvious that the time *t* in the equation cannot be zero, since one cannot measure a buildup of drug molecules in a vesicle at just one time point. In any case, the mathematics also tells us that as *t* goes to zero, $c_{in}\ (t)$ also goes to zero and the equation is satisfied. One must recall that, even though we are using the change in drug concentration inside the vesicle to measure the permeability, *P* is a physical constant for a given drug-lipid combination.

Furthermore, we have assumed in our model that the drug equilibrates within the vesicle as soon as it is past the membrane barrier. In practice of course this cannot be the case, and the drug molecules will take a finite amount of time to diffuse in the vesicle volume. A rough estimate for a vesicle with a radius of 10 μm reveals a diffusion timescale on the order of 50-100 ms for norfloxacin, which is well below the timescales that we analyse. Similarly, in the long time limit, c_{in} will exponentially converge to c_{out}, and again the formula holds true.

Let us now look at our equation in terms of the parameters that we actually measure in the experiment. The drug concentration outside the vesicle is directly proportional to the fluorescence intensity I_{out}. However, since the optical setup used in the microfluidics experiments is not a confocal microscope, the drug concentration inside the vesicle ($c_{in}(t)$) depends on the fluorescence intensity inside the vesicle I_{in} in a more complicated manner. We can split the intensity contribution inside the vesicle into two parts, one that is the contribution of the drug ($I^{true}{}_{in}(t)$) and another that is simply due to the out of focus light from outside the vesicle that has entered into the region being studied,

that we label *F*. *F* is independent of time (since it is independent of drug concentration) but has a dependence on the vesicle radius. Now,

$$\frac{c_{out} - c_{in}(t)}{c_{out}} = \frac{I_{out} - I_{in}^{true}(t)}{I_{out}} \tag{2.8}$$

We detect vesicles at an initial point that we define as $t = 0$ and at a later time point $t = t_f$. Vesicle detection is performed in a two-step process during image processing[3]:

- Firstly, deviations from the mean image intensity are detected, and if the difference from the baseline is more than a suitable multiple of the median absolute deviation (MAD), the frames are considered for potential vesicle detections. This condition may be varied depending on the SNR of the experiment. Initially, we used 3×MAD as our criterion, but noticed that we were then missing a significant fraction of events. We therefore reduced this to just 1×MAD for the home-built setup.

- Secondly, the vesicles are identified in each of the candidate regions. A background is calculated as the averages of the frames just before and after each detection event. This background is then subtracted from each of the images in the candidate region in order to enhance the vesicles, as they are the main source of intensity variation. A binary mask with the vesicle outline is obtained using the threshold given by the Otsu method.

- Finally, the 'regionprops' function in MATLAB is used to obtain information about the major and minor axes, the centre of the shape, amongst other parameters. The vesicle radius is determined by taking an average of the semi-major and semi-minor axes. Since we capture the vesicles for multiple frames, we can track the movement of the centre position and use this to determine the vesicle velocity. Around the centre, a 5×5 pixel box is created and the average intensity within this box is determined. The average intensity of exactly the same 5×5 pixel box is determined in the background image for each event. This gives us the values of I_{in} and I_{out}, which are used in the calculations.

[3]The MATLAB programs were written in collaboration with Dr. Avelino Javer (formerly of the Cicuta group, Cavendish Laboratory).

For clarity, let us introduce the convention that all intensities related to the interior of vesicles (I_{in}) at the initial detection point $t = 0$ will be denoted as $I_{(0)}$ and at later times as $I_{(t)}$. We reiterate that the intensities outside the vesicles I_{out} remain constant with time, and will always be written as I_{out}. Our image analysis program outputs the following value for each vesicle at the two time points:

$$\Delta I(0) = \frac{I_{out} - I_{(0)}}{I_{out}} \tag{2.9}$$

$$\Delta I(t) = \frac{I_{out} - I_{(t)}}{I_{out}} \tag{2.10}$$

Now,

$$I_0 = I_0^{true} + F = F \tag{2.11}$$

since we assume that the drug concentration inside the vesicle is 0 at $t = 0$. Furthermore,

$$I_{(t)} = I_{(t)}^{true} + F = I_{(t)}^{true} + I_{(0)} \tag{2.12}$$

Therefore,

$$I_{(t)}^{true} = I_{(t)} - I_{(0)} = I_{in}^{true}(t) \tag{2.13}$$

Thus,

$$\frac{c_{out} - c_{in}(t)}{c_{out}} = \frac{I_{out} - I_{in}^{true}(t)}{I_{out}} = \frac{I_{out} - (I_{(t)} - I_{(0)})}{I_{out}} = \Delta I(t) + \frac{I_{(0)}}{I_{out}} = \Delta I(t) + 1 - \Delta I(0) \tag{2.14}$$

Substituting this in our equation for P equation (2.7), we finally obtain:

$$P = -\left(\frac{R}{3t}\right) \times \ln(\Delta I(t) - \Delta I(0) + 1) \tag{2.15}$$

This is the equation we use to calculate the permeability coefficient for individual vesicles. As mentioned in the discussion above, this model is applicable when the time between detection points is greater than about 100 ms. However, we should also note that our experimental resolution fixes a finite upper bound on the time differences as well. As the time between the detection points increases, ΔI(t) becomes smaller and smaller as the drug concentration within the vesicle approaches the external concentration. ΔI(t) will approach zero exponentially, but our measurement timeframe depends on our detector being able to distinguish the vesicle from the background via its intensity contrast. Therefore, in practice there is also an upper bound on the timeframes that can be studied, which depends on the speed of drug uptake and also on the vesicle radius.

However, using our microfluidic approach, hundreds of vesicles can be detected and analysed with this equation within the experimental timescales. In the following chapters, we shall apply this technique to the study of passive norfloxacin transport across phospholipid bilayers. In addition, we perform measurements with different antibiotic-lipid combinations, and show how the same detection technique can be extended to studying the interaction of other nanoparticles with lipid membranes.

2.3.6 Data Analysis

We have two MATLAB analysis codes; the first studies the images in the TIFF stacks obtained (the raw experimental data) and obtains all the desired information on a frame by frame basis. We then process this data set with a 'post-process' code that averages all the relevant values on a vesicle-by-vesicle basis. Thus, if a single vesicle is detected for, say, 10 frames, the values of ΔI and R will be averaged over the values in all 10 frames – it is this average value that is used in the calculations. Furthermore, the first code measures the minor and major axes of the vesicles on a frame by frame basis, and reports a circularity criterion defined as:

$$Circularity = \frac{MinorAxis}{MajorAxis} \tag{2.16}$$

The theoretical analysis is based on the vesicles being circular. Therefore, we apply a filter in the post-process code that deletes all vesicles detected with a circularity lower than a defined value (the optimum value for this filter was found to be 0.7, although 0.75 can also be used). The code also tracks the centre position of each vesicle. The post-process code uses this information (and a knowledge of the camera frame rate) to determine the vesicle velocity. A knowledge of the chip geometry and vesicle velocity determines the time t taken by the vesicle to travel the intervening distance between two detection points.

The final analysis is performed manually with OriginPro software. In addition to the circularity filter, at this stage filters are applied on the radius and vesicle velocity which help avoid the detection of false positives generated due to the detection of lipid aggregates. With regards to the radius, the width of the microfluidic channel is 40 μm. Therefore, vesicles with radii greater than 20 μm are discarded – these are prone to shear by the channel walls. It was also observed that detections with radii less than approximately 8.5 μm were often due to lipid aggregates, and were thus discarded. When considering vesicle velocities, experience showed that if the velocity was less than ∼0.4 mm/s, the detected objects were either vesicles rolling along the channel walls (in which case they were prone to shear) or lipid aggregates. Velocities above 1.5 mm/s were almost always small lipid aggregates, and not vesicles. The events were filtered accordingly.

At the different vesicle detection points, there might be slight changes in the measured vesicle radius due to optical or fluidic effects. However, our calculation relies on R being unchanged for the measurement of $\Delta I(0)$ and $\Delta I(t)$. To solve this problem, we plot $\Delta I(0)$ vs R (for a typical example, see Figure 2.13) and use the resultant linear relation as a calibration for $\Delta I(0)$. The linear relation between ΔI and R is a direct consequence of the imaging technique being a brightfield rather than a confocal measurement (for details, please refer to appendix C). Now, for all the vesicles detected at the later detection point, we measure the radius, and use this value of R to obtain a corresponding $\Delta I(0)$ value from the calibration plot. It is this 'recalculated' value of $\Delta I(0)$ that is used, along with the radius measured at the later detection point, in the equation for permeability above (equation (2.15)).

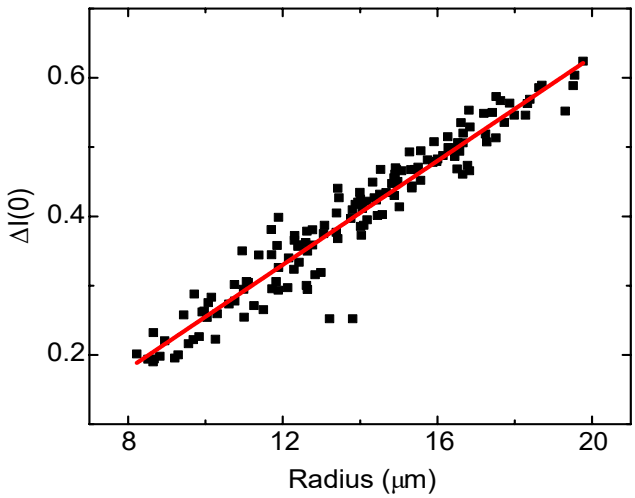

Figure 2.13 – Typical calibration plot of $\Delta I(0)$ *vs* R. This linear fit is used to recalculate $\Delta I(0)$ for vesicles using the radius measured at time t (the final detection point). This 'recalculated' $\Delta I(0)$ is used in the calculation of the permeability coefficient using equation (2.15).

We thus have all the quantities required to determine the permeability coefficient of each vesicle to the drug under investigation.

It should be mentioned here that the MATLAB code separately saves the frames (from the original image stack) in which vesicles are detected. This allows us to visually check the raw images corresponding to a data point on the scatter plot (of course, it is possible to find the same vesicle in the original video, but that would be rather more tedious). This acts as a further check that can be used to weed out false positives.

2.4 Conclusions

We have thus set up a novel, label-free technique of studying passive drug transport across lipid membranes that directly determines drug permeability coefficients using lipid vesicles. It is experimentally simple and can be adapted for cell work. The experiment itself is robust and can be run for hours at a stretch; it is thus capable of generating a much higher throughput than older vesicle-based techniques. It can be used to study passive transport in membranes of varying lipid compositions and also to study the effect of membrane-bound transporters on drug transport. In the next

chapter we shall discuss the use of this technique to study the permeability of drugs and nanoparticles through pure phospholipid membranes, before moving on to the investigation of pore mediated drug transport in chapter 4.

Chapter 3

Transport Across Pure Phospholipid Membranes

> "There is a tide in the affairs of men, which taken at the flood, leads on to fortune."
>
> Brutus (*The Tragedy of Julius Caesar*)

3.1 Introduction

In this chapter, we shall apply our new technique to the study of antibiotics and other nanoparticles as they diffuse across pure phospholipid membranes. The technique was validated by studying the transport of norfloxacin across DPhPC vesicle bilayers, and we shall begin with a description of the results and analysis of this system. One major advantage of this technique is that the lipid membrane composition can be changed easily – we shall show that changing the type of phospholipid in the vesicle membranes can have dramatic effects on the permeability of norfloxacin.

To demonstrate the versatility of the technique, measurements were also performed using a different class of antibiotics. The permeability of a broad spectrum polyketide antibiotic, tetracycline, is investigated, thus showing that the technique is not limited to fluoroquinolone antibiotics. Finally, the interaction of nanoparticles such as Quantum

Dots (QDs) with lipid membranes is an important field of study, especially in light of concerns raised about the toxicity of nanoparticles and their accumulation in cells. QDs are also autofluorescent in the UV, and we report some measurements on the interaction of Cadmium Selenide QDs with DPhPC lipid vesicles.

Before reporting these results, we shall briefly introduce some basic concepts about the phospholipid bilayer.

3.1.1 Phospholipid Bilayers

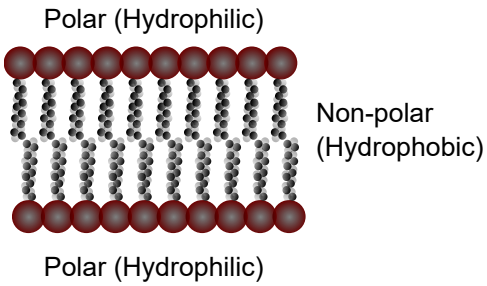

Figure 3.1 – The Phospholipid Bilayer.

The cell membrane of almost all biological organisms contains, as its core foundation, a double layer of lipid molecules. The most commonly found, naturally occurring lipid molecules are the phospholipids. These are amphipathic molecules, which contain a polar (hydrophilic) head group and two non-polar (hydrophobic) hydrocarbon chains. When suspended in an aqueous solution, the amphipathic character of these molecules governs their self-assembly; the polar headgroups preferentially align to remain in contact with the aqueous phase, whereas the hydrocarbon chains do all they can to avoid the polar water molecules. This inevitably leads to the formation of lipid bilayers (Figure 3.1), where the lipid molecules pack together in their energetically most favourable configuration – polar groups on the outside, non-polar chains on the inside.

The non-polar core of lipid bilayers is crucial – this is what keeps polar molecules and ions from flooding the cell and causing osmotic shock. It is central to the so-called 'semi-permeability' of cell membranes. Besides acting as a barrier, the lipid bilayer also behaves as a solvent for the numerous membrane spanning proteins that catalyze the transport of ions and molecules across the lipid permeability barrier [62]. Studies on

the permeability of small molecules across lipid bilayers have concluded that water and non-electrolytes cross the barrier via the solubility-diffusion mechanism predicted by Overton, and also conclude that the bilayer **barrier** (i.e, excluding the headgroups) may be approximated as a thin sheet (∼3 nm thick) of liquid hydrocarbon [62, 63].

Phospholipids always contain a phosphate moiety in the headgroup, but otherwise may possess a variety of different headgroups and hydrocarbon chain lengths. Considerable effort has been expended on the study of phospholipid bilayers, in order to better understand their role in cellular membrane transport. Their interaction with membrane proteins is another major avenue of research, and we shall discuss one such process of protein mediated membrane transport in chapter 4.

Of the various types of phospholipids, the phosphatidylcholines (PC) were amongst the first to be discovered. These form a major component of cellular membranes and are routinely used to form artificial bilayers. We developed our technology using this class of phospholipid, and shall introduce some of its properties in the following section.

3.1.2 Phosphatidylcholine lipids

Phosphatidylcholine (PC) lipids are phospholipids that contain choline as a headgroup. PC is an essential phospholipid in mammalian cells, and is made in all nucleated cells via the choline pathway [64]. It is the major structural component of eukaryotic cell membranes, and also plays an important role in lipid mediated signal transduction [65, 66]. Although less common in prokaryotes, it is estimated that more than 10% of all bacteria contain PC as a membrane phospholipid [67]. PC lipids in bacteria are generally formed by the enzymatic methylation of the commonly found phosphatidylethanolamine (PE) class of phospholipids, although choline dependent pathways for PC production have also been reported [67].

The PC lipids found in biological membranes also tend to form lamellar phases (bilayers) in water over a wide range of temperatures [68]. This makes them suitable for use in the formation of giant unilamellar vesicles, our model system. Thus PC lipids are both biologically interesting systems to investigate and convenient lipids to work with, making them an obvious choice for our assay.

We chose to work primarily with the artificial PC lipid DPhPC. This phospholipid molecule is commonly used to form artificial bilayers since it can be produced synthetically and hence free of impurities. Furthermore, it is known to form very stable bilayers and is not autoxidizable [69]. The high degree of stability arises from the fact that the hydrocarbon chains in DPhPC are composed entirely of saturated bonds [70]. Since DPhPC bilayers show very low ion leakage, they have been the lipid bilayers of choice for studying lipid-protein interactions; they have been used extensively for the study of membrane channel activity [71].

3.2 pH dependence of norfloxacin transport

3.2.1 Norfloxacin charge dependence on pH

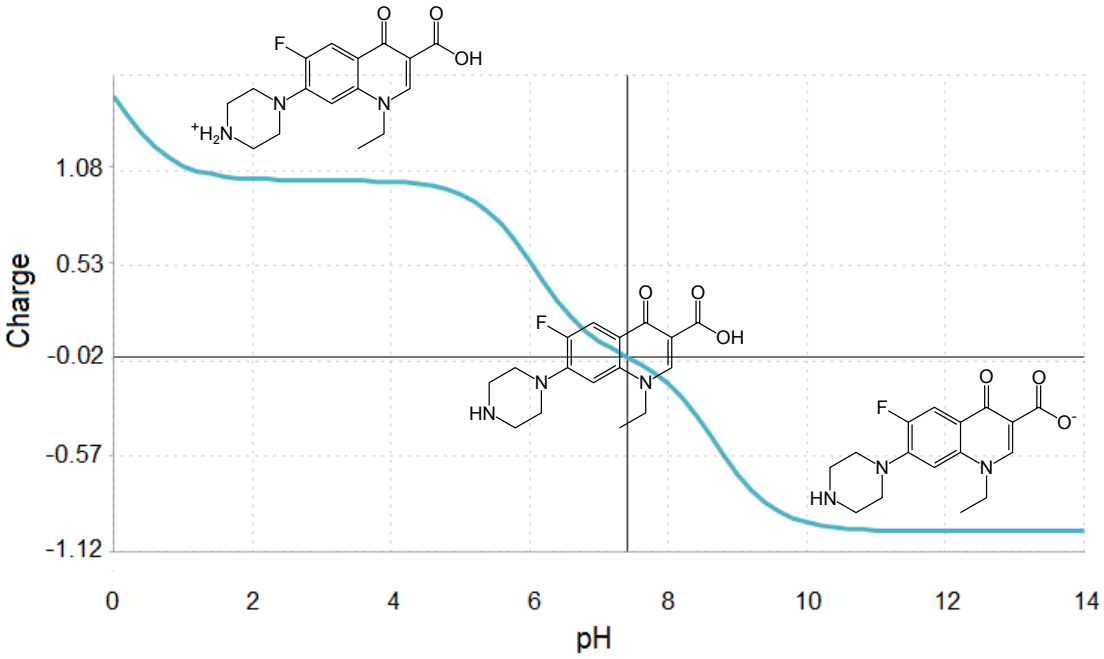

Figure 3.2 – pH dependence of norfloxacin charge. Isoelectric point 7.37. Source: www.chemicalize.org

Norfloxacin, along with other fluoroquinolones, contains two proton binding groups. The first, with a pK_a value of 6.34, is the 3-carboxyl group and the other, with a pK_a

of 8.75 (PubChem data), is the outer nitrogen on the piperazine substituent [72]. The multiple protonation sites indicate that the norfloxacin molecule can exist in different charge states. A detailed analysis based on microscopic dissociation constants predicts that at physiological pH values, a significant proportion of the norfloxacin molecules exist in their uncharged state, whereas at acidic pH values the molecule is protonated and has a net positive charge [72]. More precisely, at pH 7.4, the molecules are generally zwitterionic, but approximately 10% of the molecules are uncharged and it is these uncharged molecules that are expected to contribute to the passive diffusion of norfloxacin across lipid bilayers [72, 73]. The predicted pH dependence of norfloxacin charge is summarized in Figure 3.2. As discussed earlier, polar charged molecules have very little affinity for the non-polar core of lipid bilayers. We would therefore expect the permeability of the uncharged form of norfloxacin to be significantly greater than its charged, protonated form. We can thus use the charged form as an effective control experiment, to test whether our vesicles are prone to leakage in the flow system developed.

3.2.2 Calibrating the autofluorescence on our microscope

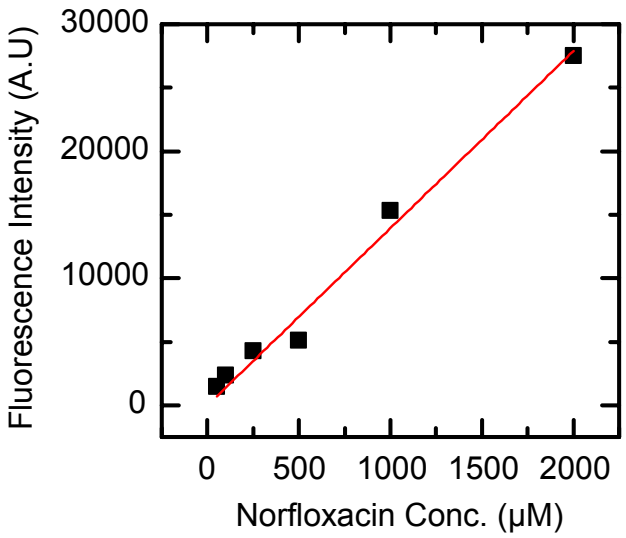

Figure 3.3 – Fluorescence intensity profile of norfloxacin at 340 nm excitation. Camera EM gain 20, 2ms exposure, bin 2, clearing pre-sequence. Published in [13].

To determine the minimum concentration of norfloxacin that could be detected by our camera, we performed a calibration by pipetting droplets of different norfloxacin concentrations (prepared in the pH 7 buffer used in experiments) in between two glass coverslips. The results are shown in Figure 3.3. The droplets were suspended between the two coverslips as measuring the intensity in a droplet simply placed on a single coverslip is susceptible to variation due to the curvature of the droplet. The EM gain was set at 20, to ensure that the intensity histogram peaks were in the middle of the camera range. The minimum concentration of norfloxacin that could be detected (over the background noise) using its autofluorescence at an excitation wavelength of 340 nm was found to be around 50 μM. As expected with an autofluorescent molecule, the fluorescence intensity showed a linear increase with norfloxacin concentration. Furthermore, no self-quenching was observed.

3.2.3 Results of the optofluidic assay

Preliminary single vesicle experiments implied that the time scale of norfloxacin diffusion through DPhPC vesicle membranes was on the order of a few minutes at pH 7. Furthermore, microfluidics experiments revealed a vesicle speed of 0.8-1 mm/s to be the optimum for detection in our system. Based on these considerations, we designed the 'Long' chip as a network of microfluidic channels which the vesicles would take around 5-6 minutes to traverse and used this device for the norfloxacin-DPhPC measurements.

To assess the diffusion through the membrane, we measure the intensity within the vesicles at different points in the chip. Figure 3.4 shows data for vesicles at pH 5 and pH 7. The microscopy images show vesicles (dark) in the microfluidic channels at different points, surrounded by the autofluorescing norfloxacin. Data is shown for two lengths travelled, $L = 45.5$ mm and $L = 182$ mm; data for other lengths is presented in Figure 3.5. From the images it is clear that vesicles at pH 5 remain dark as they travel through the network, whereas at pH 7 they become progressively brighter. At pH 7, as the length travelled increases, I_{in} increases and there is a corresponding decrease in ΔI. Almost no significant change is observed at pH 5 (green triangles). Thus the autofluorescing norfloxacin permeates the membrane at pH 7 far more readily than at pH 5. The radial dependence of ΔI at $t = 0$ (black squares) occurs since our

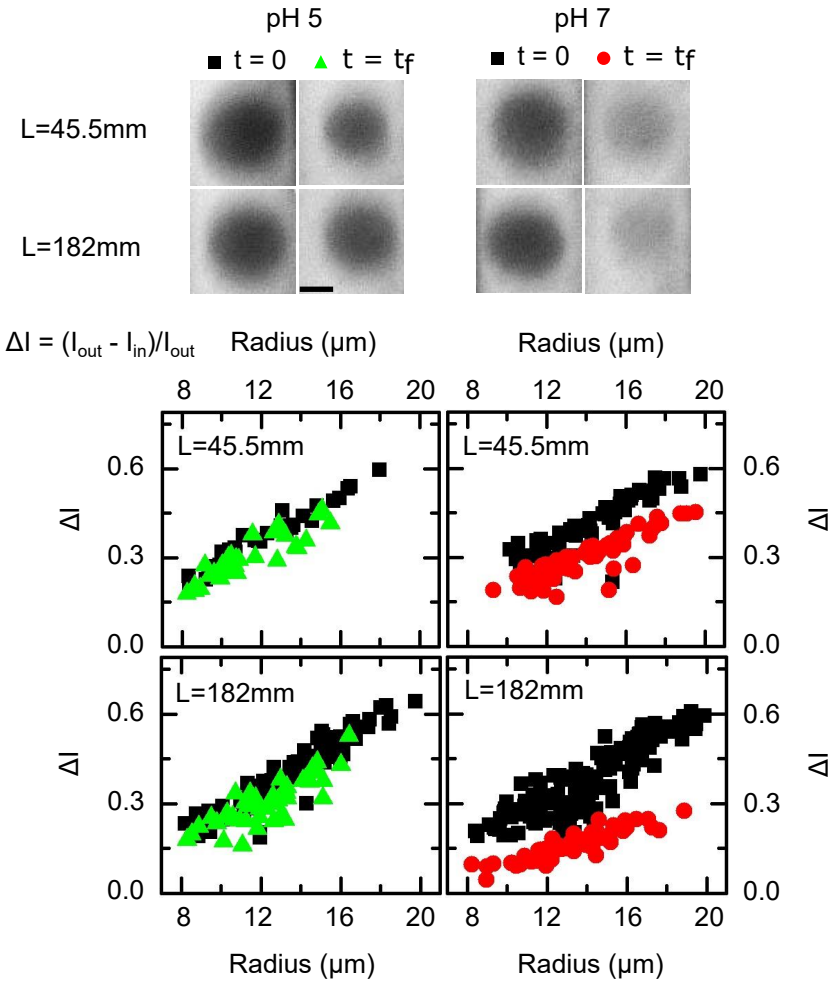

Figure 3.4 – Norfloxacin diffusion into single lipid vesicles. Images of autofluorescent norfloxacin diffusing into vesicles (λ_{ex} = 340 nm) at pH 5 (left) and pH 7 (right). L is the length travelled from the initial ($t = 0$) to the final ($t = t_f$) vesicle detection point. It is evident that there is an increase in the fluorescence intensities inside the vesicles (I_{in}) at pH 7, and a corresponding decrease in ΔI. The decrease in ΔI is proportional to the length (L) travelled, as seen in the plots (the difference between the black and red points becomes larger as L increases). At pH 5, the decrease in ΔI is much less apparent (the green and black points overlap) and I_{in} shows a much smaller increase within the timescales measured. It is thus clear that the permeability of norfloxacin through the lipid bilayer is much higher at pH 7 than at pH 5. Scale bar = 10 μm (in all images). Each data point in the plots represents a measurement on an individual vesicle. Published in [13].

measurements are in brightfield rather than confocal mode; at later times, the radial dependence is both due to this effect as well as due to drug diffusion. This was addressed in the analysis in the previous chapter section 2.3.5.

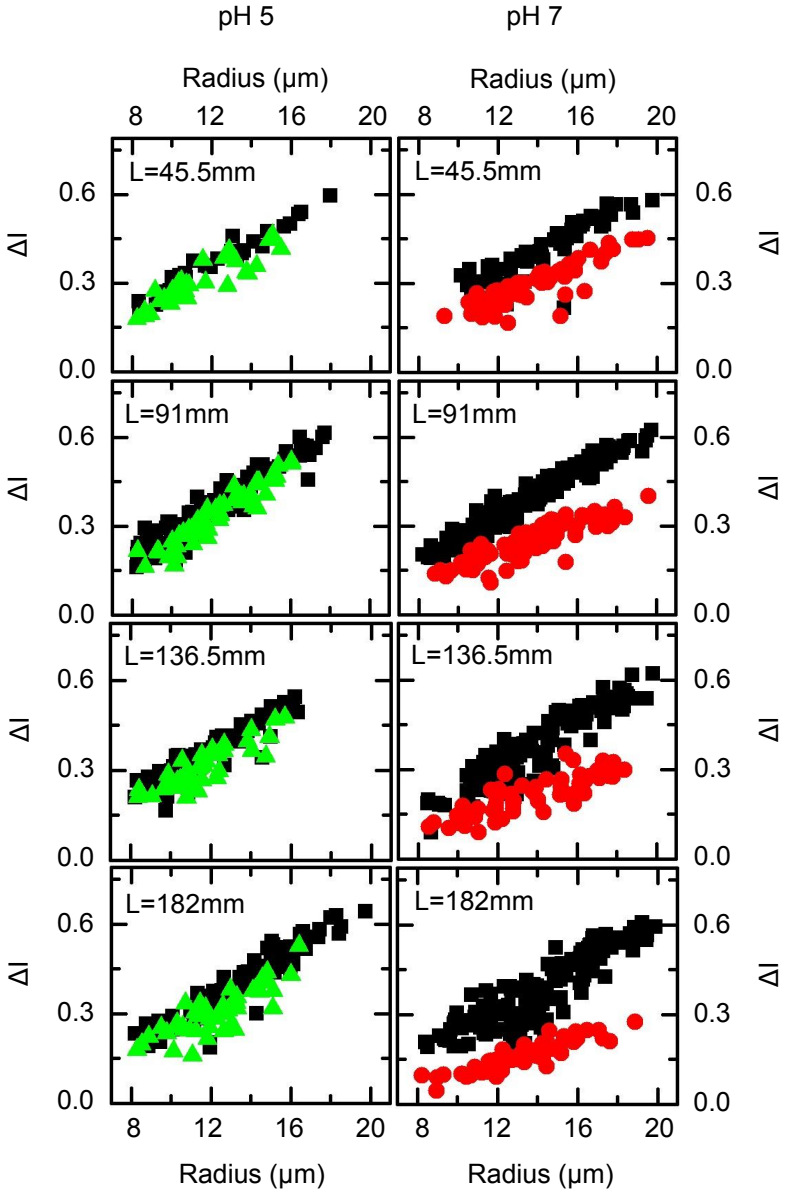

Figure 3.5 – Data shows that as the length travelled by the vesicles increases, $I_{in} \rightarrow I_{out}$ at pH 7 (ΔI decreases), showing that the drug is diffusing across the lipid membrane. This decrease is seen over a much longer time scale at pH 5. Published in [13].

Different Analysis Techniques

Figure 3.6 shows three different techniques used to analyse the data and determine the permeability coefficient of norfloxacin.

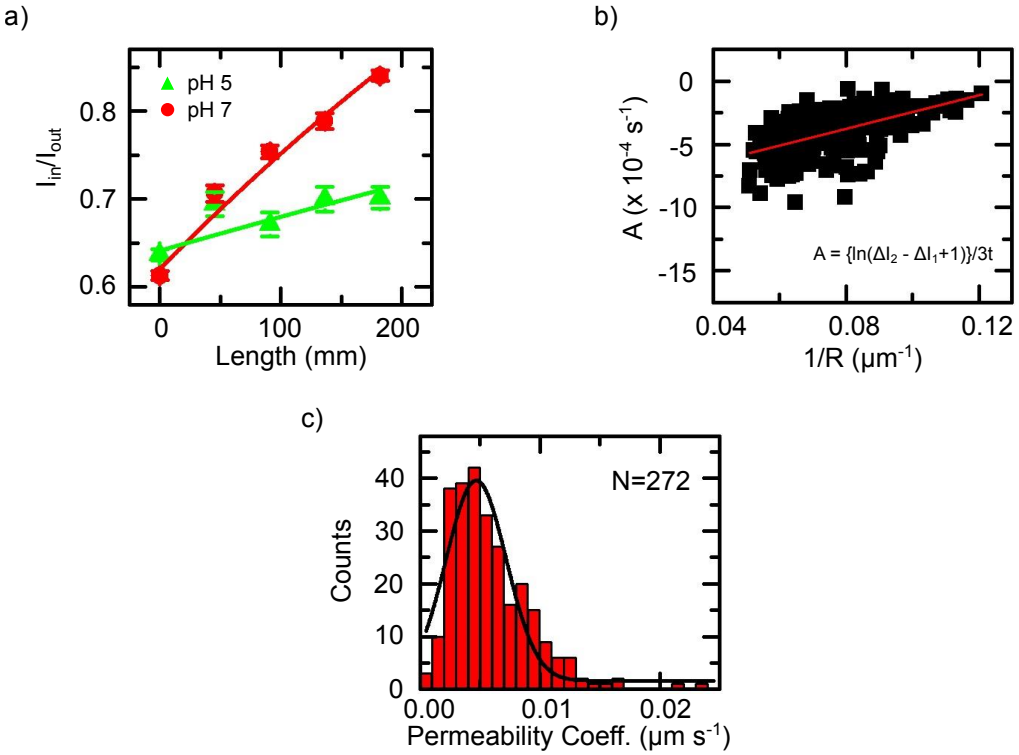

Figure 3.6 – Measurements of the permeability coefficient (P). **a)** Dependence of I_{in}/I_{out} with respect to the length L travelled by vesicles from the initial to the final detection point. The solid lines are fits based on our theoretical expectation of a diffusive process governing the transport of norfloxacin across lipid membranes. Error bars represent standard errors of the mean. From the fit, we have extracted $P = 5.2 \pm 0.4 \times 10^{-7}$ cm/s at pH 7. **b)** Dependence of parameter A (defined in the figure) on $1/R$. The slope of the linear fit gives us another technique of determining P. The value obtained (pH 7) was $P = 6.6 \pm 0.6 \times 10^{-7}$ cm/s. **c)** Histogram of P values for individual vesicles. Values determined using equation (2.15). The average value of these single vesicle calculations gives $P = 5.9 \pm 0.2 \times 10^{-7}$ cm/s (N = 272). All reported values are mean ± s.e. Published in [13].

The intensity within the vesicles (Figure 3.6(a)) increases as the length travelled in the presence of the drug increases. We can use this trend to extract P. Let us first rearrange our permeability equation (2.15) as follows:

$$\frac{I_{(t)}}{I_{out}} = 1 + \frac{I_{(0)}}{I_{out}} - \exp\left(-\frac{3Pt}{R}\right) \tag{3.1}$$

To make this consistent with the length dependence shown in Figure 3.6, we can explicitly relate the time (t) to the length (L) using the average velocity (v_a) of the vesicles. Further, since we defined $I_{(0)} = I_{in}$ (L=0, t=0) = F and $I_{(t)} = I_{in}$ (L=L, t=t_f) in section 2.3.5, we can write:

$$\frac{I_{in}(L)}{I_{out}(L)} = 1 + \frac{I_{in}(0)}{I_{out}(0)} - \exp\left(-\frac{3PL}{v_a.R_a}\right) \tag{3.2}$$

where R_a is the average radius of the vesicles. Though I_{out} $(L) \sim I_{out}$ (0), they have been written out explicitly since we measured the background intensities at both points.

Since the transport process is diffusive, we expect to see an exponential dependence of I_{in} on time (and hence length L). This analysis requires values of vesicle velocity and radius, for which the average velocity (0.81 ± 0.01 mm/s) and average radius (13.6 ± 0.1 μm) measured (pH 7) were used. Using these and the data from the exponential fit, we obtain a permeability coefficient (pH 7) of P = 5.2 ± 0.4×10^{-7} cm/s.

Furthermore, since we determine the flow speed for each vesicle, we can calculate the time taken by each vesicle to travel the length L from the initial to the final detection point. Collating this with our measurements of ΔI and the radius of each vesicle, we know all the parameters required to determine the permeability coefficients for each vesicle detected using the permeability equation (2.15). Histograms of these values for the pH 7 experiments are shown in Figure 3.6(c). The average permeability coefficient determined is P = 5.9 ± 0.2×10^{-7} cm/s (N = 272). Finally, we can use the same equation to determine the permeability coefficient (pH 7) from the slope of Figure 3.6(b). This gives P = 6.6 ± 0.6×10^{-7} cm/s. All values reported are mean ± s.e. Thus there is good agreement using all three analysis techniques.

At pH 5, the majority of the norfloxacin molecules are positively charged, but at pH 7 a significant proportion of the molecules exist in their uncharged form [72]. As indicated in the figures, it is clear that at pH 5 fewer norfloxacin molecules permeate the membrane. This is as expected, since polar charged molecules have a low affinity for the non-polar core of the bilayer. This also means that the SNR for the pH 5 data is too

low to allow the calculation of the permeability coefficient on the single vesicle level accurately. We can estimate the permeability, however, from the trend in Figure 3.6 (a). From our data we estimate a permeability coefficient of 0.5-1.5 $\times$ 10^{-7} cm/s at pH 5, a 6-fold decrease as compared to pH 7. This also confirms that our vesicles are indeed a stable model system not susceptible to leakage.

With fluoroquinolones there is significant discrepancy among the published values of apparent partition coefficients, and hence in the predicted permeability coefficients [28]. Apparent partition coefficients for norfloxacin have been reported as 0 (pH 7) [74], 0.003 (pH 7.2) [72] and 0.01 (pH 7.2) [25], which would imply a permeability coefficient ranging from 0 to around 10^{-5} cm/s. Importantly, our method does not require knowledge of the partition coefficient; we provide a direct measurement of the permeability coefficient, and the values we obtain are well within the range predicted in the literature [72].

We have described three ways of analysing our data to obtain the permeability coefficient, to show that the norfloxacin diffusion is correctly predicted by solving our diffusion equation model. Two of these techniques involve averaging over the properties of all the vesicles and were only described to show that our model works. One of the advantages of this technique is that single vesicles can be detected, analysed and their norfloxacin permeability determined – the value of each vesicle's permeability measurement is depicted in the histogram in Figure 3.6(c) above. Thus for the rest of this Thesis, we shall describe our results only in terms of the permeability coefficients measured on the single vesicle level, as in the histogram above. Furthermore, since we shall not need to discuss the length dependence further, we shall translate all future length dependencies into time dependencies using the vesicle velocities measured.

The microfluidic flows do not affect the permeability measurement

To study any potential effect of hydrodynamics or vesicle shear on the determination of the permeability coefficient (P), we have plotted the values of P obtained (at pH 7) for individual vesicles against the corresponding vesicle velocities in Figure 3.7. This includes preliminary measurements performed on stationary vesicles (N=7) in a confocal microscope (λ_{ex} = 351 nm, red circles in Figure 3.7 – the confocal measurements

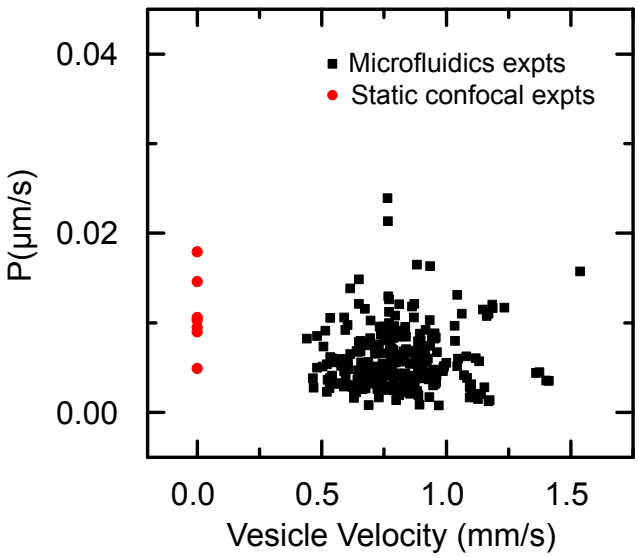

Figure 3.7 – Plot of permeability coefficient (P) against vesicle velocity. No significant dependence is seen, indicating that hydrodynamic effects do not significantly influence the permeation of norfloxacin in our microfluidic environment at the relevant flow velocities. Published in [13].

were performed by Dr. Catalin Chimerel [60]). It is clear from the plot that there is no influence of vesicle velocity on the permeability coefficient at the relevant flow velocities. If there were indeed an influence of hydrodynamics on drug permeation, one would have expected to see a dependence of P on the vesicle velocity. We therefore believe our technique and analysis to be robust in the microfluidic regime. We reiterate here that we define a strict circularity condition to ensure that we perform the permeability analysis only on vesicles that are suitably circular, and thus reject vesicles that are damaged by shear. Besides the circularity condition, vesicles of diameters larger than the channel width are rejected before analysis, since these are more susceptible to shear and rupture due to contact with the channel walls. Furthermore, we are also capable of checking the vesicles manually by viewing the raw images of vesicle detection events. These are used to reject the few out-of-focus events that evaded our strict applicability criteria.

Summary

We have thus validated our technique of measuring the permeability coefficient of drugs passively diffusing across lipid membranes. In contrast to previously described methods, we do not require any labelling or chemical complex formation in order to track the drug molecules. We further do not need to determine the drug partition coefficients in artificial aqueous-organic phase systems; we directly obtain the permeability coefficient across the membrane of interest, which is the quantity required when designing and testing new drugs.

The rest of this chapter will describe the results obtained when applying this permeability assay to a range of systems.

3.3 Changing the lipid composition affects norfloxacin permeability

Now that we have a technique to quantify the permeability of drugs across membranes, it makes sense to investigate what factors affect the permeability. One of the first variables we decided to investigate was the lipid composition. Our earlier measurements were performed using DPhPC lipid vesicles. We decided to investigate another type of PC lipid, DOPC (1,2-dioleoyl-*sn*-glycero-3-phosphocholine), which has the same headgroup as DPhPC but a different chain structure. We observe that even lipids from the same lipid 'family' can have dramatically different drug permeabilities.

3.3.1 Norfloxacin transport through DOPC lipids[1]

To study the effect of changing the lipid composition on the permeation properties of norfloxacin, we performed our optofluidic assay using DOPC vesicles. The DOPC stock used was obtained from Sigma Aldrich. The vesicles were prepared in exactly the same manner as for the earlier DPhPC experiments, in 200 mM sucrose in pH 7 phosphate buffer.

[1]The results from this section have been submitted for publication as a journal article.

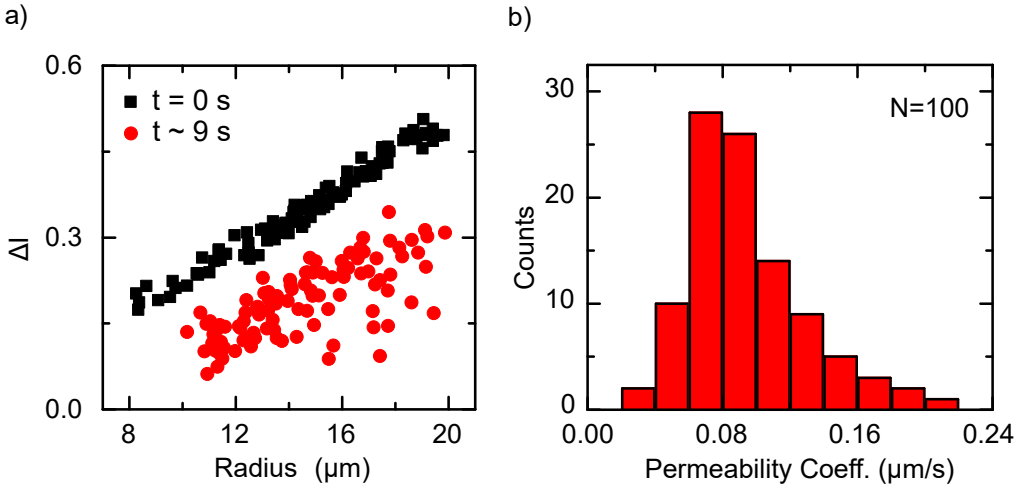

Figure 3.8 – Norfloxacin transport through DOPC vesicles at pH 7. **a)** Scatter plot showing the rapid uptake of norfloxacin into DOPC vesicles. The black squares reference vesicles at the initial detection point and the red circles reference vesicles at the later detection point, about 9 s further downstream. The scatter plot shows a considerable shift in ΔI within just a few seconds of the vesicles being exposed to norfloxacin. Drug uptake is thus much faster in DOPC vesicles compared to the corresponding DPhPC experiments (Figure 3.5). **b)** The permeability coefficient histograms reflect this greater permeability of DOPC membranes to norfloxacin. The average value of P was determined to be $9.4 \pm 0.4 \times 10^{-6}$cm/s (N = 100, mean ± s.e), a 15-fold increase in permeability compared to DPhPC vesicles.

However, while performing the experiment it immediately became apparent that norfloxacin transport through DOPC was much faster than through DPhPC lipid membranes. This was surprising, considering that both lipids are from the same lipid family and differ only in the structure of their hydrocarbon tails (Figure 3.9). We therefore had to view the vesicles within a few seconds post mixing with the drug; if we had viewed the vesicles at the longer timescales used for the DPhPC experiments, there would have been too little contrast in intensity between the vesicles and the background since too much of the autofluorescent drug would have been present within the vesicles. Hence for all fast permeation experiments, we used the 'Short' microfluidic chip (appendix B). In this chip design, the initial viewing point ($t = 0$) is immediately after the drug and vesicles mix at the T junction. The $t = 0$ point is chosen to be the earliest point at which the norfloxacin diffuses across the entire width of the channel (as observed by measuring the norfloxacin autofluorescence intensity profile within the channel) at

the flow rates used in the experiment (3-4 μl/hr). The corresponding detection point further downstream that falls in the same field of view is at a distance of 7.4 mm further along the channel. The DOPC vesicles took, on average, 9 ± 1 seconds (mean ± s.d) to traverse this distance.

The results are displayed in Figure 3.8. The measurements were performed at pH 7, in order to compare the permeability coefficient of DOPC with the DPhPC experiments at the same pH. The scatter plot (a) immediately tells us that norfloxacin diffuses across the DOPC bilayer much faster – we see a shift in ΔI within a time period of 9 seconds which is comparable to the corresponding shift in ΔI in the DPhPC experiments over a period of minutes.

This increase in permeability is reflected in the histograms (b) referencing the permeability coefficient of the individual DOPC vesicles in the experiment. The average value of the permeability coefficient (P) is determined to be $9.4 \pm 0.4 \times 10^{-6}$cm/s (N = 100, mean ± s.e). Thus the permeability of the DOPC lipid bilayer to norfloxacin is approximately 15× the corresponding permeability of the DPhPC bilayer. This is remarkable, considering the fact that both DPhPC and DOPC are PC lipids containing the same headgroup. They only differ in the structure of their hydrocarbon chains, and naïvely one would expect the solubility of norfloxacin in the hydrocarbon tails to be similar.

3.3.2 Why is permeation through DOPC faster?

The first thing to question was whether the 340 nm UV radiation damaged the DOPC membrane – the unsaturated double bonds (Figure 3.9) in the hydrocarbon chain could have been sensitive to oxidation due to UV exposure. However, when experiments were performed with DOPC vesicles at pH 5 (by Dr. S. Purushothaman, a post-doctoral researcher in the group), norfloxacin permeability retreated to the levels observed in the DPhPC pH 5 experiments. If UV induced oxidation was a problem, the pH 5 vesicles should also have been permeable to the drug. Since this was ruled out, we had to look into some lipid chemistry to try and understand the difference.

Investigations into the permeability of small molecules (such as water) across different lipid membranes have been performed by using X-ray scattering techniques to study,

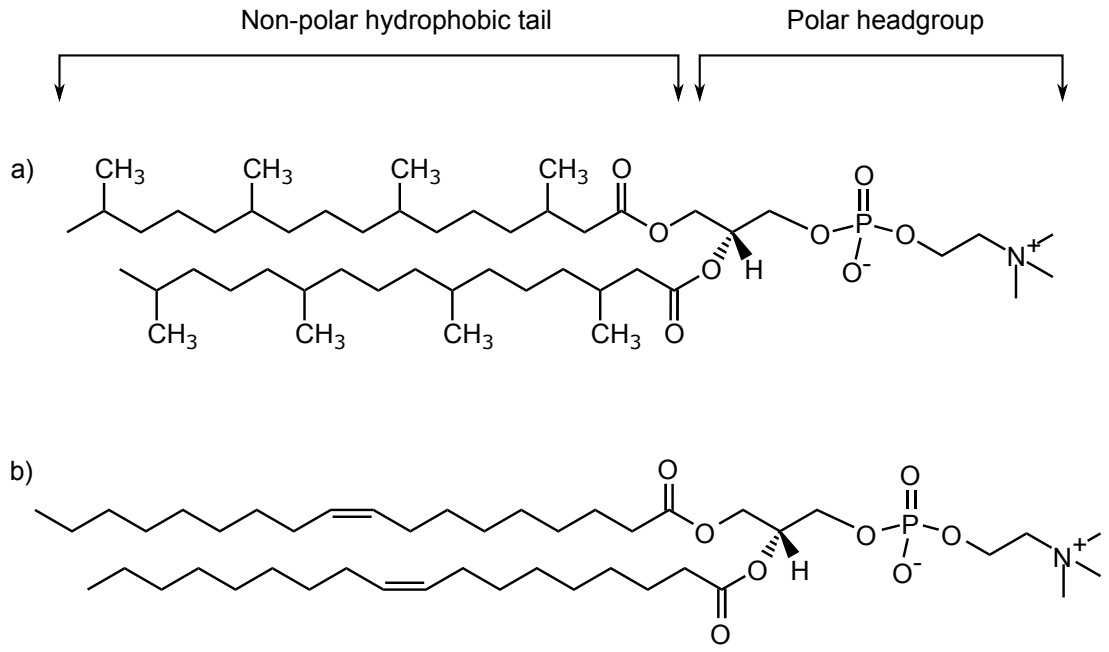

Figure 3.9 – Chemical structures of: **a)** DPhPC and **b)** DOPC lipid molecules. DPhPC has highly branched chains, whereas DOPC has unsaturations (double bonds) in both chains. Source: www.avantilipids.com

quantitatively, different lipid molecules. One such recent study, by Mathai and coworkers [75], suggested that the water permeability of a lipid bilayer correlated well with the **area per lipid** of each molecule. The average interfacial area per lipid molecule value is a quantity used to describe the bilayer microstructure with reference to molecular packing; it is defined in reference to the average hydrocarbon thickness and the hydrocarbon chain volume [76]. Mathai and coworkers found that the water permeability of lipid bilayers correlated only with this Area/Lipid quantity, and not with the hydrocarbon thickness, bending modulus nor with the compressibility modulus. They investigated a number of different lipid types, but importantly did not investigate DPhPC.

Now, the area per lipid of DOPC was measured to be 72.4 $\pm$ 0.5 Å^2 [75]. A couple of years later, the same group discovered a problem. They had decided to investigate the properties of DPhPC, and found that although its area per lipid value was considerably larger (80.5 $\pm$ 1.5 Å^2) than that of DOPC, it had a much smaller water permeability [77]. However, molecular dynamics (MD) studies had been performed previously [78] comparing the free volume distribution in the hydrophobic

part of the (branched) DPhPC molecule and its straight chain counterpart DPPC (1,2-dipalmitoyl-*sn*-glycero-3-phosphocholine). The simulations showed that the branched chains present in DPhPC reduced the free volume available in the hydrophobic region of the molecule, thus lowering the rate of diffusion of small molecules such as water [78]. They thus concluded that when lipid molecules have branched chains, the permeability to small neutral molecules is reduced.

This work led Tristram-Nagle and coworkers [77] to postulate that the biophysics of DPhPC is substantially different to other straight chain PC lipids, and that this chain branching is the cause of the reduced water permeability when compared with DOPC. This explanation also accounts well for our results. As our pH dependent measurements have shown, it is the neutral form of norfloxacin that translocates across the lipid bilayer, and this small, neutral molecule shows similar permeability characteristics to water when comparing DPhPC and DOPC lipids.

Perhaps more importantly, however, this example demonstrates precisely why it is important to perform drug permeability studies directly on the lipid system of interest. On the face of it, DPhPC and DOPC are both PC lipids with the same headgroup, differing only in the structure of their hydrocarbon chains. However, that very difference in chain structure leads to a 15-fold difference in norfloxacin permeability across membranes of the two lipid types. Real cell membranes are highly dynamic; bacteria in particular are known to change their lipid composition depending on their growth conditions [17]. It should also come as no surprise that they can change their lipid composition in response to antibiotic stress; significant changes in lipid structure were observed when comparing lipids from antibiotic resistant versus sensitive bacteria grown under identical conditions [79]. It is imperative that future drug development processes take this lipid dependence into account. At present, other group members are using the optofluidic assay to investigate the drug permeability of the different types of lipids found in *E. coli* membranes in an attempt to understand what lipid composition a bacteria might adopt to reduce antibiotic accumulation.

3.4 Tetracycline transport

In order to demonstrate that our technique is capable of studying antibiotics other than those of the fluoroquinolone family, we used it to study the permeability of tetracycline across DPhPC vesicle membranes. For ease of comparison with the norfloxacin measurements and for physiological relevance, we again performed the measurements at pH 7.

3.4.1 Tetracycline

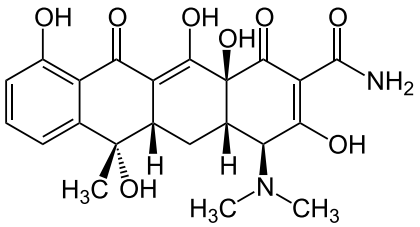

Figure 3.10 – Tetracycline chemical structure. Source: www.wikipedia.org

Tetracyclines were amongst the first antibiotics to be discovered, back in the 1940s. They are broad spectrum antibiotics that function against both Gram-positive and Gram-negative bacteria, as well as acting against a range of other aerobic and anaerobic microorganisms. Their mechanism of action involves the inhibition of protein synthesis; this is achieved by preventing the attachment of the aminoacyl-tRNA to the ribosomal acceptor (A) site [80]. Tetracycline remains an extremely important antibacterial, named on the World Health Organization's list of essential medicines [81]. However, as with all older antibiotics, many human pathogens are now resistant to the drug, and efforts are ongoing to better understand the molecular mechanisms of resistance [80].

Tetracycline has three proton-binding groups with macroscopic pK_a values of approximately 3.3, 7.7 and 9.7 in aqueous solutions [82]. As with norfloxacin, a study of the microscopic dissociation constants reveals that, at physiological pH values (pH 7.4), a significant fraction ($\sim$7%) of the tetracycline molecules exist in an uncharged form

[72, 82] and it is expected that this uncharged fraction contributes most to the passive diffusion of the drug across lipid bilayers.

Tetracycline fluorescence is well known, though not all that well understood [83]. It shows autofluorescence in the near UV at excitation wavelengths of around 360-365 nm. Its autofluorescence is weaker than that of norfloxacin, which is why we had to use higher concentrations of the drug (8 mM). The fluorescence intensity increases when the drug chelates divalent metal ions such as Ca^{2+} or Mg^{2+} [83], but we refrained from using these since we wanted to determine the permeability coefficient of pure tetracycline across the lipid bilayer. Needless to say, biologists interested in studying the membrane transport of metal ion chelated antibiotics can use the assay to determine how metal ion chelation affects drug transport.

Before discussing the results, a small technical point – we found it difficult to produce a stable stock solution of tetracycline (Sigma Aldrich) in water, and therefore dissolved it in ethanol before diluting it to 8 mM in the (aqueous) buffers used for the experiment. To keep the properties of the two solutions being mixed constant, an equivalent amount of ethanol was added to the vesicle solution. This helps ensure that the microfluidic flow profiles from the two inlets are similar (i.e, the fluidic resistances are the same), and is recommended when performing the assay with tetracycline.

3.4.2 Tetracycline transport across DPhPC bilayers

DPhPC vesicles were produced using the same protocols as before, prepared in the pH 7 phosphate buffer containing 200 mM sucrose (section 2.3.3). As with the norfloxacin-DOPC measurements, it was noticed in preliminary experiments that tetracycline transport was significantly faster than norfloxacin across DPhPC membranes, and therefore the 'Short' microfluidic chip (appendix B) was employed for these measurements.

The results are shown in Figure 3.11. We looked at two viewing positions (and hence 4 different spatial locations) along the channel in our microfluidic chip. The first viewing point was the same as that used in the DOPC measurements – the $t = 0$ point chosen was the earliest point post vesicle-drug mixing where the tetracycline had diffused across the channel width. The other point in the same field of view was 7.4 mm further downstream along the channel. The second viewing position contained

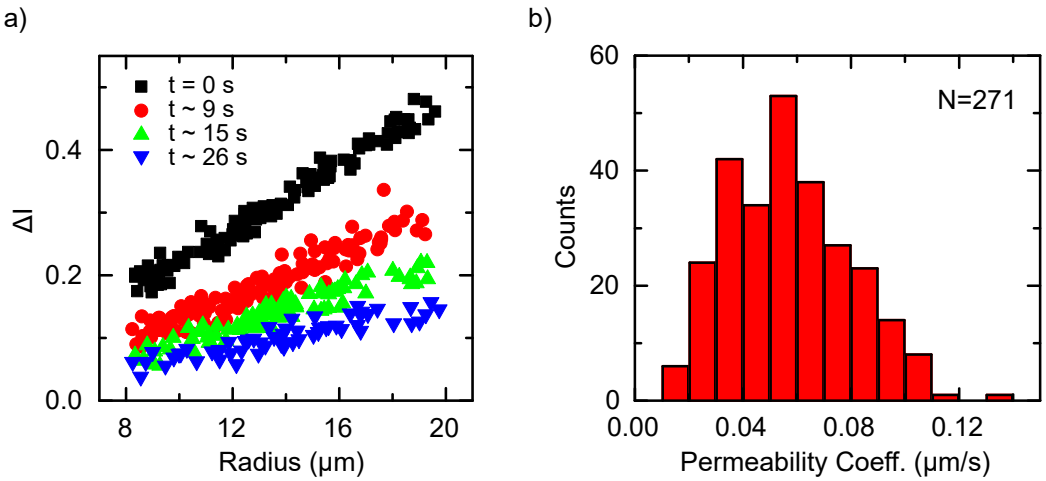

Figure 3.11 – Tetracycline transport through DPhPC vesicles at pH 7. Excitation wavelength λ_{ex} = 360 nm. **a)** The scatter plot shows the decrease in ΔI as the time of vesicle exposure to the drug increases. The different time points clearly correspond to different bands in the scatter plot, providing direct visualisation of drug uptake. The timescales involved show that tetracycline transport through DPhPC bilayers is significantly faster than norfloxacin transport. **b)** Permeability coefficient histogram representing individual vesicle measurements. The average value of P was found to be 5.7 ± 0.1×10^{-6}cm/s (N=271 events, mean ± s.e). Thus tetracycline permeability is an order of magnitude higher than norfloxacin at pH 7.

detection points at 11.7 mm and 19.5 mm respectively after the $t = 0$ position. On average, vesicles took 9 ± 1 seconds to the first (7.4 mm) point, 15 ± 2 seconds to the second (11.7 mm) position and 26 ± 3 seconds (all values are mean ± s.d) to reach the final detection point (19.5 mm). It must be noted here that there is some redundancy in vesicle detections, since the vesicles whose permeability was measured at the 11.7 mm point include most of those whose permeability was measured at the 19.5 mm point, since both positions were recorded simultaneously.

The uptake of tetracycline is beautifully visualised in the scatter plot of Figure 3.11 (a). As the distance travelled along the chip by the vesicles (and hence the time spent exposed to the drug) increases, the internal tetracycline fluorescence increases and ΔI decreases. The shift in ΔI from one detection point to the next is unambiguous and clear. The histogram (b) of the permeability coefficients for the vesicle detections also behaves as expected, and on average P = 5.7 ± 0.1×10^{-6}cm/s (N=271 events, mean ± s.e). This shows excellent agreement with the permeability coefficient of 6 × 10^{-6}cm/s

predicted [72] for the passive diffusion of tetracycline through typical biological membranes (at a pH of 7.2). This prediction was based on the fact that the protonation of the tetracycline molecule leads to approximately 7% of the molecules being uncharged at a pH of 7.2, which itself is based on considerations of the microscopic dissociation constants that govern the acid-base equilibria of tetracycline [72, 82]. This further emphasises the importance of studying the pH dependent protonation states of drug molecules and their effect on the lipid permeability of the drug. Our optofluidic assay provides an ideal platform for performing these tests on a range of different drug and lipid combinations.

We have thus shown that our assay is applicable to different classes of drugs. As a first iteration, it could be used to study the permeation properties of different molecules from the fluoroquinolone and tetracycline families, and there are many such molecules to investigate. But perhaps more importantly, it could be used to replace existing assays when testing the lipid permeation of new drugs; it would be most satisfying if this technique eventually gets used in the drug discovery process.

3.5 Interaction of Quantum Dots with lipid membranes

To demonstrate the versatility of our technique, we now apply it to the study of a completely different field – the interaction of Quantum Dots with lipid membranes.

3.5.1 Quantum Dots in Biology

Quantum Dots (QDs) are spherical nanocrystals with diameters in the range of 1-10 nm [84, 85]. They are typically made of semiconductor materials, since it was noticed that the optical and electronic properties of these materials at the nanoscale were strongly dependent on particle diameter [85]. The strong size dependence of these properties arises due to two major reasons [84]: firstly, the number of surface atoms in a nanocrystal is a large fraction of the total. These surface atoms make a significant contribution to the free energy, and hence control the thermodynamic properties of the material. The number of surface atoms depends on the size of the nanocrystal, and hence changing the diameter can have a dramatic bearing on the properties of the QD. Secondly, the

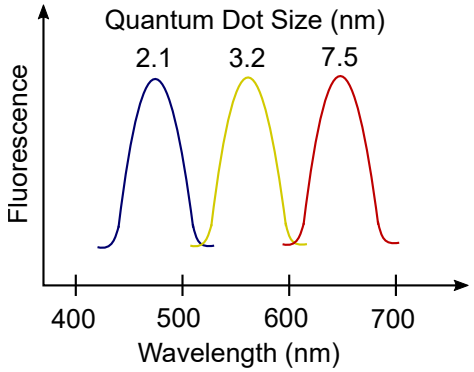

Figure 3.12 – The emission wavelength of a CdSe Quantum Dot can be tuned in the visible region of the spectrum by changing its diameter between 2 and 7.5 nm. Image adapted from [85].

intrinsic properties of the interior of nanocrystals are governed by quantum size effects, which alter the electronic properties of the material on the basis of its diameter.

One of the most important properties that is controlled by tuning the size of the QD is the wavelength of its fluorescence emission (Figure 3.12). QDs absorb strongly in the UV, but by changing their radius and chemical composition, their emission wavelengths can be made to span an extremely wide range, from 400-2000 nm [85–89]. For example, the emission of a Cadmium Selenide (CdSe) QD can be tuned between 450-650 nm within the visible spectrum by varying the nanoparticle diameter between 2 and 7.5 nm [85].

This is of obvious interest from an imaging and labelling perspective – if one were to use QDs with a range of radii to label specific biomolecules within a cell, one could excite all their fluorescence using the same light source, and each species would emit at a different wavelength. Furthermore, current techniques for the chemical synthesis of QDs allow for excellent control over the mean particle size and particle size distribution, enabling the production of QDs with narrow, symmetric emission peaks and spectral properties far better than that of typical organic dye molecules [85].

These properties thus sparked a flurry of research activity aimed at making QDs viable for use with cells. In 1998, the research groups of Alivisatos and Nie independently achieved this feat. Alivisatos and coworkers demonstrated the use of these nanocrystals as fluorescent markers for investigating mouse fibroblasts, using a dual emission, single

excitation labelling experiment [90]. Nie and Chan used Zinc Sulphide coated CdSe QDs and covalently attached these to biomolecules for ultra-sensitive biological detection [91]. They claimed that this class of fluorescent probes was "20 times as bright, 100 times as stable against photobleaching, and one-third as wide in spectral linewidth" as compared to standard organic dyes. These ZnS-CdSe conjugates were also water soluble and biocompatible [91]. The QDs were attached to the transporter protein transferrin and taken up by HeLa cells via receptor-mediated endocytosis. Within the cells, the QDs were used to recognize specific antibodies or antigens [91].

Since then, considerable research has gone into developing QDs as probes to detect, for example, cancer markers in live tumour cells [92], for multicolour optical coding in bioassays [93], for single particle tracking within a live cell [94] – the list is extensive. Furthermore, these probes have been used for live animal imaging, in the hope of developing novel imaging techniques for the early detection of cancer and other diseases [95]. There is thus tremendous scope for this technology; it has the capacity to truly revolutionize medical diagnostics. But, as always, there is a catch.

3.5.2 Quantum Dot Cytotoxicity

The spectral characteristics of QDs might be fantastic, but the fact remains that the most commonly used QDs, especially those used for biological applications, have CdSe as their core material. Cadmium is a notorious heavy metal, linked with all sorts of undesirable health effects, from renal failure to cancer [96]. It is a Red List chemical and its use and disposal are tightly regulated.

It is thus natural that concerns were raised regarding the use of cadmium in the core of QDs [97–100]. Studies revealed that the main source of cytotoxicity was the release of Cd^{2+} ions into cells; thus, the development of appropriate surface coatings for the QDs that prevented the release of these ions became a major priority. Comprehensive studies were undertaken to study the effect of various different chemical modifications to the cytotoxicity of the QDs. It was found that a ZnS shell surrounding the CdSe core rendered the QD biocompatible, with little cytotoxicity reported even at high QD concentrations [98, 99].

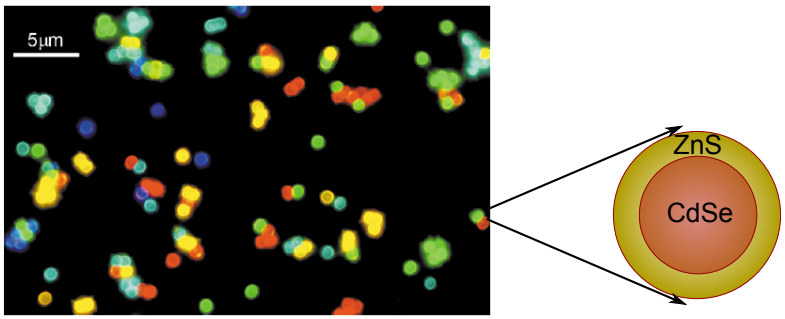

Figure 3.13 – Fluorescence micrograph showing beads labelled with a range of CdSe-ZnS QDs emitting at 484, 508, 547, 575 and 611 nm. Image adapted from [93].

However, before the use of QDs becomes routine for animal and human imaging, longer term studies will have to be performed to ensure that there is no build up of cadmium in the body, and that the risk associated with the use of these QDs is acceptable. Experiments with different coatings (such as Polyethylene glycol) are also being undertaken, in order to reduce the accumulation of these QDs in the liver and kidneys [101].

Interestingly, there is not much in the literature about the interaction of QDs with lipid membranes. One report claims that 12 nm diameter CdSe QDs can form aggregates on lipid bilayers leading to the formation of nanopores with diameters of about 2 nm [102]. Such pores could seriously undermine the integrity of a cellular membrane. We therefore decided to exploit the UV autofluorescence of QDs to investigate their interaction with our DPhPC vesicle lipid bilayers, and to see whether the vesicle membranes ruptured or allowed for the passive transport of these nanoparticles across the lipid barrier.

3.5.3 Interactions with Vesicle membranes

Understanding how QDs interact with and permeate lipid bilayers is important both for investigations into their cytotoxicity, and also for better understanding their use as intracellular fluorescent probes. To this end, our collaborators Dr. Teresa Pellegrino and Dr. Alberto Curcio from the Italian Institute of Technology sent us samples of CdSe-ZnS QDs. The CdSe core had a diameter of approximately 3 nm, surrounded by a ZnS shell. The final QDs had a mean diameter of 4.3 $\pm$ 0.5 nm, with maximum

absorbance in the UV and an emission maximum at 561 nm (when excited at 400 nm). Our goal was to determine whether the QDs were capable of passively diffusing across lipid bilayers within the timescales of our permeability assay.

We performed the experiment with DPhPC lipid vesicles, prepared at pH 7. As usual, vesicles entered from one inlet and the QDs from the other.

The diffusion of QDs across the width of the fluidic channel obviously takes a longer amount of time compared to norfloxacin or other small molecules, so we reverted to using a chip that was based on our initial design, where the two solutions are given ample time to mix (∼20 seconds) before the first ($t = 0$) detection point. To simplify the preliminary experiments, we used a slightly shorter version of the initial design (appendix B 'Medium' chip) which allowed us to view the vesicles over a period of approximately 100 seconds after complete mixing with the QDs.

Rather surprisingly, the UV autofluorescence of the QD sample was quite weak, and higher concentrations of the QDs had to be used than initially expected. The stock QD concentration was 8.49 μM, which was diluted 50 times for use in the experiments. The SNR was therefore not ideal, but we were still able to obtain results. It is possible that some degradation occurred during storage and/or transport, and fresh samples should be obtained for any follow up experiments.

Figure 3.14 shows the results obtained at the longest timescale (t ∼ 101 seconds) viewed. To reiterate, the autofluorescence intensity here is due solely to the presence of QDs in the solution. The majority of the vesicles show no shift in ΔI over the timescales measured, which seems to suggest that the QDs do not permeate across lipid bilayers passively. This is in line with previous reports [91] where the cellular uptake of CdSe-ZnS QDs required functionalization with transferrin for receptor-mediated uptake. We do notice a slight decrease in ΔI for a few (2-3) vesicles, but considering the weak SNR in these experiments, it is likely that these are artefacts or just damaged vesicles. The experiments at shorter timescales gave similar results as expected.

Thus it appears as though CdSe-ZnS QDs require functionalization for their cellular uptake. We are interested in studying the effect of a Polyethylene glycol (PEG) coating, which will reside over the ZnS shell of the QD. PEG is being used to make QDs more biocompatible [101], and it would be interesting to check if it has any effect on the lipid

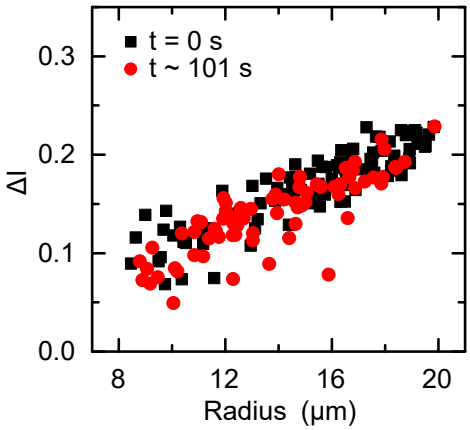

Figure 3.14 – Scatter plot for CdSe QD permeability experiment. λ_{ex} = 350 nm. The black squares represent vesicles at the initial detection point, whereas the red circles reference vesicles detected about 101 s later in the channel. Both populations show almost complete overlap, indicating that no significant QD transport is observed at the timescales measured.

permeability of these QDs. Indeed, with the permeability measurement technique in place, the lipid permeability of a range of different QDs could in principle be tested.

3.6 Conclusions

To summarize the picture thus far, we have applied our newly developed technique, a UV autofluorescence based permeability assay, to study a variety of different problems in membrane transport. We have shown that it can be used, first and foremost, to quantify passive antibiotic diffusion across vesicle lipid membranes, and have demonstrated its feasibility for at least two major classes of antibiotics, the fluoroquinolones and the tetracyclines. We further demonstrated that the assay can be used to study the effect of lipid compositions on drug transport, and reported an order of magnitude difference between the norfloxacin permeability of DPhPC and DOPC lipid membranes. Finally, we showed that the same technique can be applied to transport studies of a completely different type of particle, the Quantum Dot.

Each of these topics – antibiotic diffusion, the effect of lipid composition on drug permeability, the interaction of QDs with lipids – is a distinct field of study in its own right. This is an apt demonstration of the power of technological development – one new assay can be applied to answer a range of biologically relevant questions. And this is just the tip of the iceberg, there are many more questions in membrane transport that remain to be studied. We shall discuss a few current investigations in our Outlook chapter 6 at the end of this Thesis.

For the moment however, we shall turn our attention to the study of nanopores – specifically, the biological protein nanopores that form a vital component of all cell membranes. These protein pores are responsible for controlling the transport of a multitude of molecules, including drugs, across cellular membranes. The following chapter is devoted to the application of our technique for measuring antibiotic transport through bacterial membrane pores.

Chapter 4

Exploring the role of Nanopores in Membrane Transport

> "Everything should be made as simple as possible, but not simpler."
>
> Albert Einstein (*attributed*)

4.1 Introduction[1]

Our focus until now has been on the transport of antibiotics and other particles of interest across a pure phospholipid membrane. However, the structure of biological membranes is far more complex, consisting of a large variety of proteins. These are found both on the surface of the membrane (peripheral membrane proteins, or PMPs) and inside the lipid bilayer (integral membrane proteins, or IMPs). A subset of the IMPs contains proteins that span the length of the lipid bilayer; these *transmembrane* proteins play a vital role in regulating the passage of hydrophilic molecules and ions into cells. These transmembrane protein nanopores are in many cases the route of choice for antibiotics attempting entry into bacterial cells. *Porins* are a subset of these protein nanopores that facilitate transport across the membrane via passive diffusion. This chapter is devoted primarily to the study of one particular porin, the *E. coli* Outer

[1] We published the work presented in this chapter in reference [103].

Membrane Protein F (OmpF); its role in fluoroquinolone transport is investigated at physiological pH values. Microfluidics and electrophysiology are combined to obtain a detailed understanding of the mechanisms of fluoroquinolone uptake in *E. coli*, in particular explaining previously measured pH dependencies in the uptake process. Results from the OmpF transport studies are correlated with results from the previous chapter to provide a quantitative understanding of norfloxacin transport across both the *E. coli* outer and inner membrane, in a manner not accessible to previously available technologies.

4.1.1 The Outer Membrane of the Gram-negative Cell Wall

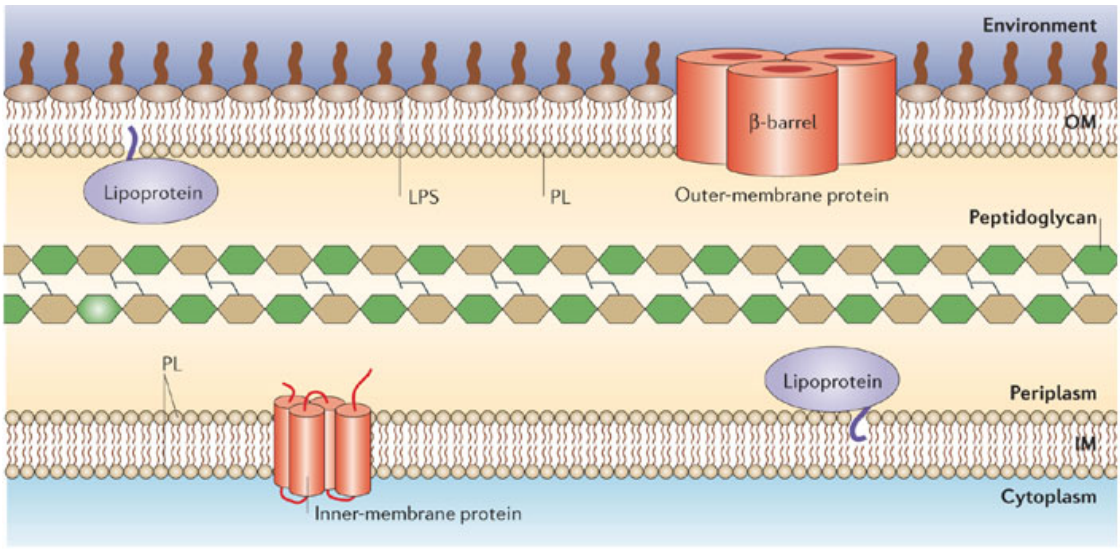

Figure 4.1 – Schematic of the *E. coli* cell envelope showing the double membrane cell wall. The outer membrane (OM) is an asymmetric membrane with phospholipids (PL) in its inner leaflet and lipopolysaccharides (LPS) in its outer leaflet. The OM also contains barrel shaped protein porins, such as OmpF. The periplasm, an aqueous compartment between the two lipid membranes, contains the peptidoglycan layer. The inner cytoplasmic membrane (IM) is a symmetric phospholipid bilayer which also contains various integral membrane proteins. Image taken from [104].

Gram-negative bacteria such as *E. coli* are characterised by the presence of a double membrane cell wall (Figure 4.1). There are thus two hydrophobic barriers that a drug must overcome in order to enter the cell cytoplasm, generally the location of antibi-

otic targets. The outer membrane (OM) is separated from the inner "cytoplasmic" membrane by a periplasmic space containing a peptidoglycan layer. In most Gram-negatives, the OM is an asymmetric bilayer of phospholipids and lipopolysaccharides (LPS) [105]. LPS molecules generally consist of a hydrophobic domain known as lipid A (or "endotoxin"), a non-repeating "core" oligosaccharide and a distal polysaccharide (or O-antigen) [106]. The strong lateral interactions between LPS molecules and their low fluidity make the asymmetric OM much more hydrophobic than a typical phospholipid bilayer [105]. In fact, such is the level of interaction that the core region of LPS provides a strong barrier against the entry of even certain hydrophobic antibiotics; pure phospholipid membranes are much more permeable to lipophilic compounds [105]. Transmembrane porins found in the OM are thus the main port of entry for most extracellular molecules entering the cell. These porins are generally water filled channels, and the narrowest constriction in the porin determines the maximum solute size that can pass through it [107, 108].

Before moving on to a detailed description of the OmpF porin, we must mention here an important physical property of these bacterial membranes. There exists an electrical potential across the cytoplasmic membrane, $\Delta\psi$, which is negative inside the cell relative to the outside. A combination of this potential and a pH gradient (ΔpH) across the cytoplasmic membrane gives rise to a Proton Motive Force (PMF), an electrochemical gradient of protons across the membrane that is crucial for the metabolism of the cell [109]. Given its obvious importance, this electrical property of the cytoplasmic membrane has been extensively studied and will not be described in further detail here. Of more interest to our study of porins is the existence of potentials across the OM, and it is to these that we now turn our attention.

In 1973, the discovery of a new *E. coli* cell constituent, the membrane-derived oligosaccharide (MDO) was reported [110]. These oligosaccharides consist of about 8-10 glucose units/mol in a highly branched structure, and are variously substituted with *sn*-1-phosphoglycerol and phosphoethanolamine residues that derive from membrane phospholipids (hence the name) [111]. These MDO molecules are localized to the periplasmic space of *E. coli* [112], and their synthesis plays a crucial role in the osmoregulation of *E. coli* [111]. However, our interest in them stems from the fact that these molecules are highly anionic; on average each MDO molecule contains a total net negative charge

of 5 [111]. This negative charge anchored in the periplasm leads to the development of Donnan potentials across the *E. coli* outer membrane. The magnitude of this Donnan potential is highly dependent on the cation concentration of the medium surrounding the bacterium; potentials in the range of about 5-100 mV have been measured as a result of varying the external cation concentrations [113]. In the presence of typical physiological ion concentrations, the magnitude of this potential is in the region of 20-30 mV [113].

Thus it is apparent that the OmpF porin resides in a landscape with an electrical potential that can vary over a large range; one would expect that these electric fields influence the transport of compounds through the porin. One would also expect such effects to be intricately related to the charge of the compound attempting to pass through the porin. Building on the work presented in chapter 3, we investigate how the pH dependent charge on our model molecule, norfloxacin, influences its transport through the OmpF porin. Combining results from both chapters will allow us to present a physical mechanism that explains previous observations of the pH dependence of bacterial susceptibility to fluoroquinolones.

The OmpF Porin

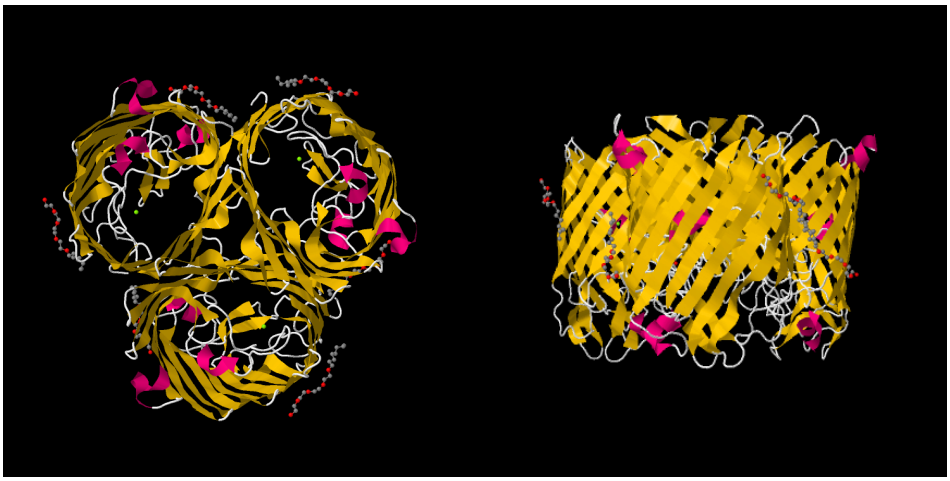

Figure 4.2 – The OmpF porin. Top and side views of the trimeric protein structure. Crystal structure image adapted from the Protein Data Bank [114].

Outer Membrane Protein F (OmpF) porins are amongst the most abundant protein porins found in *E. coli* OMs; it is estimated that they are found in excess of 10^5 copies per cell [105]. The OmpF porin is a symmetric trimer that consists of three copies of a barrel-shaped, 340-residue monomeric unit [114, 115]. It forms a water filled channel in the OM that functions as a weakly cation selective and size selective filter with an exclusion limit of approximately 0.6 kDa for hydrophilic solutes [114, 116, 117]. It is one of the relatively few OM proteins for which high resolution crystal structures exist [114, 115], enabling an in depth study of its solute selective properties. In fact, OmpF was amongst the first membrane proteins to be studied by X-ray crystallography [115, 118].

Unusually for a membrane protein, the OmpF sequence is predominantly polar; there are no long hydrophobic segments such as those found in other transmembrane proteins [115]. However, the external surface of the barrel contains lipophilic side chains that help the protein straddle the lipid membrane [116]. Its secondary structure consists almost entirely of β-sheets [115, 119]. The β-strands are tilted by between 30-60° in relation to the barrel axis, and this tilt leads to an increase in the pore diameter [116]. The crystal structure showed that the 'eyelet' of the channel, i.e., its constriction site, was 1.1 nm by 0.7 nm [115, 116]; it is this constriction that determines the size selectivity of the channel. At these length scales, the diffusion of solutes is also determined by the amino acid residues lining the internal channel wall, and indeed a study of the residues explains the slight cation-selectivity of the OmpF porin [116].

The role of porins in Fluoroquinolone Transport

In chapter 3, we saw that the fluoroquinolone antibiotic norfloxacin easily diffuses across a pure phospholipid membrane when in its neutral form; when it is protonated (positively charged) at acidic pH values, this diffusion is much slower [13].

However, the diffusion of even the neutral, lipophilic version of norfloxacin through the OM is hindered by the presence of LPS. Thus porin mediated diffusion becomes vital for the entry of these antibiotics into the bacterial cell. Inevitably, one of the primary mechanisms of fluoroquinolone resistance in bacteria is thus the downregulation of these porins, which dramatically decreases the accumulation of these antibiotics in

the cell [23, 105, 120]. A reduction in OmpF expression has been directly associated with decreased fluoroquinolone uptake [23, 121–123]. Moreover, antibiotic therapy has been associated with a shift in porin expression *in vivo* from OmpF to the narrow OmpC family of porins, whose smaller channel constriction reduces the passage of antibiotics through the OM [23].

However, a response to antibiotics is not the only mechanism by which porin mediated transport is regulated; the environment around the bacterium also plays a crucial role. The expression of the OmpF and OmpC porins in *E. coli* is governed by the OmpR/EnvZ two component system, and is affected by both the osmolarity and the pH of the surrounding medium [124]. In addition, the nutrients present in the surroundings also influence porin expression [124]. However, OmpF and OmpC proteins were also expressed in experiments with EnvZ mutants at a low pH, suggesting that alternative porin regulation pathways might be used in this regime [124]. Though the pH dependence of porin expression still needs further clarification, it has been reported that high osmotic pressure, high temperature and acidification of the medium leads to a switch in porin expression from OmpF to OmpC [125] which should lead to a decrease in antibiotic uptake, as mentioned above.

In fact, changes in bacterial susceptibility to fluoroquinolones due to changes in pH have been reported previously. An increase in external pH from acidic (5.6) to basic (8.3) was shown to correspond to a reduction in the minimum inhibitory concentration (MIC) of norfloxacin [126]. It was proposed that this pH mediated change in fluoroquinolone susceptibility is related to changes in the uptake of fluoroquinolones due to alterations of the electric charge on the antibiotic molecule [72, 127]; norfloxacin, as we know, is positively charged at pH 5 and neutral (zwitterionic or uncharged) at pH 7. It thus seems reasonable to assume that the fluoroquinolone susceptibility of bacteria in response to pH changes is a complicated process, involving both changes in porin expression and changes in drug transport properties, both through porins in the OM as well as through the phospholipid inner membrane.

One might ask whether the study of pH dependent antibiotic transport is worthwhile. However, it should be obvious that an ability to survive in varying habitats is fundamental to the ubiquity of bacteria. In particular, they have developed various mechanisms for coping with changes in external pH [109]. To colonize the human

gastrointestinal (GI) tract, for example, *E. coli* must be capable of surviving in a pH range of 4.5-9 [128, 129]. For a drug to be effective in all regions of the GI tract, an understanding of the pH dependence of antibiotic uptake is thus imperative. Our measurements were performed within this range, at pH 5 and pH 7, in order to elucidate the effect of the pH dependent norfloxacin charge state on its transport through OmpF.

4.1.2 Traditional Experimental Techniques used in Porin transport

The study of the diffusion of solutes through porins has previously been conducted using one of two general techniques. The first involves the use of multilamellar liposomes in 'liposome swelling assays'. These involve reconstituting porins into multilayered proteoliposomes and measuring solute diffusion rates in relation to another solute, generally a fully permeable sugar like arabinose [23, 116]. The second popular technique involves the reconstitution of porins into planar lipid bilayers, and studying blockages in the ionic current passing through the porin in the presence of an antibiotic/solute molecule [105, 130]. Such electrophysiology measurements enable measurements on single porins, and can boast single molecule resolution. A less common approach involves porin studies in intact cells, where the influx of a hydrophilic solute is coupled with another process such as hydrolysis of the solute in the cytoplasm; the hydrolysis can be monitored using optical density measurements [116, 131]. However, since some form of solute hydrolysis is required, this naturally limits the different types of solute that can be used in such an assay [132]. The other problem inherent in the technique is a lack of precise control over the influx pathways, since any number of different transport pathways could be used. We shall therefore not discuss this further. All three techniques thus have their strengths and weaknesses, and their relative merits are fiercely debated [116]. We shall briefly introduce liposome swelling assays and electrophysiology techniques, before we move on to discuss our own novel technique for porin studies and the results we obtained.

Liposome Swelling Assays

Liposome swelling assays (Figure 4.3) involve the reconstitution of pure porin preparations into multilamellar liposomes [108, 131, 132]. The liposomes are prepared in the presence of a polymer (generally a type of sugar); these are mixed in an isotonic polymer-free solution containing the solute of interest and the optical density (OD) is measured. If the solute is impermeable, the OD does not change. However, if the solute is permeable, this creates an osmotic gradient which leads to the influx of water, thus swelling the liposome (hence the name, swelling assay). This will eventually lead to the bursting of the liposome and a corresponding decrease in OD [23].

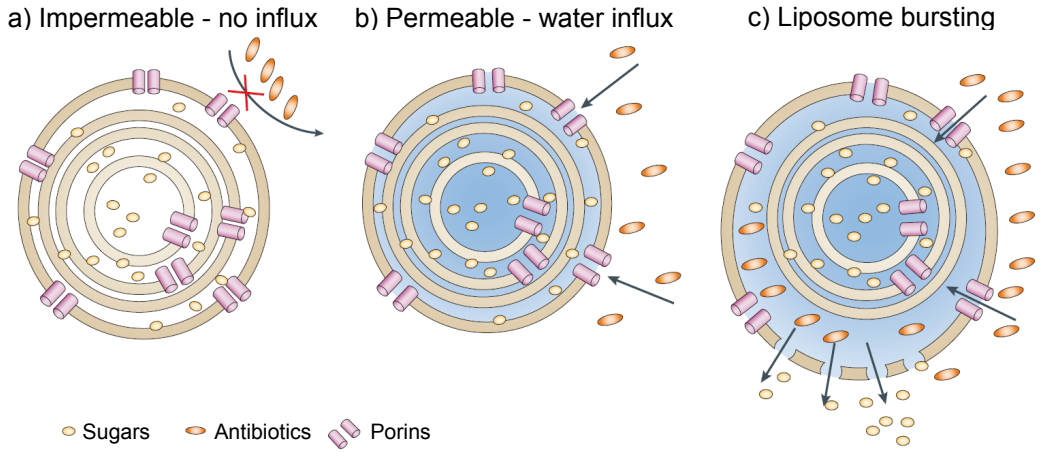

Figure 4.3 – Liposome swelling assays. a) Multilamellar liposomes are prepared encapsulating a polymer (sugar). These are mixed with an osmotically balanced polymer free solution containing the molecule (antibiotic) of interest. If the molecule is impermeable, the OD stays the same. b) If the molecule is permeable, this creates an osmotic gradient and water will swell the liposome, changing the OD. c) Eventually, this leads to the bursting of the liposome and the release of the polymer, which reduces the OD. The permeation rate is inferred by studying the decrease in OD. Image taken from [23].

This technique has been used to compare the diffusion of solutes of various sizes through porins. The channel size predicted by this method (based on solute exclusion) was remarkably accurate when compared with the known porin crystal structures [116]. The technique measures the flux of the solute by comparing its diffusion against a permeable sugar (generally arabinose); thus only relative rates of diffusion can be measured

[133, 134]. However, there are other, more serious, problems. The liposomes respond non-specifically to any solute, and hence one has to take great care in ensuring that any swelling observed is due to the solute of interest. Furthermore, when dextrans are used in liposome formation, it leads to the accumulation of cations inside the liposomes due to the build up of Donnan potentials. Thus the isoosmotic concentration for solutions of test solutes cannot be found by simply measuring the osmotic activity of the dextran [133]. The pioneer of this technique, the 'porinologist' Nikaido, has himself warned of the dangers of modifying any of the protocols involved; the possibility of misinterpreting results or observing artefacts is high [133]. Finally, since here porin incorporation is uncontrolled, one must always estimate the flux per porin; single channel resolution is not possible. Thus there are intrinsic problems inherent in the technique, and alternative technologies for porin studies were sought.

Single Channel Electrophysiology

Single channel electrophysiology has become the method of choice in the study of porins [23, 105, 130], since it provides single porin resolution and enables the study of molecular interactions with the porin. The experimental setup generally involves a teflon membrane with an aperture (normally 60-80 μm in diameter) separating two symmetrical reservoirs (cuvettes). Electrolyte solutions are present in both chambers and an ionic current is driven across the aperture via the application of a transmembrane voltage. An artificial lipid bilayer is painted across the aperture and a stock solution of porin added to one of the chambers; insertion of the porin across the lipid bilayer leads to a well-characterized jump in the ionic current. Using appropriate porin concentrations, and with appropriate dilution protocols, single channel reconstitution can be achieved. The electrical properties of the membrane and porin can then be characterized. The addition of sugars or antibiotics to one chamber and their subsequent diffusion through the porin leads to blockages in the ionic current; high resolution analysis of these ionic current fluctuations leads to a detailed understanding of the transport of single solute molecules through the porin, making this a powerful technique [23].

However, for all its success, electrophysiology has its own problems. For example, when used to measure channel size in some mutants of the *E. coli* OmpF porin, elec-

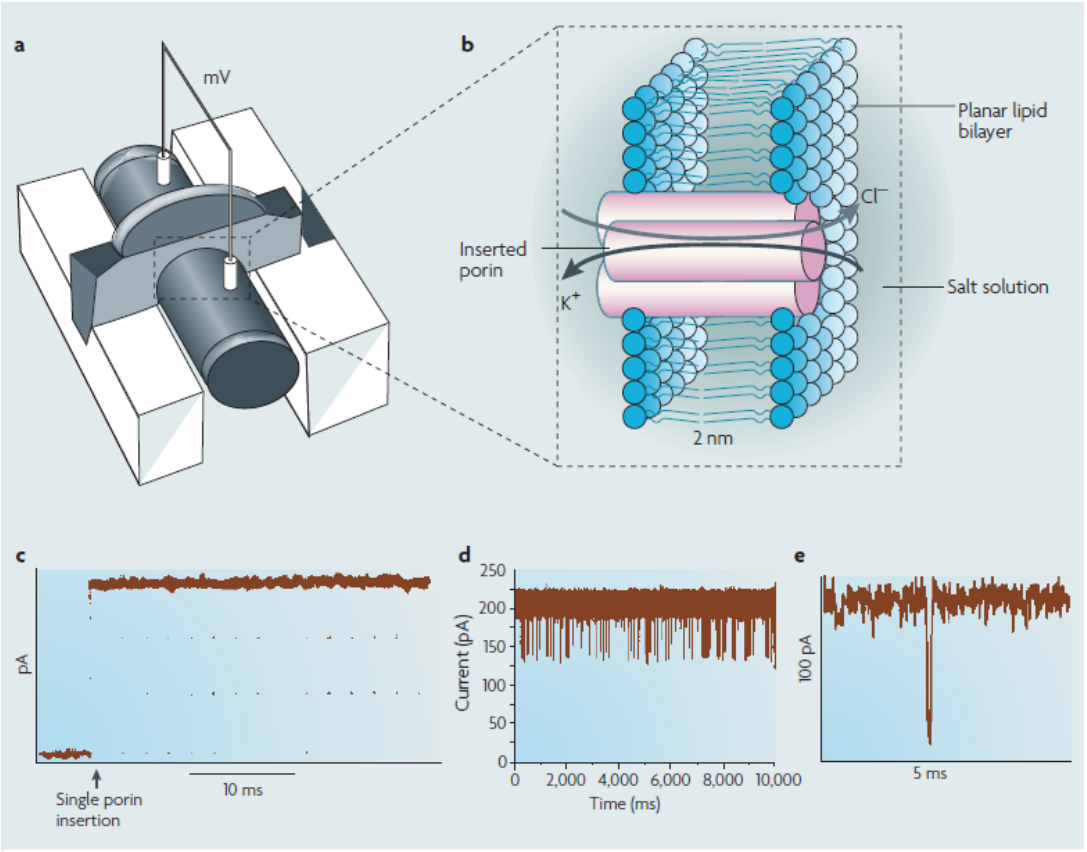

Figure 4.4 – Single channel electrophysiology. a) Experimental apparatus ('cuvette') used to create the artificial membrane. The two chambers are filled with an electrolyte and ionic currents are driven across the membrane by applying an electric potential. b) Schematic view of a single porin in the lipid bilayer. c) The ionic current across the membrane increases in a stepwise manner on the incorporation of a porin in the bilayer. d) When antibiotics are added, they permeate inside the channel and block the ionic current. e) A single antibiotic blocking event takes about 1 ms. Data obtained using 1 M KCl, a transmembrane potential of 50 mV and 5 mM ampicillin. Image taken from [23].

trophysiology showed a decrease in size whereas swelling assays and crystallography both showed the opposite [116]. Another issue with electrophysiology is that it cannot differentiate between translocation and binding events, since molecule transport is not directly observed [135]. Finally, the technique necessarily involves the application of transmembrane voltages; although important in the study of the voltage dependence of porin transport, in some cases these voltages have been suspected of producing artefacts in the results [130]. Thus, although single channel electrophysiology is widely used, there are problems associated with it that need to be addressed.

There is therefore a need to find alternative techniques capable of studying solute transport through porins, which could circumvent the flaws inherent in traditional methods. We therefore decided to modify our optofluidic assay to make it viable for the study of porin embedded proteoliposomes.

4.2 Experimental Techniques and Materials

4.2.1 Optofluidic Permeability Assay

The optofluidic permeability assay builds on the work described in the previous chapters studying the permeability coefficient of norfloxacin across lipid membranes. It was designed to explore properties of porin mediated transport not accessible to electrophysiology and other traditional techniques. It enables the study of drug transport through porins without the application of a transmembrane voltage. The optofluidics assay also presents a direct visualisation of norfloxacin uptake across a proteoliposome membrane and enables the measurement of contributions to diffusion from pure lipids and through porins, which cannot be done in a quantitative manner using the older liposome swelling assays [23, 108, 132].

As described in Figure 4.5, the optofluidic permeability assay involves the 'Short' T junction microfluidic chip where the vesicles (liposomes/proteoliposomes) and the drug molecules are mixed in a channel (via the application of suction at the outlet). The T junction geometry of the chip leads to an equal mixing of vesicle and drug solutions. The inlet norfloxacin concentration is 2 mM and hence the vesicles are exposed to a

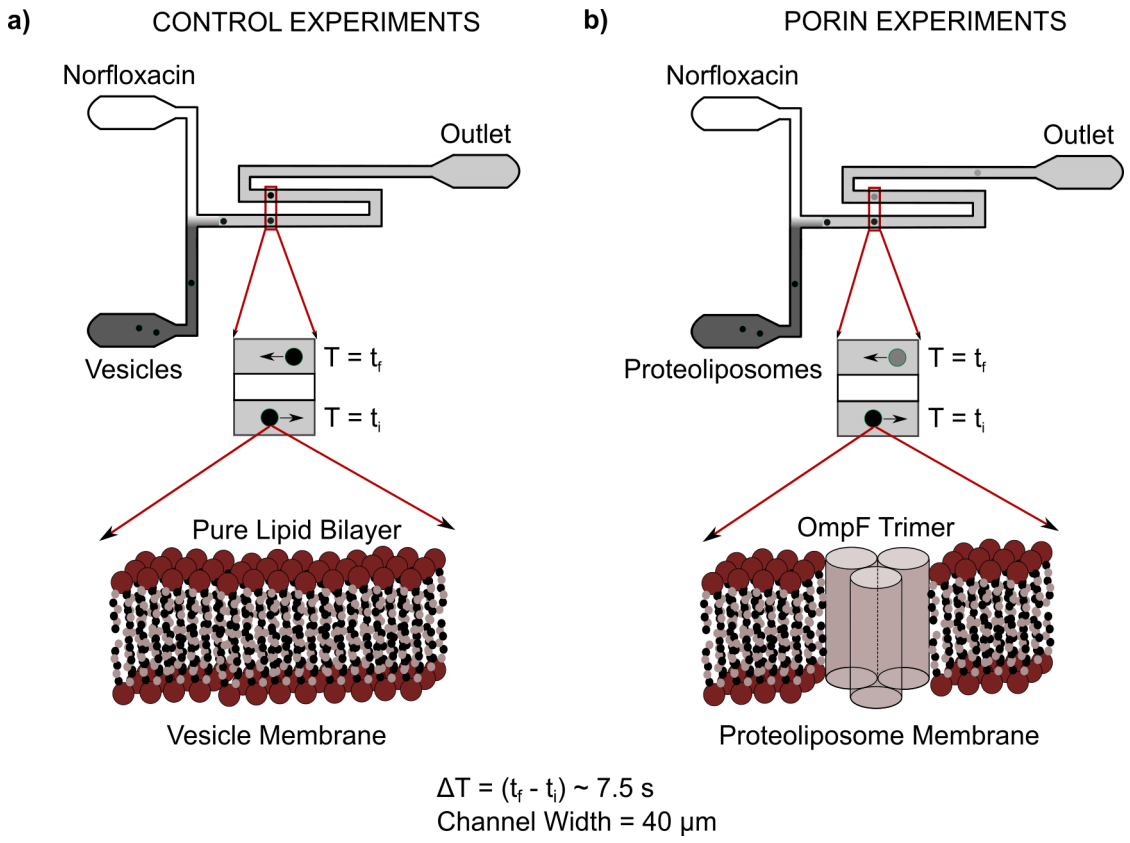

Figure 4.5 – Schematic of the OmpF optofluidic permeability assay. Control experiments (no porin) are represented in (a) and proteoliposome experiments (containing OmpF) in (b). Vesicles (liposomes/proteoliposomes) are mixed with norfloxacin in a T junction microfluidic chip by applying suction at the outlet reservoir with a syringe pump; norfloxacin autofluorescence is stimulated with a UV epifluorescence microscope. The vesicles are detected at an initial time t_i immediately post mixing and at a later time t_f, a distance 7.4 mm further downstream. Vesicles took, on average, about 7.5 s to travel the intervening distance. Both time points are observed in the same field of view. Detection of the autofluorescence intensities within the vesicles at both points enables the calculation of the drug permeability coefficient for each vesicle. Published in [103].

final norfloxacin concentration of 1 mM. The vesicles are imaged immediately post mixing with the norfloxacin and at a distance 7.4 mm further along the channel, both points being observed in the same field of view.

The work described in chapter 3 involved the use of our custom built UV epifluorescence microscope with an EMCCD camera, a setup that was tailored for this experiment. However, to demonstrate the versatility of the technique, we performed all the OmpF optofluidics experiments described in this chapter on a commercial Olympus IX73 microscope, using a DAPI filter set (Chroma) and an arc lamp (Prior Lumen 200). A 60× air objective was used (Olympus LUCPlanFLN, NA 0.70). Images were recorded using a scientific CMOS camera (optiMOS, QImaging) which enabled recording at 100 fps (10 ms exposure, bin 4).

4.2.2 Vesicle formation and OmpF incubation

GUVs of DPhPC lipids (Avanti Polar Lipids) were prepared via electroformation using a Nanion Vesicle Prep Pro (Nanion Technologies GmbH, Germany) setup as described previously (section 2.3.3). The GUVs were prepared in 200 mM sucrose with 5 mM phosphate buffer (pH 7) or 5 mM acetic acid (pH 5).

The OmpF incubation followed previously established protocols [136]. Purified stock OmpF (5.5 mg/ml) was provided (courtesy the Winterhalter laboratory, Jacobs University Bremen) in a detergent, a 1% solution of n-Octylpolyoxyethylene (octyl-POE, Bachem) prepared in Millipore water. The stock OmpF was diluted 1:1 in the same detergent and vortexed; 1 µl of this freshly diluted OmpF solution was added to 199 µl of the vesicle stock solution and incubated at room temperature for an hour. Biobeads® SM-2 (Bio-Rad) were added to remove the detergent and the mixture was incubated at room temperature for 45-60 minutes followed by storage at 4 °C overnight. The next day, the OmpF embedded proteoliposome solution was separated from the Biobeads with a pipette and the sample used directly in experiments. For the control (liposome) experiments, 1 µl of 1% octyl-POE (instead of the OmpF solution) was added to 199 µl of the vesicles; the rest of the incubation protocol remained unchanged.

4.2.3 OmpF insertions counted using ionic current sensing

In order to calculate the norfloxacin flux per OmpF porin in the optofluidics assay, we needed a calibration measurement that would allow us to estimate the number of porins embedded in each proteoliposome. This measurement was done by our collaborators in Jacobs University Bremen, Germany (Winterhalter group). Briefly, proteoliposomes were prepared in a similar manner as for the optofluidics assay; however, the OmpF concentrations used were a factor of 500×, 250× and 100× smaller, so that single insertions could be measured. Higher porin concentrations could not be used because the resultant patches were unstable. A planar lipid bilayer containing the proteins was formed by pipetting 5 μl of the proteoliposomes into a similar amount of the electrolyte solution (200 mM KCl, 5 mM acetic acid for pH 5 or 5 mM phosphate for pH 7). The resulting solution was placed on a microstructured glass chip (grounded side) containing an aperture approximately 1 μm in diameter. The vesicles burst once they touch the glass surface of the chip thus forming a planar lipid bilayer; additional suction was applied to patch the proteoliposomes across the aperture. Ionic current measurements were performed using an Axopatch 200B amplifier in voltage clamp mode. An on board low pass Bessel filter was used at 10 kHz; the sampling frequency was 50 kHz.

From the calibration curve (Figure 4.6), we see that the number of porins per patch increases linearly with porin concentration. The large errors in the measurements indicate the variability in OmpF insertion efficiency in different vesicles. This can be due to various reasons – all electroformation protocols lead to a small population of multilamellar vesicles [36], and in these the porins will not be able to insert. Furthermore, OmpF mixing with vesicles is not controlled in our protocol, and hence is not expected to be uniform. However, for the purposes of estimating the flux per porin, this calibration measurement is sufficient; the large error in insertion efficiency is reflected in the spread in permeability coefficients obtained in the experiments.

Extrapolating from the calibration curve, we obtained a value of ∼1,800 porins per μm^2 for the proteoliposomes used in the optofluidics assay (for comparison, it is estimated that general diffusion porins are present at $>10^5$ copies per bacterial cell [105], which translates into an approximately 6-7× higher [porin]:[lipid surface area] ratio than in

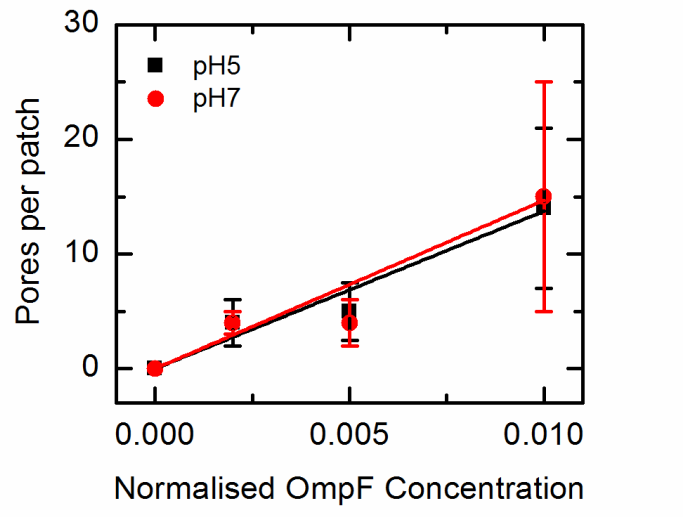

Figure 4.6 – OmpF insertion efficiency calibration. A range of OmpF concentrations were measured in proteoliposomes in a Port-a-Patch setup. The number of OmpF porins per membrane patch (d = 1 μm) were counted and used to plot a calibration curve. The OmpF concentrations displayed are normalised with respect to the concentrations used in the optofluidics assay. Within error, we observe a linear increase in the number of porins measured per patch. Extrapolating to the concentrations used in the optofluidics assay, we estimate 1750 ± 114 porins per μm^2 in the vesicles at pH 5 and 1871 ± 137 porins per μm^2 at pH 7 (values are mean ± s.e). For each OmpF concentration, four batches of vesicles were prepared at both pH 5 and pH 7. The number of proteoliposome patches measured for each OmpF concentration (at each pH) was, in order of increasing OmpF concentration, N = 17, N = 6 and N = 11. Measurements performed by Dr. Harsha Bajaj. Published in [103].

our experiment). The vesicle radius is measured in the optofluidic assay; one can thus calculate the surface area of each vesicle and use the calibration measurement to estimate the number of porins per vesicle. The permeability coefficient of the vesicle contains information about the total flux of drug molecules into the vesicle, and hence a rough estimate of the flux per porin can be calculated.

4.2.4 Flux calculations

The flux (J) through a proteoliposome can be calculated from its permeability coefficient (P) as follows:

$$P = -\left(\frac{R}{3t}\right) \times \ln(\Delta I(t) - \Delta I(0) + 1) \tag{4.1}$$

$$J = 4\pi R^2 \times P \times (\Delta I(t) - \Delta I(0) + 1) \times c_{out} \tag{4.2}$$

where c_{out} is 1 mM. The main contribution to J is the flux through the OmpF porins in the proteoliposomes. There is a small contribution that arises due to norfloxacin diffusion through the pure lipid bilayer. This can be quantified using known values of the permeability coefficient of norfloxacin across DPhPC vesicle membranes, reported in chapter 3. The control measurements show that in the absence of porins, $\Delta I(t) \sim \Delta I(0)$ on the timescales measured. Therefore, the (maximum) contribution of the diffusion through lipids, J_{lipids}, to the total flux measured is given by:

$$J_{lipids} = 4\pi R^2 \times P_{lipids} \times c_{out} \tag{4.3}$$

where c_{out} is 1 mM, as usual. From chapter 3, we know that P_{lipids} = 0.006 μm/s at pH 7 and $P_{lipids} \sim$ 0.001 μm/s at pH 5.

The actual flux through all the porins in a proteoliposome, J_{porin}, is thus:

$$J_{porin} = J - J_{lipids} \tag{4.4}$$

Dividing J_{porin} by the number of porins in the proteoliposome gives us the flux per porin for that proteoliposome.

4.2.5 Data Analysis

In the data analysis of the optofluidic assay, four filters were applied to separate genuine vesicle detection events from lipid aggregates.

- The circularity criterion (as defined in equation (2.16)) was 0.7.
- Only those vesicles with radii between 20 and 45 pixels (i.e. 8.8-19.7 μm) were chosen for analysis; vesicles with radii below 20 pixels were difficult to distinguish

from lipid aggregates, and were hence discarded. Since the microfluidic channel width is 40 μm, vesicles with radii greater than 20 μm were subject to shear by the channel walls, which can affect drug uptake. Therefore these events were discarded as well.

- Vesicles with velocities only between 0.4-1.5 mm/s were chosen for analysis. Events with velocities above 1.5 mm/s were generally false positives; events below 0.4 mm/s were either false positives or cases where vesicles were moving along the channel walls and were hence subject to shear.

- Finally, it was observed that ΔI values below 0.05 were associated with lipid aggregates and false positives. Therefore all events with $\Delta I < 0.05$ were discarded.

The main purpose of the selection criteria is to speed up the analysis process. However, as mentioned earlier, the frames corresponding to vesicle events are saved separately during image analysis in MATLAB, and hence each point in the scatter plots can be checked visually as well if desired.

4.3 Results

4.3.1 Optofluidic assay reveals norfloxacin uptake through OmpF

The results of the optofluidic permeability assay are illustrated in Figure 4.7 – results from other proteoliposome experiments are presented in Figure 4.8. As before, the graphs show a normalised intensity difference ($\Delta I = \{(I_{out} - I_{in})/I_{out}\}$) between the background autofluorescence intensity (I_{out}) and the autofluorescence intensity inside the vesicle (I_{in}), versus vesicle radius (R). Each point represents a single vesicle measurement. The grey squares reference vesicles at the initial viewpoint immediately post mixing with the norfloxacin (which for convenience we set to $t = 0$). The green triangles (pH 5) and red circles (pH 7) reference vesicles once they have travelled along the channel to the next detection position.

The norfloxacin concentration present in the channel after diffusive mixing is about 1 mM; at $t = 0$, there is no norfloxacin inside the vesicles, whereas outside the vesicles

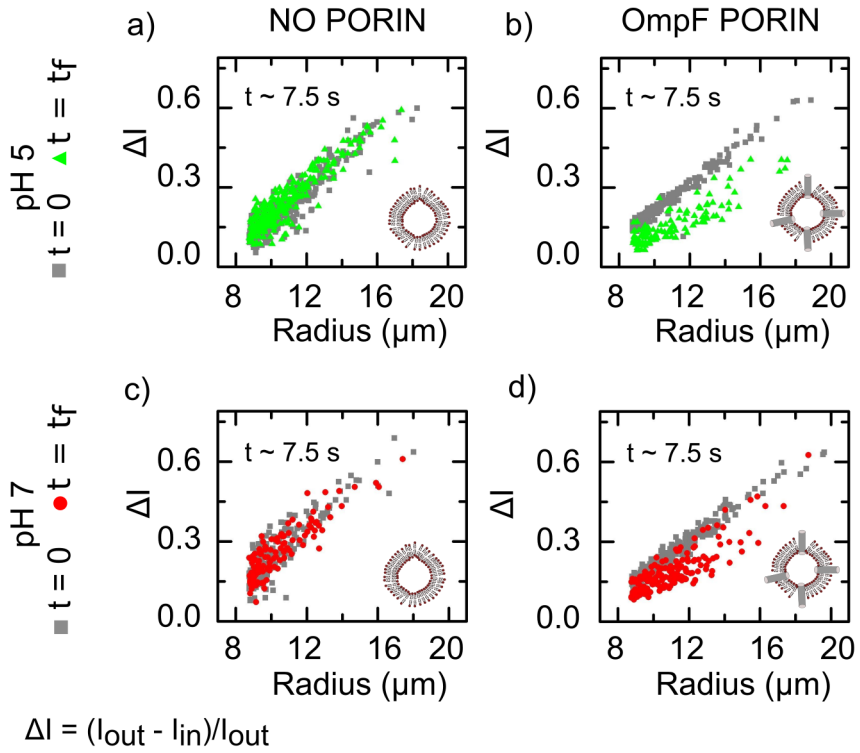

Figure 4.7 – Optofluidic permeability assay shows the rapid uptake of norfloxacin in OmpF embedded proteoliposomes. Comparison of the uptake measurement in liposomes and proteoliposomes at pH 5 **(a, b)** and pH 7 **(c, d)**. Each point references an uptake measurement at the single vesicle level, the grey points being $t = 0$ and the green (pH 5) and red (pH 7) being the final detection point $t = t_f$. On average it took vesicles about 7.5 s to move from the initial to the final detection point. In the absence of porins **(a, c)**, there is no shift in ΔI values observed at the later time at either pH. The presence of porins **(b, d)** leads to a marked downward shift in ΔI for the majority of proteoliposomes at the later detection point, both at pH 5 and pH 7. The downward shift in ΔI corresponds to an increase in the norfloxacin autofluorescence intensity within the proteoliposome (I_{in}), and is thus a direct measure of drug uptake. Published in [103].

the concentration is 1 mM. At both pH 5 and pH 7, the presence of the OmpF causes a marked downward shift in the ΔI values of vesicles at the final viewpoint as opposed to the control experiments, indicating rapid accumulation of the drug inside the proteoliposomes. In the absence of the porins, a similar degree of drug accumulation is only observed over much longer timescales (as presented in chapter 3), indicating that OmpF porins significantly enhance the permeability of the membranes to norfloxacin.

This can be seen in the repeat porin measurements presented in Figure 4.8 as well.

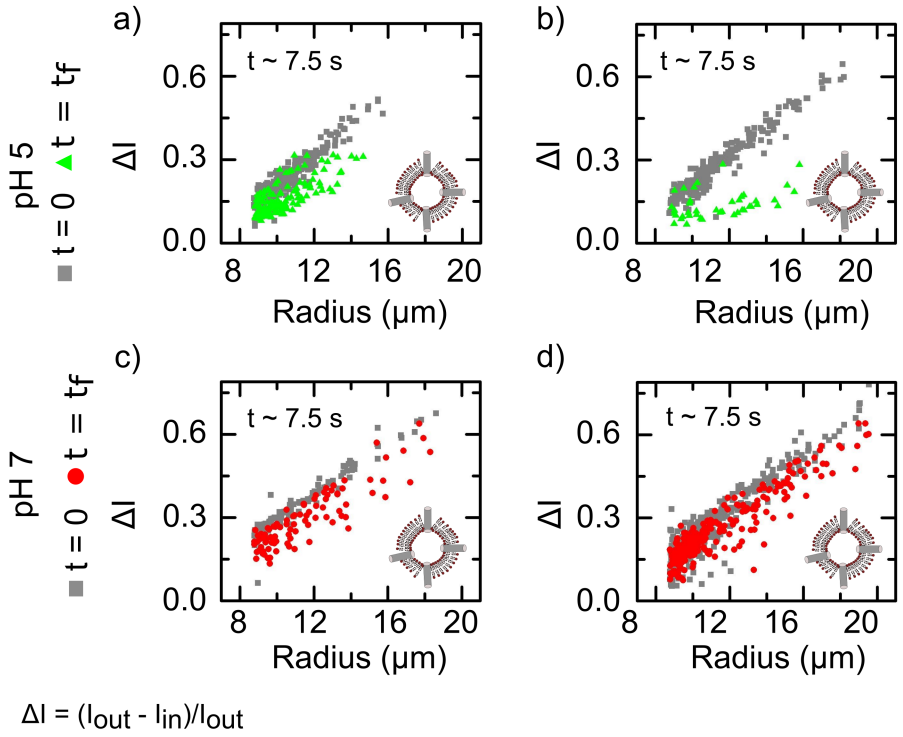

Figure 4.8 – Norfloxacin uptake measurements of OmpF-embedded proteoliposomes in the optofluidic assay. **a)** and **b)** show results from two individual experiments at pH 5 with different batches of vesicles. Likewise, **c)** and **d)** show the results of two experiments at pH 7, conducted with different vesicle batches. The same porin concentration was used for all the experiments. Differences in the nature of the spread can be attributed to variations in the vesicle batch quality and porin insertion efficiency. However, in all plots enhanced uptake is observed for a significant proportion of the proteoliposomes. Published in [103].

Histograms representing the combined results of 3 separate proteoliposome experiments at each pH are presented in Figure 4.9.

The presence of the porins leads to similar permeability coefficients at both pH 5 and pH 7, suggesting that the charge of the molecule does not play a significant role in influencing its transport through the porin in the absence of a transmembrane potential. The spread in the permeability coefficient histograms is caused by the inevitable variability of OmpF insertion into individual vesicles prepared for the optofluidics experiments. This can be seen in the scatter plots Figure 4.7 and Figure 4.8 as well

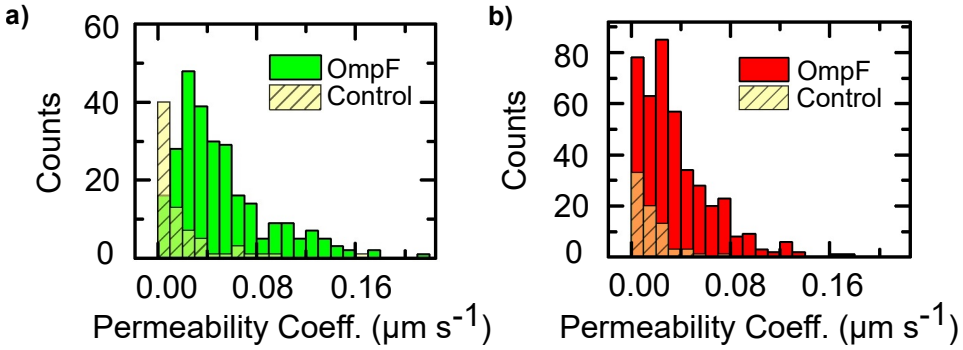

Figure 4.9 – The histograms are a record of permeability coefficients (P) measured for individual porin-embedded proteoliposomes, and summarize the data from 3 separate experiments at each pH. Histograms from the control measurements with liposomes (no porins) are overlaid to show the shift in P due to the presence of porins in the membrane. Total liposomes/proteoliposomes detected were N = 268 (pH 5, with porins), N = 74 (pH 5, no porins), N = 420 (pH 7, with porins) and N = 74 (pH 7, no porins). Published in [103].

– it is clear that, at both pH conditions, a handful of vesicles do not show significant transport. It is known, however, that electroformation produces some multilamellar vesicles [36], and in these the porins cannot insert across the membranes; this would account for the few negative observations.

Norfloxacin Flux Calculation in the Proteoliposomes

Our Port-a-Patch calibration curve (Figure 4.6) yielded an estimate of ~1,800 porins per μm^2 for the proteoliposomes used in the microfluidics assay. Since we measure the vesicle radius in the optofluidic assay, it is straightforward to calculate the surface area of each vesicle and use the Port-a-Patch calibration measurement to estimate the number of porins per vesicle. Using the equations in section 4.2.4, an average over all events (neglecting the contribution of flux through pure lipids) gives a flux value of 10 ± 8 norfloxacin molecules/s per porin at pH 7 (N = 420) and 15 ± 10 molecules/s (mean ± s.d) per porin at pH 5 (N = 268). Subtracting the contribution due to the diffusion through pure lipids leaves the flux values unchanged, as expected considering the timescales over which the measurements were performed [13, 103].

4.3.2 Single OmpF Channel Electrophysiology measurements

The measurements presented in this subsection were performed by our collaborators in Bremen (Harsha Bajaj, Winterhalter group). We shall therefore not go into great detail, and will only briefly summarize the technique and results obtained, since these results are relevant to the model for norfloxacin accumulation in *E. coli*.

This experiment involves the study of single OmpF channels reconstituted in a planar lipid bilayer using the technique pioneered by Montal and Mueller [34]. Traditionally, a lipid bilayer is formed across an aperture (diameter $\sim$ 30-60 μm) in a teflon film that separates two reservoirs in a cuvette. The reservoirs are filled with an electrolyte solution and a potential difference is applied across the lipid membrane via electrodes in the reservoirs. Porins are reconstituted in the lipid bilayer and their conductance properties studied by measuring the ionic current flowing through the membrane. The addition of antibiotics leads to blockages in the ionic current, since the antibiotic molecules displace ions flowing through the porin. By studying properties such as the residence time of the antibiotic in the channel and the frequency of blockage events, it is possible to infer kinetic association and dissociation rates that characterize the interaction of the antibiotic with the porin [137]. Using these measured properties, it is possible to calculate the antibiotic flux through the porin based on a suitable transport model [138–140].

Measurements were performed using transmembrane voltages of 25 mV and 50 mV, and a norfloxacin concentration difference of 250 μM between the two reservoirs of the cuvette. In both instances, it was found that the residence time of norfloxacin in the channel at pH 5 was an order of magnitude lower than the corresponding residence time at pH 7. This immediately suggests that the positive charge on the drug molecule at pH 5 leads to it being driven through the channel in the presence of a transmembrane voltage. At pH 7, the overall charge on the norfloxacin molecule is neutral and therefore the voltage is less important; free diffusion is the primary driving agent for transport through the porin. However, there might still be some small voltage dependent effects since the molecule is zwitterionic at pH 7 – this requires further investigation.

The above interpretation seems validated by the flux values obtained. At an applied transmembrane voltage of -25 mV, the norfloxacin flux value (per porin) was found to

be $\sim$ 1 molecule/s at pH 7 and $\sim$ 2 molecules/s at pH 5. An increase in the transmembrane voltage to -50 mV results in an increase in the flux at pH 5 to 5 molecules/s; the flux at pH 7 remains unchanged. Note that the flux was calculated using $\Delta c = 1$ mM, to compare with the optofluidic permeability assay results described previously. This is justified since it was observed that the number of antibiotic events in the ionic current recordings increased linearly with an increasing concentration of the antibiotic, and hence the rate constants measured with a concentration difference of 250 μM were equally applicable at a concentration difference of 1 mM.

4.4 Discussion

In this study, we used an optofluidic permeability assay alongside traditional porin electrophysiology to explore the pH and voltage dependence of norfloxacin transport through OmpF porins. The optofluidic assay directly proves that the uptake of norfloxacin in the proteoliposomes is much faster due to the OmpF porins embedded in the proteoliposome membranes, as compared to pure lipid membranes (no porins).

An interesting pattern emerges: in the absence of any transmembrane potential, the optofluidics assay shows that the flux per porin is essentially the same (within error) at both pH 5 and pH 7. However, as the transmembrane voltage is increased (electrophysiology), the flux at pH 5 starts to increase over the flux at pH 7. At a transmembrane voltage close to typical physiological OM Donnan potentials [113] of -25 mV, the flux at pH 5 is twice as large compared to the observation at pH 7. On increasing the transmembrane voltage to -50 mV, the flux at pH 5 increases to five times that at pH 7. This confirms that the positive charge on norfloxacin at pH 5 contributes significantly to its transport across porins in the presence of transmembrane voltages.

It has been reported that a change in the pH from acidic to basic reduced the minimum inhibitory concentration (MIC) of norfloxacin [126]; furthermore, the cytoplasmic accumulation of norfloxacin peaks at a pH of 7.5 [72]. This agrees well with the data obtained in our study. As mentioned above, our experiments suggest that norfloxacin will accumulate in the periplasm of an *E. coli* bacterium at a 2× faster rate at pH 5 than at pH 7 under typical physiological conditions, due to porin mediated transport across

the OM. However, the drug molecules now encounter the phospholipid inner membrane (IM). Our previous results [13] showed that the direct diffusion of norfloxacin through a pure vesicle lipid bilayer is more effective (by a factor of approximately 6×) at pH 7 than at pH 5. It is also known that the periplasmic pH is the same as the external pH [128]. Considering the relative rates of norfloxacin transport across the two membranes at pH 5 and pH 7 thus explains the greater cytoplasmic accumulation at the higher pH. This suggests that diffusion through the inner membrane might present the rate limiting step. However, the permeation of Mg^{2+} chelated antibiotics could further influence the uptake process through both the OM and IM. It should also be remembered that medium acidification leads to the preferential expression of the narrower OmpC porins over OmpF [125], which would further reduce norfloxacin accumulation at acidic pH values.

Our analysis of norfloxacin transport through porins and lipids has thus clarified some of the mechanisms by which drug transport is affected under changing external conditions. The optofluidics assay also presents a direct visualisation of norfloxacin uptake across a proteoliposome membrane in a label-free assay not previously possible, and unambiguously confirms the importance of these porins in facilitating the transport of fluoroquinolone antibiotics across lipid barriers. In addition, our optofluidic technique enables the measurement of contributions to diffusion from pure lipids [13] and through porins, which cannot be done in a quantitative manner using the established liposome swelling assays [23, 132]. Furthermore, our microfluidic based approach has the potential to explore a wide range of porins. Proteoliposomes could be devised containing a combination of passive diffusion porins and active transporters, to study competition between these processes. New vesicle preparation techniques [141] have shown considerable promise for integration into lab-on-a-chip devices, which should translate into better control over porin insertions and proteoliposome modification. A combination of traditional and advanced single vesicle techniques can thus be used to investigate a variety of drug transport phenomena, an urgent need in medicine today.

4.5 Conclusions

Our investigations into norfloxacin transport across phospholipid membranes and the OmpF porin have thus yielded a more detailed, quantitative understanding of its passive transport rates across bacterial membranes. We have experimentally demonstrated that the charge state of the drug molecule (and by association, the pH of the surrounding environment) dramatically influences its transport across lipid membranes; we have thus validated theoretical predictions [72] on this topic. The technology developed is capable of studying these processes in proteoliposomes of varying lipid and porin constitutions, and indeed the next steps in this direction would involve the use of lipids that more closely resemble those found in bacterial cells (already under investigation) and combinations of import and efflux pathways to study the effect of these competitive processes.

A lack of control over protein incorporation in the vesicles is the obvious roadblock to such further investigations. However, microfluidic vesicle preparation techniques [141, 142] have recently been demonstrated that should enable much better control of protein insertion, by incorporating all the mixing steps into lab-on-a-chip devices. This is the great advantage of microfluidic techniques – one can replace traditional bulk pipetting procedures with finely controlled mixing on the single vesicle level. Clever design of the chip geometry could suitably enhance protein insertion efficiency, and step by step, a better approximation of a true bacterial membrane could be developed.

Further experimental capabilities of this technique will be discussed in chapter 6. Before that, however, we shall delve next into a discussion on bacterial signalling, an ongoing investigation that has great potential with regards to understanding the antibiotic stress response in bacteria.

Chapter 5

Indole signalling in *Escherichia coli*

> "Are we [humans] in charge, or are we simply hosts for bacteria? It all depends on your outlook."
>
> Neil deGrasse Tyson (*Space Chronicles: Facing the Ultimate Frontier*)

5.1 Introduction[1]

This Thesis has thus far been devoted to studying the passive transport of antibiotics across artificial cell membranes, and to the development of new techniques to measure the same. However, such transport studies can be applied to other small molecules as well. Cellular signalling, in both prokaryotes and eukaryotes, is governed by the transport of small, drug-like molecules and ions across cell membranes [144–147]. In bacteria, the indole molecule has generated interest as an inter-species and inter-kingdom signal [144, 145, 148]. By tracking indole molecules using their UV autofluorescence, previous work in our laboratory showed that indole can passively diffuse across *E. coli* lipid membranes [149].

The rate at which indole diffuses out through the cell membrane is critical – when produced rapidly within the cell, its lipophilicity means that indole accumulates in the membrane before diffusing into the surrounding medium. This leads to transiently

[1] We published the work presented in this chapter in reference [143].

high concentrations of cell associated indole, which we have termed the indole 'pulse' [143]. This was a hitherto unknown aspect of indole signalling, that governs the entry of *E. coli* cells into their stationary growth phase.

This project was carried out in collaboration with the group of Dr. David Summers (Dept. of Genetics, Cambridge). The work described in this chapter to elucidate the indole pulse is a small part of the much larger story of indole signalling in *E. coli*, but it is of particular interest because it stands as the culmination of many years of both pure biological and biophysical investigations performed in our laboratory.

5.1.1 Indole

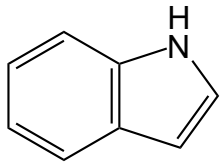

Figure 5.1 – The indole molecule. Source: www.wikipedia.org

Indole (Figure 5.1) is a molecule that is ubiquitous in the bacterial community – it is known to be produced by at least 85 different species of bacteria, spanning both Gram-positive and Gram-negative species [144]. It is produced by the degradation of the amino acid tryptophan. In the presence of the enzyme tryptophanase (tnaA), tryptophan is converted into indole, pyruvate and ammonia [150].

Indole is known to be a key bacterial signalling molecule – it is involved in regulating plasmid stability [151], acid resistance [152] and the expression of efflux pumps in *E. coli* [153]. It plays a role in the modulation of biofilms [154], and has been linked to a number of stress response mechanisms in bacteria, including an antibiotic response [155]. Perhaps even more interestingly, indole is found in considerable quantities (0.5-1.0 mM) in the human gut, a consequence of the trillions of bacteria present there [156] – it has been found to regulate gene expression in human enterocyte cells, and is believed to play an important role in the response of epithelial cells in the gut to pathogens [145]. Recent work has also shown that indole can affect the hormone secretion of enteroendocrine cells in the gut, with significant effects on the host's

metabolism [148]. All these signalling mechanisms are active at indole concentrations typically ranging between 0.5-1.0 mM.

An investigation into the electrical properties of indole revealed that it also behaves as a proton ionophore, capable of shuttling protons across cellular membranes [157, 158]. At high enough concentrations (3-5 mM), it was shown that this ionophore activity of indole was capable of blocking *E. coli* cell division by depolarising the membrane potential [157]. However, such high concentrations of indole are not typically found in bacterial culture supernatants [159], and hence the biological relevance of these effects was open to question.

However, it was also known that tryptophanase expression is strongly up-regulated by the stationary phase sigma factor RpoS [160], which leads to an increase in indole production as cells approach stationary phase [151]. We postulated that, if the indole production rate in a cell exceeded the rate at which indole left the cell, there could transiently exist a state in which the cell experienced high concentrations of indole. This pulse could, we believed, lead to indole concentrations that were capable of shutting down the cell division machinery via the ionophore effect.

In order to observe this pulse, it was necessary to devise an assay that allowed us to measure the internal indole concentration associated with bacterial cells. Previously, all discussion about the effects of indole involved using the supernatant concentration of the molecule, but we needed to measure cell associated indole to validate our theory. Two independent methods were used to probe this [143]. Dr. Hannah Gaimster (Summers's laboratory) used a modified Kovacs assay – this is the standard fluorimetric assay [161] used to determine indole concentrations. However, the Kovacs assay has limited sensitivity at low indole concentrations, and the modifications required to study cell associated indole reduced the SNR considerably. We therefore devised a complementary technique to measure cell associated indole via its UV absorbance characteristics, and it is this assay and its results that form the basis of this chapter.

5.2 Measuring Cell Associated Indole

5.2.1 UV Absorbance Assay

Cell associated indole was determined by measuring the reduction in supernatant indole concentration due to the presence of bacterial cells. Briefly, indole is added externally to a bacterial suspension, and the solution is centrifuged to separate out the cells. Some of the indole is absorbed by the cells, thus reducing the supernatant indole concentration. This is at least partly due to the fact that indole is lipophilic, and preferentially partitions into lipids [143].

The reduction in supernatant indole concentration was quantified by measuring the UV absorbance of the indole in the supernatant and comparing it with a calibration control in which no bacteria were present. To avoid any contamination from intracellular indole, a tryptophanase knockout strain of *E. coli* (W3110 ΔtnaA) was used – since they lack tryptophanase these bacteria cannot produce indole, and the only indole in the experiment is that which is added externally. The outline of the assay is shown schematically in Figure 5.2 and the exact experimental procedure is provided below.

5.2.2 Experimental details

Cells were cultured overnight to stationary phase in a Luria Bertani (LB) medium (Sigma Aldrich) at 37 °C in shake flasks at 250 rpm. The strain used was Kanamycin resistant, so 30 μg/ml Kanamycin (Sigma Aldrich) was added to the growth culture to prevent contamination from other strains. The strain itself was grown on an LB-Agar plate (Sigma Aldrich) with the appropriate amount of Kanamycin added. Generally, about 30 ml of each culture was prepared.

The cells were resuspended in Phosphate Buffered Saline (PBS, Sigma Aldrich) for use in the absorbance measurement. The buffer was autoclaved prior to use and stored at 4 °C. Before each experiment, the buffer was also sterile filtered through 0.22 μm filters (Millipore).

A 75 mM stock solution of indole was prepared by dissolving indole (>99% pure, Sigma Aldrich) in absolute ethanol (Sigma Aldrich).

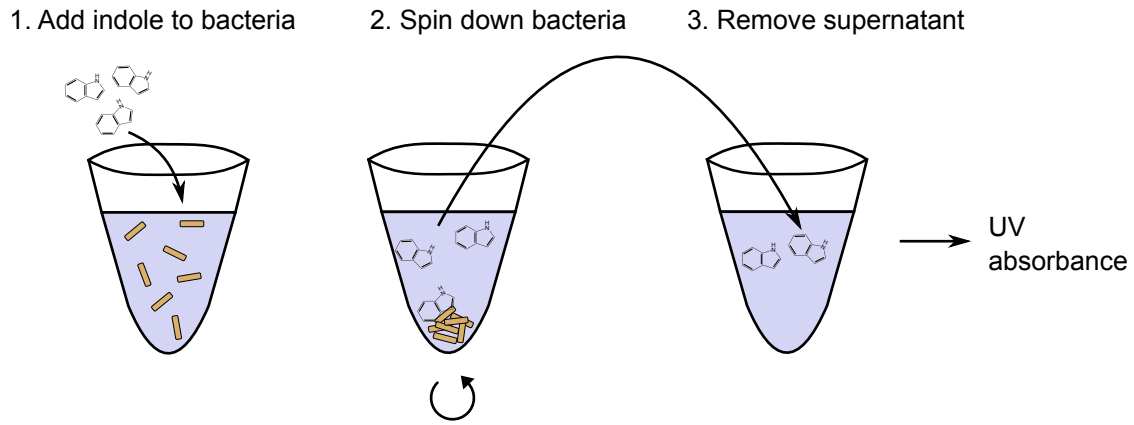

Figure 5.2 – UV absorbance assay to determine the absorption of indole by cells. Indole is added externally to a suspension of *E. coli* bacteria that are incapable of producing their own indole. Since indole diffuses freely across cell membranes [149] and is lipophilic [143], a fraction of the externally added indole is absorbed by the cells. The solution is centrifuged and the indole that was absorbed by the bacterial cells is thus separated from the supernatant. The bacterial pellet is discarded, and the amount of indole left in the supernatant quantified by measuring its absorbance in the UV. Comparing this with a calibration curve enables us to determine the amount of indole associated with the cell pellet.

The spectrophotometer used was a UV VIS Varian spectrometer (Cary 300 Bio) and the software package used was the accompanying Cary 'Scan' program. The same quartz cuvette (Sigma Aldrich Z276677-1EA) was used for all experiments. After each spectrophotometer measurement involving indole, the cuvette was rinsed with 96% ethanol and dried with nitrogen before the next measurement to remove any trace indole contamination.

After all mixings/resuspensions, the samples were vortexed to ensure a uniform distribution of bacteria and indole.

The basic protocol was as follows:

1. The bacteria (in LB) were spun down in a Harrier 18/80 Refrigerated Centrifuge at 4,000 rpm (2,685 × g) for 10 minutes. The supernatant was discarded, and the bacteria resuspended in a similar amount ($\sim$ 30 ml) of PBS. This was then again centrifuged at 4,000 rpm for 10 minutes, so that the bacteria were washed with the buffer.

2. After the PBS wash, the supernatant was again discarded and the bacteria resuspended in a suitable amount of PBS. It is at this stage that one can modify the bacterial number density in the culture; we chose to concentrate the bacteria by resuspending them in 7.5 ml of PBS. The higher bacterial density improves the SNR in the assay.

3. We measured the optical density at 600 nm (OD_{600}) of the bacterial culture in the PBS. This is a standard method of determining the number density of bacterial cells in a culture. The higher the number of cells, the higher the optical density. As with all other measurements in the experiment, this was repeated thrice and the average value taken. Our final experiments used samples with an OD_{600} of between 4.0-5.0.

4. Once the OD_{600} measurements were complete, we took 1 ml of the bacterial sample in a microtube (Axygen boil-proof 1.5 ml) and added the appropriate amount of 75 mM indole stock to it to obtain the desired indole concentration. For our 'blank', we used 1 ml of the bacterial sample without indole. After spinning these samples down in a centrifuge (Thermo Scientific Heraeus Fresco 17) at 6,000 rpm (3,500 $\times$ g) for 5 minutes, we saved the supernatants for analysis and discarded the pellets.

5. Since the indole concentrations we studied were in the range 0.5-2.0 mM (which saturated the UV VIS reading), we had to dilute all our samples 1:20 by volume in PBS.

6. Finally, the absorbance curves (in the 250-300 nm range) of the samples were measured in the spectrophotometer. These absorbance curves were normalised by subtracting the absorbance curves of the backgrounds – for the bacterial solutions, we used the bacterial sample without indole (the 'blank').

To check that the basic premise of the experiment was correct, we added 1.5 mM indole externally to two samples of bacteria, one at a low OD_{600} (1.8) and one with a very high OD_{600} (16.7). Since the sample with the high OD_{600} contains many more bacterial cells (for the same volume) than the low OD_{600} sample, one would expect more indole to be removed from the supernatant in the high OD_{600} case. The absorbance curves

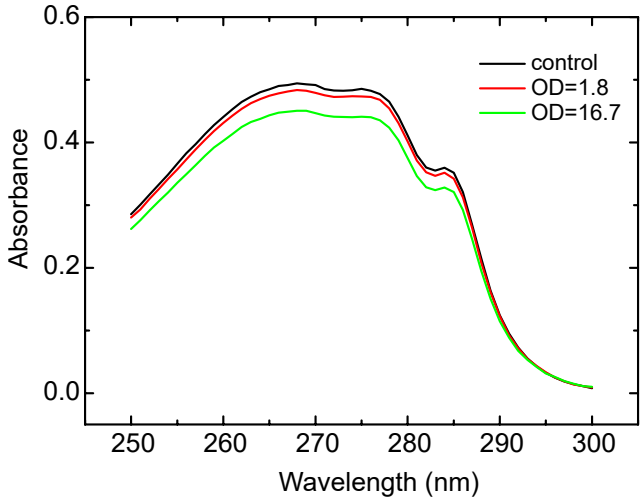

Figure 5.3 – UV absorbance curves for the supernatant when an indole concentration of 1.5 mM was added externally to control/bacterial solutions. The solutions were all diluted 20-fold to ensure the absorbance values remained within the linear regime of the spectrophotometer. A small decrease in absorbance was observed between the PBS control and the low OD_{600} bacterial sample (OD_{600} = 1.8). However, the high OD_{600}(OD_{600} = 16.7) sample absorbed significantly more indole, as evidenced by the shift in the indole absorbance curve. This suggested that the bacteria were indeed capable of absorbing indole, and the amount absorbed increased with the number of cells present.

of the supernatants should reflect this OD_{600} dependent change in supernatant indole concentration. This was observed as expected (**Figure 5.3**).

5.2.3 Calculation of Cell Associated Indole

To calculate the internal cell indole concentrations from the differences in the absorbance curves, we needed a calibration curve of absorbance versus indole concentration. We therefore prepared solutions of 0.5 mM to 2.5 mM indole in PBS, performed the necessary dilutions and measured the absorbance curves. After subtracting the background, we picked the peak wavelength in the absorbance curves (268 nm) and plotted a calibration curve of these peak absorbance values against the external indole concentration.

For elucidating the cell associated indole, we used the calibration curve to determine the indole concentration in the supernatant of our bacterial samples (again using the absorbance values of the samples at 268 nm), and subtracted this value from the external concentration. Since we always used 1 ml of sample, we could calculate the number of moles of indole that were transferred to the bacterial pellet. Using the OD_{600} obtained (in PBS), one could then calculate the total cell volume in the bacterial pellet [162], and hence the apparent cell associated indole concentration.

5.2.4 Results

The results of the absorbance assay are depicted in Figure 5.4. At each external concentration, 4 independent bacterial cultures were tested. The mean OD_{600} of the samples used was 4.5 ± 0.2 (after concentration in PBS). As expected, we observed a linear increase in the cell associated indole concentration as the external concentration was increased. We also calculated that the cell associated concentration was typically 5-fold higher than the added external concentration.

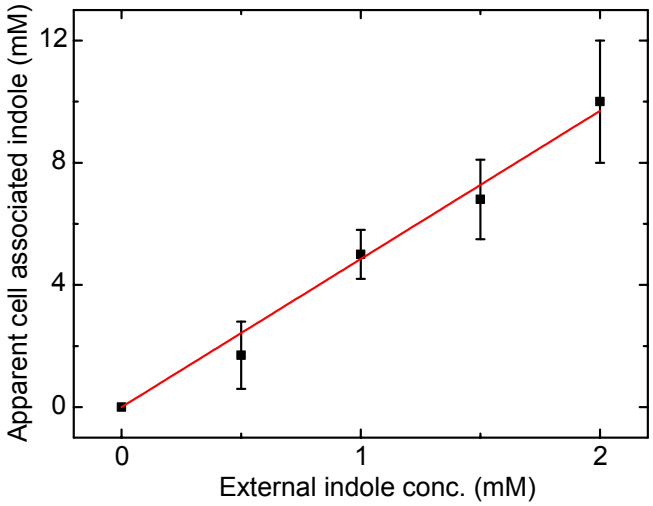

Figure 5.4 – Results of the UV absorbance assay. The apparent cell associated indole concentration rises linearly with externally added indole, as expected. Error bars represent standard deviations. We see that the cell associated indole is significantly higher than the supernatant indole concentration, indicating the cellular absorption of indole.

We were particularly interested in the 1 mM external indole case, since this is the value generally found in culture supernatants. Therefore, we tested the effect of 1 mM external indole without concentrating the samples in PBS (the mean OD_{600} for these samples was 1.3 ± 0.1, N = 4, mean ± s.d). As mentioned earlier, the SNR for these experiments was worse, but the final result, combining both the high and low OD_{600} calculations, revealed that at 1 mM external concentrations, the apparent cell associated indole concentration was 7 ± 3 mM (mean ± s.d, N = 8).

It is thus apparent that bacterial cells absorb indole from the supernatant, and that the cell associated indole concentration can be significantly higher than the external (supernatant) indole concentration.

5.2.5 Results on cell associated indole using the Kovacs assay

Dr. Gaimster used a complementary approach to measure cell associated indole (Figure 5.5). In her assay [143], known concentrations of indole were added to ΔtnaA *E. coli* cells in stationary phase, similar to the UV assay described previously. However, after vortexing and centrifuging the solutions, the cell **pellet** was analysed for indole, and the supernatant discarded. So whereas the UV assay measures indole in the cell pellet indirectly, by measuring how much indole the cells removed from the solution, this approach measures the indole associated with the bacterial cells directly. The cells are incubated with Kovacs Reagent (made by dissolving 10 g of *p*-dimethylaminobenzaldehyde in a mixture of 50 ml HCl and 150 ml amyl alcohol) for two minutes, which leads to cell lysis. This allows the Kovacs Reagent to react with the indole present in the pellet, and the level of indole is quantified with an absorbance measurement at 540 nm (for full experimental details, please refer to [143]). The calculation of cell associated indole follows the same technique as that used in the UV assay, and involves the estimation of the cell volume in the pellet from the OD_{600} [143, 162].

A comparison of the results from the two techniques shows that the cell associated indole estimated by the Kovacs assay is ∼2× higher than that estimated from the UV assay. This is likely caused by systematic errors due to the different protocols for the two assays. In the UV assay, we only take the supernatant, so contamination from the

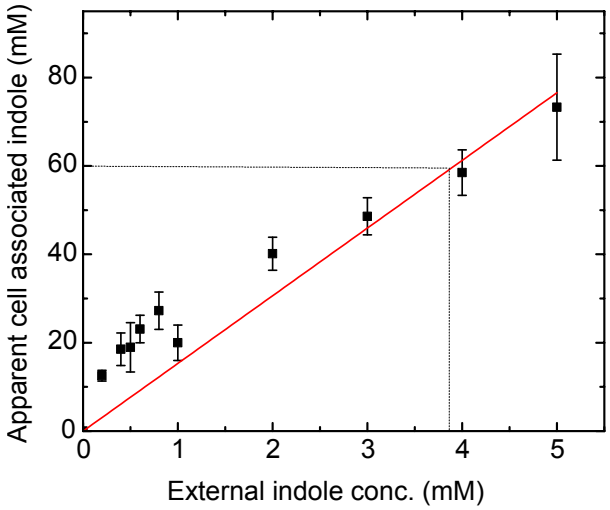

Figure 5.5 – The relation between apparent cell associated indole concentrations and the supernatant indole concentration as determined by the Kovacs assay. As with the UV assay, known concentrations of indole were added to ΔtnaA *E. coli* cells in stationary phase. The mixture was vortexed and centrifuged, but in this assay the cell **pellet** was analysed for indole using the Kovacs reagent. Dotted lines show the cell associated indole concentrations corresponding to external indole concentrations capable of shutting down cell division [157]. Data points represent mean ± s.d for at least 3 independent repeats. Data collected by Dr. Gaimster. The image is taken from [143].

bacterial pellet is unlikely. However, in the Kovacs assay, it is experimentally almost impossible to remove all the supernatant from the cell pellet before treating it with Kovacs Reagent. It is therefore likely that some of the indole detected is not associated with the pellet, which would lead to a slight overestimation of the cell associated indole. This could account for the differences in values obtained by the two assays. However, both assays show that the cell associated indole concentration is significantly higher than the supernatant concentration. This agrees with our understanding of indole as a lipophilic molecule. The partition coefficient of indole into *E. coli* total lipid extract (Avanti Polar Lipids) was measured by Dr. Silvia Hernandez-Ainsa ($\log(K) = 1.95 \pm 0.12$ ($N = 9$) [143]) and confirmed that indole has a high affinity for lipids.

5.3 Discovery of the Indole Pulse

Work by Dr. Gaimster had shown that there is a rapid increase in indole production as bacteria transition from exponential to stationary phase. This leads to indole accumulation inside the cells at a rate faster than its diffusion out through the membrane, causing a pulse in the level of indole associated with the cell, as seen in Figure 5.6. By comparing the cell associated indole to the supernatant indole concentrations (Figure 5.5), we see that the indole pulse leads to cell associated indole concentrations that are high enough to inhibit cell division via the ionophore mechanism mentioned previously [143, 157].

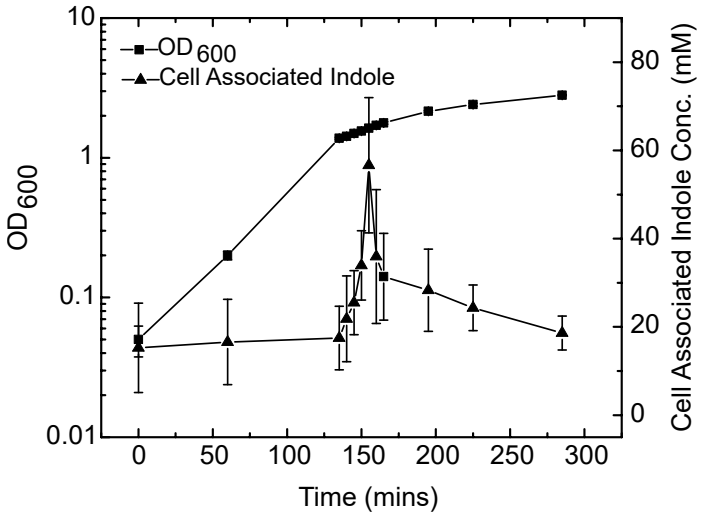

Figure 5.6 – The Indole Pulse. When *E. coli* transition from exponential to stationary growth, the rapid production of indole leads to a transient increase (i.e, a pulse) in the cell associated indole. The high cell associated indole concentration leads to the blocking of cell division via the ionophore mechanism described earlier [157]. The data for this figure was obtained by Dr. Gaimster, and the figure is taken from [143].

Furthermore, we showed that this pulse leads to better long term cell viability – cells lacking the tryptophanase gene had lower viability than the wild type strain when monitored over a period of 10 days in low nutrient settings [143]. It was also observed that simply adding 1 mM indole – the supernatant concentration generally associated with stationary phase cultures – to these tryptophanase knockouts could not restore the wild type viability, thus suggesting that the internal indole pulse is crucial for this long term survival phenotype. We proposed that the pulse signals a decline in available

nutrients, thus inducing the metabolic changes required to slow down growth in the hope of conserving the limited resources for long term use [143].

We expect most of the cell associated indole to exist within the lipid membrane. It is therefore possible that the indole pulse plays a significant role in modulating the properties of proteins anchored in the *E. coli* membranes. Since the membrane is the bacterium's main protection against external stress, it is likely that indole plays an important role in the bacterial stress response. We shall briefly discuss the role of indole in antibiotic resistance below, and shall conclude by returning to our permeability assay, to examine whether indole affects the lipid permeability of antibiotics.

5.4 Indole and Bacterial Stress Response

5.4.1 Indole response under antibiotic stress

We know that indole is a proton ionophore that is capable of depolarising the *E. coli* membrane potential and inhibiting cell division [157]. It should thus come as no surprise that cell viability is dramatically reduced when the bacteria are incubated with high concentrations (>4.5 mM) of indole [163]. In fact, ionophores are typically used as antibiotics due to their toxicity [164]. Thus too much indole is certainly problematic for a bacterium.

However, indole has also been routinely linked with stress responses in bacteria [144, 153]. While conducting experiments to determine phenotypes in the emergence of antibiotic resistance, it was discovered that when bacteria were grown under norfloxacin stress (at sub-MIC levels), a few cells became highly resistant, and these isolates started producing copious amounts of indole [155]. The presence of this indole in the medium led to an improved antibiotic tolerance for the wider population, but came at a fitness cost to the producers [155]. This 'bacterial charity work' established the existence of an indole mediated population-based resistance mechanism to norfloxacin [155]. The molecular mechanism of this process is still not well understood, although it is believed to be linked with the indole mediated overexpression of multidrug efflux pumps [153, 155].

In order to test this physically, one first needs to know whether the presence of indole affects the passive permeability of antibiotic molecules across lipid membranes. We therefore decided to test the effect of a high indole concentration (5 mM) on the permeability of norfloxacin across DPhPC vesicle membranes to see whether it changed the drug's permeation properties.

5.4.2 Lipid permeability of norfloxacin is indole independent

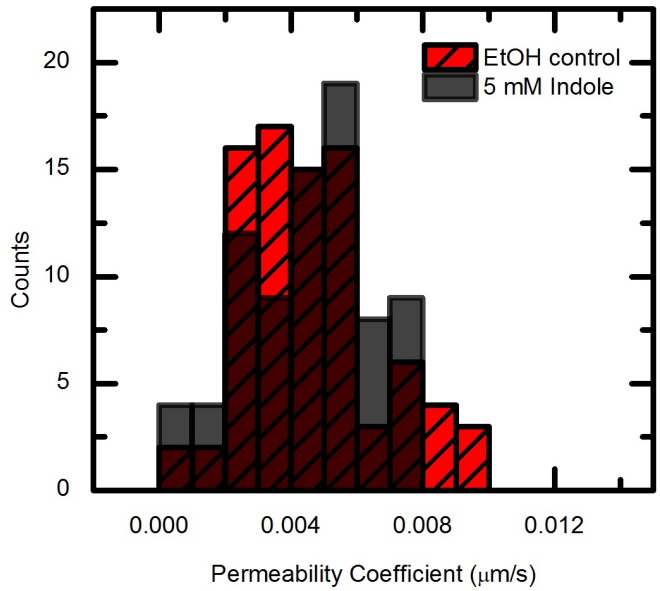

Figure 5.7 – Permeability coefficient histograms showing the permeability of norfloxacin across DPhPC lipid membranes at pH 7 in the presence and absence (ethanol control) of indole. Both populations overlap, implying that indole does not affect the passive diffusion of norfloxacin across lipid membranes.

We performed our optofluidic permeability assay on DPhPC vesicles incubated with 5 mM indole. The indole stock was dissolved in absolute ethanol, so the control experiments were performed using an equivalent amount of ethanol (without indole) in the assay solutions. The measurements were performed at pH 7 in the 'Long' chip, and the rest of the protocol was the same as the initial norfloxacin-DPhPC protocol.

The resultant histograms of the permeability coefficients are shown in Figure 5.7. As is evident, the presence of the indole has no detectable effect on the diffusion of

norfloxacin across the lipid membrane. It is therefore likely that indole does not influence passive transport, and that its effects are limited to modulating active transport processes [153]. The study of the effect of indole on these transmembrane transport proteins is an important avenue of research, but lies beyond the scope of this Thesis.

5.5 Conclusions

We have provided a small glimpse into the ever expanding field of indole signalling in bacteria. The pulse signalling mechanism is a new entrant to this field, and much work is still required to pin down its mechanisms and downstream effects. There are many examples of indole playing important signalling roles, but the molecular mechanisms involved have so far proved elusive.

Apart from the microbiology and antibiotic resistance perspective, the presence of indole and indole producers in the human gut is of great interest, especially in light of the recent results highlighting the effect of indole on the human glucose metabolism [148]. Understanding bacterial signalling processes in the gut is thus crucial for developing a broader understanding of host-microbiome interactions. And this is just one example – the number of bacteria colonizing the human body outnumber all the 'human' cells in our bodies 10 to 1. Metabolites produced by gut bacteria have been shown to affect plasma concentrations of various mammalian blood metabolites [165, 166]. Furthermore, the lining of the digestive tract is home to the enteric nervous system which consists of approximately 10^8 neurons of various different types [167, 168]. Investigations are already underway linking changes in the gut microbiome with changes in behaviour, and this promises to be an extremely interesting field of biomedical research in the near future [169]. Along these lines, it is worth considering the fact that the indole ring is found in various chemicals known to affect the nervous system, from the 'sleep chemical' serotonin to hallucinogens such as psilocybin. 90% of the serotonin in our body is produced in the gut, and experiments have already shown that both human and mouse gut microbes regulate their host's serotonin biosynthesis [170]. One could easily speculate on the role of indole, produced by gut bacteria, in controlling the human nervous system via similar pathways.

Which begs the question, who really is in charge, humans or bacteria? Only time will tell.

Chapter 6

Outlook

> "We are made wise not by the recollection of our past, but by the responsibility for our future."
>
> George Bernard Shaw

6.1 Vesicle based permeability measurements

Vesicles offer, in principle, an excellent platform for studying transport across lipid bilayers, as evidenced by the work described in this Thesis and elsewhere [13, 19, 56]. However, a lack of precise control over vesicle formation using traditional electroformation or lipid hydration techniques has placed limitations on the field. As a result, most membrane protein research today is carried out using planar lipid membranes, which lack the curvature and spherical continuity of true cellular membranes [171], in addition to being incompatible with conventional microscopy techniques.

The use of microfluidics for vesicle formation has provided a much needed impetus to the field. These techniques generally involve focussing an aqueous solution in a cross flow of a lipid/oil solution. The resultant lipid-stabilized droplets are converted into vesicles by merging the droplet flow with another aqueous solution, which is accompanied with the removal of the oil phase [43, 141, 142, 171]. The use of microfluidic flow patterns enables precise control over vesicle formation – the vesicles

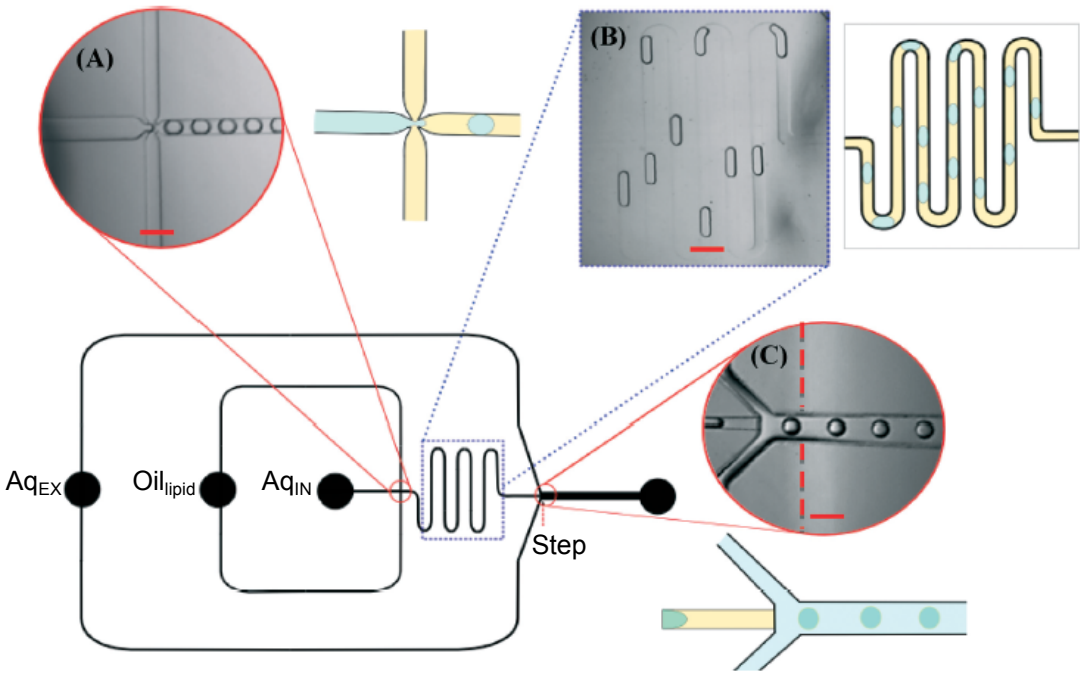

Figure 6.1 – Microfluidic vesicle formation. **A)** The internal aqueous dispersed phase (Aq_{IN}) is sheared by a carrier oil flow producing monodisperse water-in-oil emulsion droplets (scale = 70 μm). **B)** Image of channel meander, where the spontaneous formation of a lipid monolayer around each aqueous droplet can take place (scale = 80 μm). **C)** Step junction (scale = 100 μm), where the channel carrying the water-in-oil droplet changes depth from 50 μm to 100 μm. This allows the emulsions to transfer into the external aqueous phase (Aq_{EX}). The red line indicates where the PDMS has been treated in the deeper channel to prevent the wetting of each droplet on the channel wall. Image and description taken from [141].

produced are of uniform size, the diameter can be tuned and solutes can be efficiently encapsulated [171]. Preliminary studies have shown that protein pores can be inserted in these vesicles leading to the permeabilization of the membrane [171]. Although the experimental techniques involved are far more challenging than conventional electro-formation, the significant improvement in vesicle formation control offered must mean that these microfluidic techniques will soon become the norm.

This bodes well for our permeability assay. A microfluidic chip redesign would allow us to incorporate the vesicle formation on chip, significantly improving throughput and, additionally, simplifying the analysis. Lipid aggregates would not be a problem, and the

uniformity in vesicle size would make it easier to filter out false events. It should also then be possible to mix nanopores with the vesicles on chip, which should make the pore insertion efficiency more uniform across the vesicles. In principle, fluorescently tagged pores could be used to quantify the number of pores attached to the vesicle membrane, enabling a more precise measurement on the flux of the solute of interest through the pore. Thus incorporating microfluidic vesicle formation into our assay would be the obvious next step in developing the technology.

6.1.1 Antibiotic transport studies

First and foremost, our assay could be used to characterize the permeability of various antibiotics across a range of different lipids. Lipid mixtures containing the lipid molecules found in bacterial membranes could be used to create vesicles that more closely mimic true bacterial membranes. As demonstrated with norfloxacin, the pH dependence of antibiotic transport can be investigated for a host of different drug molecules. Furthermore, the effects of ions such as Mg^{2+} on antibiotic transport could be investigated. Metal ions can chelate antibiotics and this can change the solubility, pharmacokinetics and bioavailability of these drugs [172].

Secondly, the role of different membrane protein pores on antibiotic transport can be quantified using our technique. However, for this we shall first have to develop better control over quantifying the porin insertion efficiency, for which the microfluidic developments of vesicle formation and pore incubation are crucial. Nevertheless, there are many different membrane protein pores that are yet to be analysed by this technique, and the selectivity of pores for particular antibiotics could be investigated.

The technique need not be limited to passive diffusion. Vesicles have been used to study active transport using efflux pumps reconstituted in lipid vesicles [173]. Such transport processes could also be investigated using our technique, although one must bear in mind that the theoretical model will have to be modified appropriately to study active rather than passive transport.

Finally, one need not limit oneself to the study of protein pores. Our research group has recently succeeded in creating nanopores made out of DNA origami [174]. Further work has shown that these can be reconstituted into lipid bilayers, raising the possibility

that these structures could one day be used as artificial membrane channels enabling the transport of ions or drugs into target cells [175, 176]. We are in the process of optimising the insertion of these pores into vesicles to test their ability to transport drugs across the lipid bilayer.

6.1.2 Ion flux measurements

The assay we have developed is a very general technique. The experiment only requires that the entity under investigation show fluorescence. Thus we are not just restricted to antibiotics, we can study the transport of any drug or solute molecule that is fluorescent and quantify its lipid permeability.

One field that is extremely important in biology is the field of ion transport. The proper balance of ions between the interior and the exterior of a cell is critical for its survival. Besides maintaining the correct osmolarity and membrane potential, ions are involved in various cell signalling processes. For example, Ca^{2+} signalling is used to control processes ranging from fertilization, proliferation, development, learning and memory, contraction and secretion, and all this must be tightly regulated since deviations in the spatial or temporal boundaries of Ca^{2+} signalling can cause cell death [147, 177, 178]. Ca^{2+} can be derived either from internal stores within the cell, or from the external surroundings via channels in the membrane [146]. Defects in calcium channels have been linked with a number of serious neurological, cardiac, retinal and muscular disorders in humans [179].

Given the obvious importance of studying calcium signalling and transport, a number of highly sensitive dyes have been developed that are capable of detecting physiological concentrations of Ca^{2+} in cells [180]. One such dye, developed in the group of the Green Fluorescent Protein pioneer Roger Tsien, is Fura-2 [181]. The fluorescence characteristics of the dye are shown in Figure 6.2. Fura-2 is a divalent metal ion chelator that changes its fluorescence properties on complexation [182]. In the absence of Ca^{2+}, the unbound form of Fura-2 has a peak excitation wavelength around the 370 nm mark, which shifts down to around 340 nm when the Ca^{2+} is bound. By switching between 340 nm and 370 nm excitation wavelengths, one can obtain intracellular Ca^{2+} concentrations using a ratiometric approach [180].

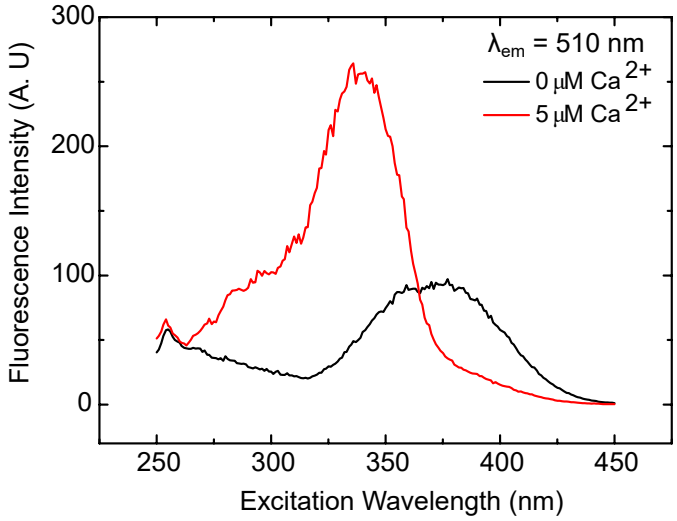

Figure 6.2 – Fura-2 pentasodium salt (Life Technologies) fluorescence characteristics. Emission wavelength λ_{em} = 510 nm. When Ca^{2+} ions are bound to the dye, the excitation maximum is at around 340 nm, whereas the unbound form of the dye has an excitation maximum around 370 nm. We can exploit this to study Ca^{2+} transport into nanopore embedded vesicles in the same way as we studied norfloxacin transport. Using 340 nm as our single beam excitation wavelength, we can track Ca^{2+} ions as they accumulate in vesicles by studying the increase in fluorescence intensity within the vesicles. The Fura-2 fluorescence characteristics were measured by T. Maier on a Cary Eclipse fluorimeter. Solutions contained 5 μM Fura-2, 140 μM EGTA as chelator for divalent impurities and 200 mM sucrose.

However, from Figure 6.2, it is clear that we can study Ca^{2+} transport across proteoliposome membranes using this dye without requiring a ratiometric measurement. By stimulating the dye's fluorescence at 340 nm, one can distinguish solutions flowing in the chip in which Ca^{2+} ions are present (bound to Fura-2) or absent. One can prepare vesicles containing Fura-2 and a chelator (Ethylene Glycol Tetraacetic Acid, EGTA, to remove any trace divalent impurities in the buffer) – this forms the solution in one inlet of the T junction, whereas the other inlet contains the same buffer with Ca^{2+} ions. The transport of the Ca^{2+} ions into the vesicles can be tracked by studying the increase in autofluorescence intensity (at an excitation wavelength of 340 nm) within the vesicles.

Of course, being charged the ions cannot simply diffuse across the lipid bilayer. We have incorporated alpha-hemolysin, a bacterial toxin nanopore, into the vesicles and

are in the process of studying Ca^{2+} transport through these pores. With the hemolysin measurement as a positive control, we can investigate the ion transport properties of new DNA origami nanopore structures by embedding these in the vesicle membranes.

Besides Ca^{2+}, there are dyes available to track Na^{+} and K^{+} ions as well, and thus our system can be used to investigate the ion transport characteristics of a range of different nanopores, thus opening up yet another field of investigation with this technique.

6.2 Transport measurements on the single cell level

The main advantage of using vesicle based model systems is that one has complete control over the transport process. One knows that all transport must be passive (unless designed otherwise), and once the baseline membrane permeability has been determined, it is possible to study the effect of additional membrane components on drug (or ion) transport.

However, in many cases one just wants to know whether a drug or nanoparticle enters a cell, and how long such a process takes. For example, if one has a sample of bacteria from a clinic, by performing a drug transport assay one could screen the population for antibiotic resistant cells based on their reduced drug uptake (Figure 6.3). In principle, our microfluidic chip could be redesigned into an autofluorescence based cell sorter which could separate bacteria based on their relative rates of drug uptake (for a review of label-free microfluidic cell sorting, the reader is referred to [183, 184]). These cells could then be analysed using genomic and proteomic techniques to study the precise mutations that led to reduced drug uptake.

Performing such studies on lab-on-chip devices would enable clinicians to spot mutations quickly and, in an ideal scenario, change the therapy such that the resistance pathway could be overcome. This could be useful not just for bacterial infections but also for cancer diagnosis and treatment, another setting in which drug resistance plays an important role.

A number of eukaryotic cell types can be analysed in the microfluidic devices we already possess. For example, we have tested HL60 cells (a leukemia cell line) in our

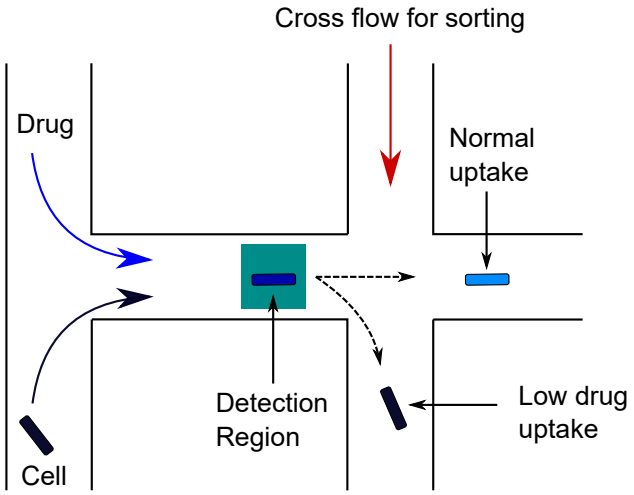

Figure 6.3 – Schematic of a proposed microfluidic system that sorts bacterial cells on the basis of antibiotic uptake. The levels of drug autofluorescence within the cell after exposure to the drug in a T junction chip determine whether the uptake is normal or reduced. Reduced uptake is often a sign of antibiotic resistance [23], and such cells would be separated using a cross flow. The cells could then be subjected to detailed biochemical analyses to determine the cause of resistance.

devices, and showed that similar transport measurements could be performed using these cells.

With bacteria, their small size becomes a challenge. We have constructed channels that are 10 μm wide and 6 μm high, in which we were able to see *E. coli* flowing through the channels. However, flow control for the long network lengths is challenging with such narrow channels, and the small size of the bacteria also makes imaging them difficult. The use of faster cameras and high magnification objectives should, however, make this system viable in the future. Another option, especially when considering making a portable device, would be using photomultiplier tubes as the detectors and designing a confocal detection system. The fluorescence intensity at particular points in the network could be monitored – the drug accumulation in an individual bacterium would be a function of the fluorescence intensity dip recorded by the detector as the bacterium passes through the detection volume. PMTs are also much faster than standard cameras, which would increase the throughput, and reduce the time taken to sample a bacterial population. Another corollary to this would be that one could obtain an accurate estimate of the bacterial concentration at the same time, which

would provide an added bonus when characterising bacterial infections in the clinic. There is thus significant incentive to develop such technology.

6.3 Future measurements on indole signalling

With the indole project, there are many possible avenues to pursue. The first thing that will need to be investigated in detail is the actual mechanism of indole production. We know that indole is produced when bacteria face external stresses, but the molecular mechanisms and pathways involved in the response are unclear.

One would also like to quantify indole production on the single cell level. We have two possibilities in this regard – indole production can be detected indirectly inside cells by using the pSTYABB plasmid, which encodes styrene mono-oxygenase. This enzyme converts indole molecules into indigo, a dye whose levels can be quantified by colorimetric assays [149, 160].

The timing of indole production can also be inferred by studying the expression of tryptophanase. This can be done using a bacterial strain in which green fluorescent protein (GFP) is tagged to tryptophanase expression. With this in hand, it should be possible to perform a number of experiments in which single bacterial cells are exposed to a range of stresses, and tryptophanase expression monitored using the GFP fluorescence to study the role of indole in the stress response.

Single cell studies, however, cannot be performed efficiently using standard microbiology protocols. Here again, microfluidics can come to the rescue. High throughput, single cell studies of bacterial growth have become technologically feasible with the invention of the "Mother Machine", a microfluidic chip used to study various aspects of bacterial growth [185]. A similar device could allow us to control the microenvironment in ways conducive to studying stress responses in growing bacteria.

Another interesting possibility is that the indole pulse might be a stochastic process occurring continuously in bacterial colonies, that preconditions certain individuals in a bacterial colony to be able to withstand any type of stress. This would have implications for the study of bacterial persistence, which is almost as great a medical problem as antibiotic resistance [186–188]. Persisters are the cells in the colony that

become dormant due to natural stresses, and their metabolic inactivity allows them to escape the effects of antibiotics. These cells can survive antibiotics without having undergone the mutations typically seen in resistant organisms. Once the stress is removed, these cells start growing again, leading to a recurrence of the infection. Their transient nature and relatively low numbers in colonies has impeded the study of persisters, and the molecular mechanisms behind their phenotype are largely unknown [188]. The indole pulse could potentially be one such mechanism regulating persistence in bacteria. Again, microfluidic investigations on single cells would offer a platform into the analysis of this phenotype, and an ability to separate these cells will hopefully open the field up to detailed biochemical investigation.

The role of indole signalling in the human gut is already under investigation [145, 148]. However, all the studies performed so far have been based on cells grown in cultures. The next step here would be to study the effect of indole positive and indole negative bacteria directly in the gut. This is typically done using 'germ-free' mice, which are grown in special aseptic conditions so that they are born free of any microbes. Growing these mice is experimentally challenging, but they are ideal systems for experiments studying the effect of particular gut bacteria on physiology [189]. Germ-free mice colonized by indole producers could be studied and compared with those colonized by indole non-producers, and effects on metabolism, blood metabolites and other physiological parameters monitored.

It is thus apparent that the indole project spans many different fields of study, and it would be presumptuous in the extreme to suppose that any one individual or research group could pursue all the leads. However, the rewards for studying these various aspects of indole signalling could be substantial, and one hopes that the elucidation of the pulse mechanism is just the beginning of a long road of discovery in the field.

Chapter 7

Concluding Remarks

> "I did, what I had to do. And saw it through, without exemption."
>
> Frank Sinatra (*My Way*)

This Thesis has been devoted primarily to the development of a new technique capable of quantitatively studying the passive diffusion of drugs through model lipid membranes. We applied this optofluidic assay to the investigation of the lipid permeability of the antibiotic norfloxacin, and validated theoretical predictions of the pH dependence of norfloxacin permeability. We also demonstrated the importance of lipid composition on drug permeability by measuring norfloxacin permeability across lipid bilayers constructed from different lipid molecules.

By reconstituting OmpF pores in our vesicle membranes, we were able to develop a new technique for investigating antibiotic transport through these membrane protein nanopores. Our reductionist approach allowed us to quantify drug transport through the lipid membranes and pores separately, and enabled us to propose a physical mechanism that explains the pH dependence of antibiotic susceptibility in *E. coli*.

We also used our technique to measure the lipid permeability of the antibiotic tetracycline. Our measurements agreed well with theoretical predictions of tetracycline permeability that were based on considerations of the multiple possible protonation states of the molecule. Our technological developments have laid the foundations for a detailed investigation into the environmental factors that affect the lipid permeability

of different drug molecules, which we believe will be of great use in optimizing drug delivery and efficiency.

Finally, we presented results on a novel signalling mechanism that we discovered in *E. coli*. In our present battle against antibacterial resistance, the importance of understanding bacterial communication and stress responses cannot be overstated. We believe that the indole pulse signal could be a vital component of the bacterial arsenal against external stress, and future investigations have been planned in an attempt to unlock the indole pulse on a molecular level.

As discussed in the Outlook chapter 6, we have many different avenues to investigate, both from the perspectives of technology development and fundamental molecular biology. With the battle against drug resistant pathogens looming large, one must leave no stone unturned in the quest for a solution that would prevent a return to the dark ages of pre-antibiotic medicine.

However, the beauty of biology is that there are many unknowns, and one hopes that with new discoveries, no medical problem will prove insurmountable. In spite of all the scientific advancement over the past century, we are still a long way from a complete understanding of how even a single living cell functions. The work presented in this Thesis is but an incremental advance in this direction. Shakespeare's words still ring true today – there are, indeed, far more things in this World, than are dreamt of in our philosophy. With perseverance, however, we might still find some of them.

Appendix A

Protocol for the Optofluidic Permeability Assay

1. Prepare DPhPC (or other lipid) vesicles (in 200 mM sucrose, in 5 mM phosphate buffer made by mixing 5 mM solutions of KH_2PO_4 and K_2HPO_4 in deionized (Millipore) water in a beaker till the pH reaches 7). For pH 5, use 5 mM acetic acid as the buffer.

2. Prepare the PDMS chip by pouring approximately 36 g of the PDMS mixture (9:1 elastomer:curing agent ratio) onto the Si mold placed in a round plastic petri dish (for smaller molds, use a flat square weighing boat, and add approximately 21 g of the PDMS mixture). Make sure the petri dish/weighing boat is lined with Aluminum foil beforehand to ease removal of the mold and PDMS after baking. The PDMS should be baked for 55 minutes in the oven at 60 °C. Removal of PDMS from the Si mold must be done carefully using a scalpel, cutting away any PDMS from the base of the mold using a shallow cutting angle. Avoid putting pressure on the mold at a steep angle with the scalpel as this can fracture the mold.

3. The PDMS chip should be cut out as a neat cuboid using a sharp blade; it is easiest to cut this while keeping the PDMS flat on a thick glass slide on a table top.

4. Inlet/outlet columns should be punched using a 1.5 mm biopsy punch (Miltex). Use some spare (flat), set PDMS as the base on top of which you hold the PDMS chip in which the columns are being punched. Punch through the entire thickness of the chip and use the plunger on the punch to remove any loose PDMS pieces from the column.

5. Plasma bind the PDMS chip to the coverslips used (for the water immersion objective, it is helpful to use 50 x 40 mm Type I coverslips, Assistent, Germany; the broader coverslips help prevent the movement and evaporation of water). For this process:

- First clean the PDMS chip with 96% ethanol and blow dry with nitrogen gas.
- Use 'magic' scotch tape to clean both sides of the chip thoroughly, especially the surface that is to be bonded. Simply deposit the tape on the side being cleaned, and peel off to remove dirt/dust. Repeat 6-8 times on the side being bonded.
- Use the tape to clean the coverslip in a similar manner.
- Place the PDMS chip and coverslip in a plasma cleaner (surfaces to be bonded facing up) and press PUMP, adjust power to full (setting 10 W), timer to 10 s and then wait 5 minutes.
- Press GAS, adjust to 25 sccm level and wait 5 minutes.
- Press GENERATE. The count down will begin and stop after 10 s.
- Immediately press (in order) GAS, VENTILATE and (after 5-10 s) PUMP. As soon as the door is released, press the two surfaces to each other and move over the edges of the chip (from the glass side) with flat tweezers to ensure bonding. This must be done within 60 seconds of the plasma being generated.
- Place the bonded chip in the oven at 60 ^{o}C for 5-10 minutes to enhance adhesion.

6. Separately, filter (0.22 μm Millipore filters) the buffer to be used in the experiment (approximately 1 ml) into an Eppendorf tube.

7. Prepare 2 mM norfloxacin in the filtered buffer. The norfloxacin stock (around 50 mM) is prepared in deionized water by reducing the pH to about 3 (using 10% HCl) and then slowly increasing it to a pH of 5 by adding 10% KOH. The norfloxacin only dissolves in water at an acidic pH and is not stable at these stock concentrations above a pH of 5.

8. Switch on the neMESYS syringe pump system. Switch on the software and fill the syringe with Millipore water through the tube that will be connected to the chip outlet. Use a flow rate **increment** of 100 μl/hr and a suitably high flow rate ($\sim$ 8,000 μl/hr) for this step.

9. Through the other tube (yellow on the graphical user interface), pour out the water till the syringe level is about 80 μl. Stop the flow.

10. Switch back to the flow channel that will be used in the experiment (blue channel in the software) and ensure the flow rate increment is set to 1 μl/hr.

11. TROUBLESHOOTING: Ensure that there are no air bubbles anywhere in the tubing/syringe. If there are bubbles, repeat the above steps till they are completely removed. If simply repeating the above process is not enough to get rid of the bubbles, unscrew the syringe from the pump and tap the syringe so that the bubbles move to the mouth of the syringe. Use the software to switch the flow to the other channel (yellow) and manually push out the liquid completely. Perform a "Reference Move" using the software (IMPORTANT: THE SYRINGE SHOULD BE REMOVED FROM THE HOLDER WHILE PERFORMING A REFERENCE MOVE); this will move the syringe holder back to the zero position. Reattach the syringe, switch back to the channel used in the experiment, and repeat steps 8-10 above. You should have now removed all the air bubbles.

12. Switch on the Monoscan 2000 (Monochromator), open the software and set the wavelength to 340 nm (norfloxacin excitation wavelength used).

13. Once the chip is bonded, use a 1 ml syringe and type 11 hypodermic needle to fill the chip with the filtered buffer. Ensure no air bubbles form in the chip. Since you are filling the chip from all three columns, there will be air trapped in

the channels. Wait till this disappears before starting the experiment (PDMS is permeable to air). If there are air bubbles in the columns, it is possible to remove them by carefully pulling them out with the syringe needle. Take appropriate (sharps) precautions while working with the needles and dispose of them in the Sharps Hazards bin.

14. Cut a pipette tip (200 µl, Axygen) near the taper at the tip to obtain a slightly wider bore. Take up 40 µl of the 2 mM norfloxacin solution into this pipette tip and stick the pipette tip into one of the inlets (it should be pressed approximately halfway down the column). Repeat the same procedure for the vesicles solution in the other inlet (the volume does not **have** to be 40 µl, it depends on how long you wish to run the experiment). Blot away any external liquid at the inlets using dust-free tissue paper (Kimtech).

15. Turn on the camera and the software (µManager 1.4). Set the exposure to 2 ms, bin 2, clearing pre-sequence (if using the Evolve) or exposure 10 ms, bin 4, clearing pre-sequence if using the optiMOS. Remove the lens cap.

16. Put a droplet of Millipore water on the objective (if water immersion) and place the coverslip/microfluidic device on it such that the T junction is in the field of view. For the moment, use the simple LED light source for viewing and aligning the position of the chip.

17. Find the T junction by moving the stage or moving the chip by hand. Once found, ensure that the channel lines are straight (if not, rotate the chip by hand till they are straight). Then fix the coverslip in position using tape.

18. Use the syringe pump to push the liquid out of the tubing (Upchurch 1520G) so that a droplet forms on the end of the tubing. Once this happens, stop the flow and insert the tubing into the outlet column in the chip.

19. Set the pump to a flow rate of -30 µl/hr flow to pull the solutions into the microfluidic network.

20. Turn on the EQ99FC light source by switching on the main power supply, toggling the ENABLE switch, waiting 5 seconds, then toggling the OPERATE

switch. Remember, for these switches, UP is ON, and DOWN is OFF. You MUST wear goggles, and keep the shielding in place when the UV light is on. On the Olympus IX73 Setup, you simply have to switch on the Prior Lumen lamp (remember, once this has been turned on it must run for at least 30-45 minutes, and after switching it off let it cool for 1 hour before using it again. These precautions are not required on the EQ99FC light source, though one should ideally avoid switching this source on and off repeatedly as well).

21. Once the EQ99FC light source is active (takes about 90-120 seconds after switching on), focus the image at the T junction. Switch off the LED light source and set the EM gain to 100 (Evolve).

22. Wait till the two flows are clearly seen (i.e, the autofluorescence of the norfloxacin will cause the flow arriving from the norfloxacin inlet to be bright whereas the vesicle flow will be dark).

23. Once the fluorescence intensity stops increasing, reduce the flow speed to about -3 μl/hr.

24. Wait till the flows settle to the lower value and vesicles start appearing.

25. Once a steady, suitably slow flow rate has been reached, move the chip into the desired viewing position.

26. Change the settings in the MultiD Acquisition tab in μManager to 5000 frames with 0 ms intervals (fastest acquisition) and run a preliminary video acquisition. Remember to save the images as a single stack file and choose an appropriate name and folder to save the stacks to. Since the amount of data generated is large, it is advisable to save the files directly to an external hard-drive. Check this video to ensure that the focal plane is appropriate for the vesicles being detected, and that each vesicle is being detected for 6-10 frames at least. Adjust the focus/flow rate accordingly.

27. Once set, go to Tools → Script Panel and run the Repeat Acquisition beanshell script as required. This basically runs the MultiD acquisition script with its current settings repeatedly for a specified amount of time.

28. IMPORTANT: If the images start going out of focus, you should immediately stop the acquisition and delete any videos it might have affected. You may need to adjust the focus quite often till it settles. If the water has dried completely, you will need to put another droplet of water on the objective. This is done by first switching off the light source via the OPERATE switch, removing the tape holding the device in place and raising the coverslip gently. This allows access by the dropper for the water on the objective. Place the coverslip back in position, make sure the viewing point is the same, tape it down, switch on OPERATE and continue the acquisition. Repeat till you have about 40-50 good movies (5,000 frames each) at one position. Ideally, do 2-3 viewing points in one experiment.

29. On occasion, there might be some imbalance in the flow due to a slight asymmetry in the optical table or the inlet fluidic resistance. It is important to balance the flows to ensure a 1:1 mixing of the two solutions. You may add/remove a small amount of solution from one of the inlets to balance this. If you suspect one of the flows has been blocked (this occasionally happens in the vesicle flow due to a build up of lipid aggregates at the vesicle inlet reservoir), increase the flow rate substantially ($\sim$ 150-200 μl/hr) till the blockage is removed (you should see it flow through your field of view). Reduce the flow rate and restart acquisition once the desired flow rate is achieved. It is also advisable to check that the lipid aggregate has completely cleared the channel and reached the outlet reservoir before restarting acquisition.

30. After acquiring your data, it is always a good idea to scan through the part of the chip you have been studying to ensure that there has been no build up of lipid deposits that could have affected the flows. You may do this at regular intervals during the experiment. Lipid deposits can block the flows and distort the measurements of time taken for the vesicles to travel between detection positions, so this is an important factor to check.

31. Once complete, switch off the light source first (turn off OPERATE, ENABLE and finally the main power switch for the EQ99FC; for the Prior lamp simply turn off the main switch). Switch off the camera (software first, then hardware; remember to cover the camera with the lens cap). Stop the flows completely and

disconnect the syringe pump from the chip by removing the tubing. Pour out the liquid from the syringe into a waste container and then switch off the syringe pump (software first, then mains). Switch off the monochromator software and then hardware. Ensure the LED light source is also off.

32. Remove the chip from the setup and dispose of it in the Sharps bin. Blot away any remaining water from the objective using lens cleaning tissues (Thorlabs).

33. Cover the objective with a lens tissue, and close down the setup.

34. All liquids should be disposed off in the Aqueous/Unchlorinated Waste bottles as appropriate.

Appendix B

Microfluidic Chip Designs

The outlines of the 3 microfluidic chip designs used are presented. In all three designs, the inlet reservoirs show the two sets of filter pillars used, the first being a coarse filter (75 μm gaps) and the second a fine filter (40 μm gaps). These were included to prevent large lipid aggregates from entering the channels and blocking the flows.

Photolithography of the 'Short' design Si mold

A silicon substrate was covered with a thin layer of adhesion promoter (Omnicoat, Microchem, spin coating: 2,000 rpm for 30 seconds) following which a layer of SU-8 2025 (Microchem) was deposited (2,000 rpm, 30 seconds). This was pre-baked (2 mins at 65 °C, 5 mins at 95 °C) and selectively exposed to UV (12 seconds, 365-405 nm, 20 $mWcm^{-2}$) through a bespoke pellicle mask created using the AutoCAD design (Photo-data Ltd.). The sample was then post-baked (1 min at 65 °C, 3 mins at 95 °C), developed for 3 mins, dried with N_2 and hard baked for 5 mins at 95 °C. This protocol yields channels with a height of 43 μm. The shallower channel is advantageous, since it keeps the vesicles in better focus during imaging.

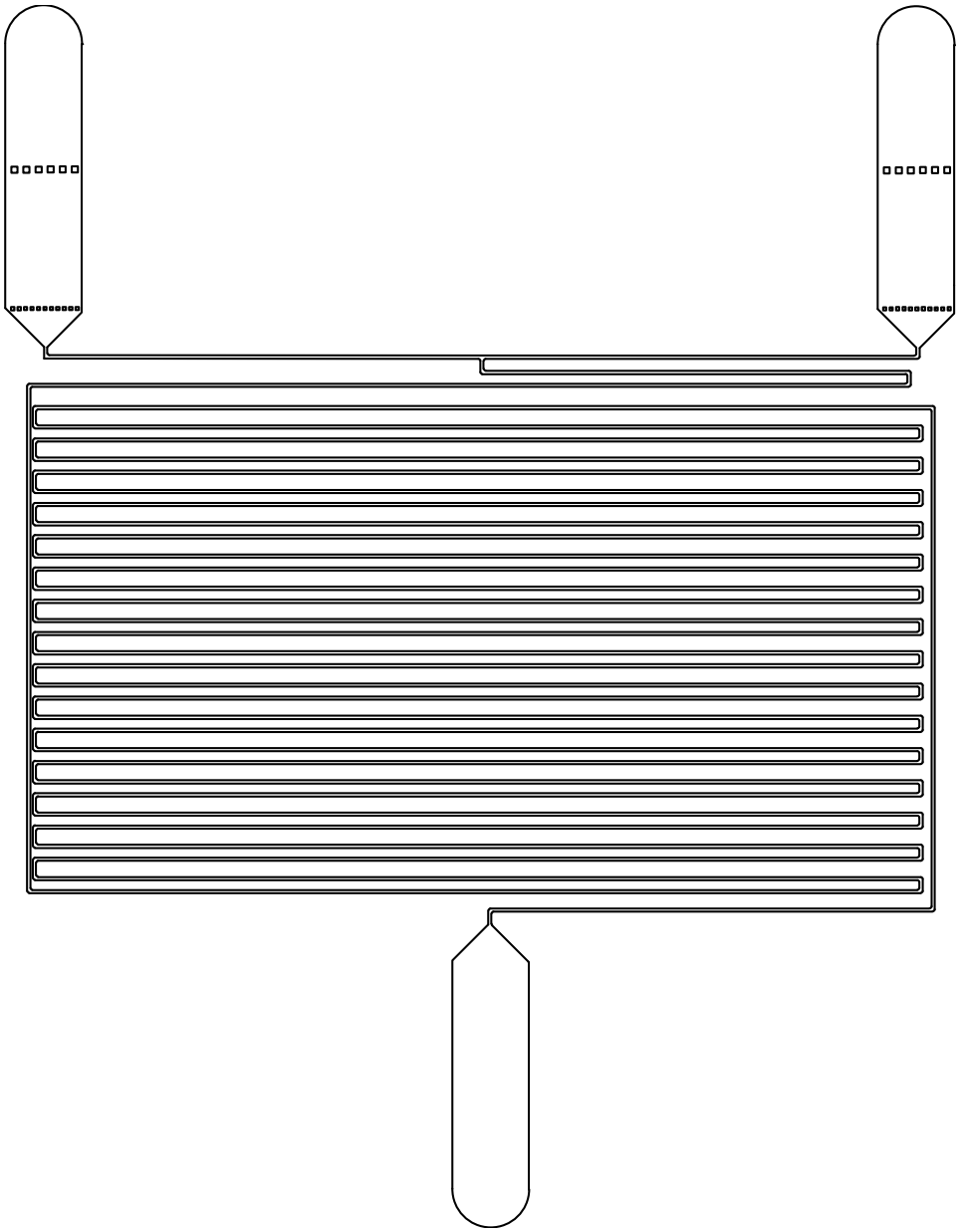

Figure B.1 – 'Long' chip design. The length from the T junction to the outlet reservoir is about 380 mm. Channels are 40 μm wide and 50 μm high. This design is used for experiments where significant drug diffusion across the vesicle membrane occurs on a timescale of minutes. The design contains 15 different viewpoints. This design was used for the norfloxacin-DPhPC results presented in chapter 3.

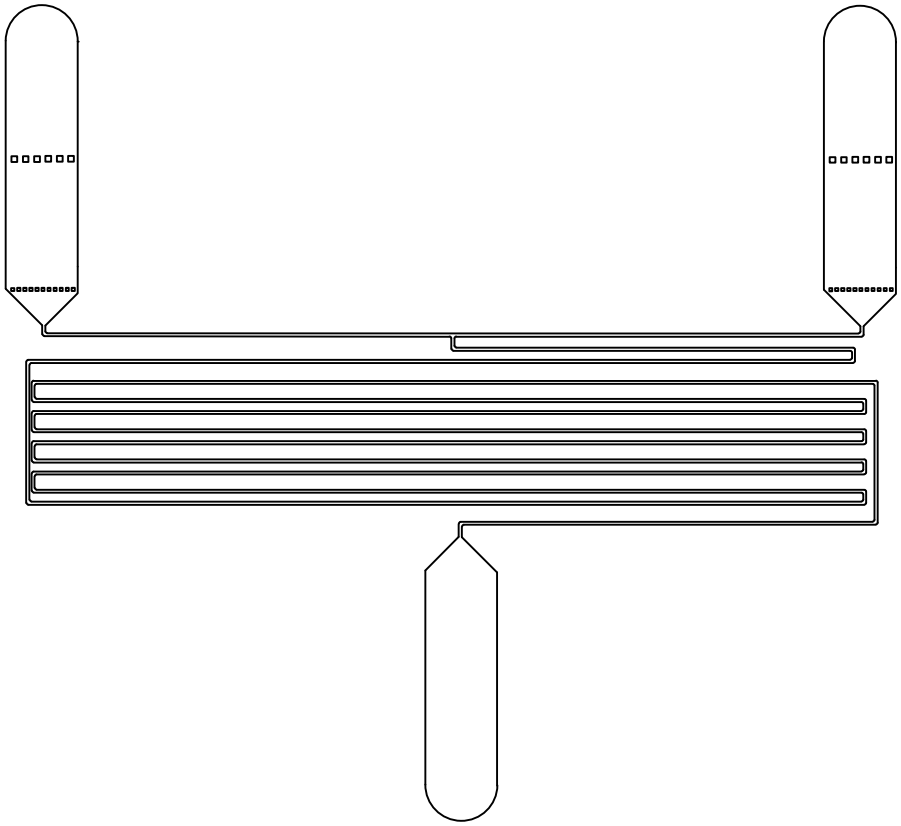

Figure B.2 – 'Medium' chip design. The length from the T junction to the outlet reservoir is about 127 mm. Channels are 40 μm wide and 50 μm high. This design is used for experiments where significant drug diffusion across the vesicle membrane occurs on a timescale of minutes. The design contains 4 different viewpoints. This design was used for the Quantum Dot measurements presented in chapter 3.

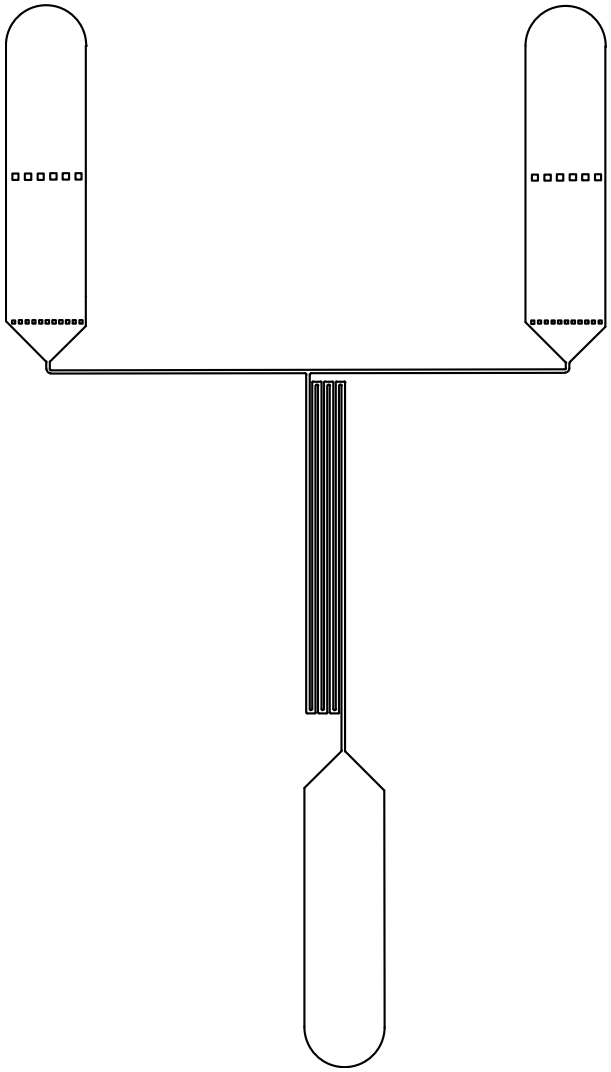

Figure B.3 – 'Short' chip design. The length from the T junction to the outlet reservoir is about 28 mm. Furthermore, the initial ($t = 0$) viewpoint can be much closer to the T junction than in the other designs; the detection point typically used was reached by vesicles within a second after passing the T junction. The channel width is 40 μm and the height is 43 μm. This design was used for all the fast permeation experiments described in this Thesis – the norfloxacin-DOPC, tetracycline-DPhPC (chapter 3) and OmpF measurements (chapter 4). It is also the design being used to study Ca^{2+} transport through hemolysin nanopores (chapter 6).

Appendix C

Theoretical basis for the linear relationship of $\Delta I(0)$ vs R

The autofluorescence intensity (I) of drug molecules is proportional to the number of molecules (N) being imaged:

$$I = \alpha N = \alpha c V \tag{C.1}$$

where c is the concentration of the drug molecules in the imaging volume V.

However, in our image analysis, we always calculate the intensities in a 5×5 pixel area around the centre of the vesicle. Therefore, we can simplify the above equation to:

$$I = \beta c l \tag{C.2}$$

where β is the modified proportionality constant which includes the constant area term, and l now refers to the height of the imaging volume.

Now, we have:

$$\Delta I = \frac{I_{out} - I_{in}}{I_{out}} \tag{C.3}$$

Using our analysis from above:

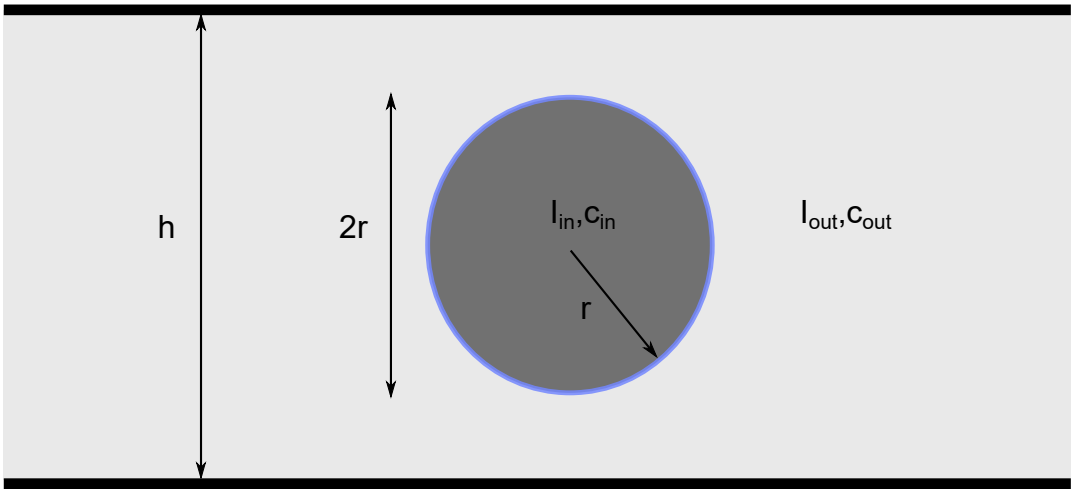

Figure C.1 – Schematic depicting a vesicle of radius r in a microfluidic channel of height h. Drug fluorescence intensity outside the vesicle I_{out} corresponds to a drug concentration c_{out}. However, the fluorescence I_{in} measured at the centre of the vesicle contains fluorescence contributions due to both the drug inside the vesicle (c_{in}) as well as background fluorescence due to the drug molecules that are present in the space between the vesicle and the channel walls.

$$I_{out} = \beta h c_{out} \tag{C.4}$$

and

$$I_{in} = \beta(h - 2r)c_{out} + \beta 2r c_{in} \tag{C.5}$$

where h is the height of the microfluidic channel and r is the vesicle radius (Figure C.1). Using the above equations, ΔI reduces to:

$$\Delta I = \frac{2r}{h} \times \left(\frac{c_{out} - c_{in}}{c_{out}} \right) \tag{C.6}$$

But at $t = 0$, $c_{in}(0) = 0$. Therefore, we find:

$$\Delta I(0) = \frac{2r}{h} \tag{C.7}$$

We thus obtain a linear relation between $\Delta I(0)$ and vesicle radius r in our calibration curves (for example, see Figure 2.13). In practice, there are other optical effects which

prevent us from realising a $\Delta I(0)$ value of 1 when $2r = h$. However, this analysis offers a simple explanation for the linear trends we observe in our experiment.

Appendix D

List of Publications

1. J. Cama, H. Bajaj, S. Pagliara, T. Maier, Y. Braun, M. Winterhalter and U. F. Keyser. Quantification of Fluoroquinolone Uptake through the Outer Membrane Channel OmpF of *Escherichia coli*. *Journal of the American Chemical Society*, 137(43):13836-13843, 2015.

2. J. Cama, C. Chimerel, S. Pagliara, A. Javer and U. F. Keyser. A label-free microfluidic assay to quantitatively study antibiotic diffusion through lipid membranes. *Lab on a Chip*, 14:2303-2308, 2014.

3. H. Gaimster, J. Cama, S. Hernandez-Ainsa, U. F. Keyser and D. K. Summers. The indole pulse: a new perspective on indole signalling in *Escherichia coli*. *PLoS ONE*, 9(4)e93168, 2014.

4. S. Purushothaman, J. Cama and U. F. Keyser. Dependence of Norfloxacin diffusion across bilayers on lipid composition. *Submitted, under revision*.

Bibliography

[1] S. Duckett. Ernest Duchesne and the concept of fungal antibiotic therapy. *Lancet*, 354(9195):2068–2071, 1999.

[2] A. Fleming. On the antibacterial action of cultures of a Penicillium, with special reference to their use in the isolation of B. influenzae. *British Journal of Experimental Pathology*, 10:226–236, 1929.

[3] A. Fleming. Penicillin. In *Nobel Lecture*, 1945.

[4] J. Davies and D. Davies. Origins and Evolution of Antibiotic Resistance. *Microbiology and Molecular Biology Reviews*, 74(3):417–433, 2010.

[5] E. P. Abraham and E. Chain. An Enzyme from Bacteria able to Destroy Penicillin. *Nature*, 3713:837, 1940.

[6] V. M. D'Costa, K. M. McGrann, D. W. Hughes, and G. D. Wright. Sampling the Antibiotic Resistome. *Science*, 311:374–378, 2006.

[7] J. Davies. Vicious circles: looking back on resistance plasmids. *Genetics*, 139(4): 1465–1468, 1995.

[8] T. Watanabe. Infective heredity of multiple drug resistance in bacteria. *Bacteriological Reviews*, 27:87–115, 1963.

[9] E. Meynell, G. G. Meynell, and N. Datta. Phylogenetic relationships of drug-resistance factors and other transmissible bacterial plasmids. *Bacteriological Reviews*, 32(1):55–83, 1968.

[10] M. A. Kohanski, D. J. Dwyer, and J. J. Collins. How antibiotics kill bacteria: from targets to networks. *Nature Reviews Microbiology*, 8(6):423–435, 2010.

[11] G. E. Flaten, A. B. Dhanikula, K. Luthman, and M. Brandl. Drug permeability across a phospholipid vesicle based barrier: A novel approach for studying passive diffusion. *European Journal of Pharmaceutical Sciences*, 27:80–90, 2006.

[12] A. K. Mandagere, T. N. Thompson, and K-K. Hwang. Graphical model for estimating oral bioavailability of drugs in humans and other species from their Caco-2 permeability and in vitro liver enzyme metabolic stability rates. *Journal of Medicinal Chemistry*, 45:304–311, 2002.

[13] J. Cama, C. Chimerel, S. Pagliara, A. Javer, and U. F. Keyser. A label-free microfluidic assay to quantitatively study antibiotic diffusion through lipid membranes. *Lab on a Chip*, 14:2303–2308, 2014.

[14] A. Leo, C. Hansch, and D. Elkins. Partition coefficients and their Uses. *Chemical Reviews*, 71(6):525–616, 1971.

[15] W. D. Stein. *The Movement of Molecules Across Cell Membranes*. Academic Press Inc., 1st edition, 1967. ISBN 978-0-12-664650-4.

[16] M. Sinensky. Homeoviscous adaptation–a homeostatic process that regulates the viscosity of membrane lipids in Escherichia coli. *Proceedings of the National Academy of Sciences of the United States of America*, 71(2):522–525, 1974.

[17] Y. Yano, A. Nakayama, K. Ishihara, and H. Saito. Adaptive changes in membrane lipids of barophilic bacteria in response to changes in growth pressure. *Applied and Environmental Microbiology*, 64(2):479–485, 1998.

[18] Y. Sambuy, I. De Angelis, G. Ranaldi, M. L. Scarino, A. Stammati, and F. Zucco. The Caco-2 cell line as a model of the intestinal barrier: Influence of cell and culture-related factors on Caco-2 cell functional characteristics. *Cell Biology and Toxicology*, 21:1–26, 2005.

[19] P. Kuhn, K. Eyer, S. Allner, D. Lombardi, and P. S. Dittrich. A microfluidic vesicle screening platform: Monitoring the lipid membrane permeability of tetracyclines. *Analytical Chemistry*, 83:8877–8885, 2011.

[20] M. Kansy, F. Senner, and K. Gubernator. Physicochemical high throughput screening: Parallel artificial membrane permeation assay in the description of passive absorption processes. *Journal of Medicinal Chemistry*, 41(7):1007–1010, 1998.

[21] A. Avdeef, S. Bendels, L. Di, B. Faller, M. Kansy, K. Sugano, and Y. Yamauchi. PAMPA-Critical Factors for Better Predictions of Absorption. *Journal of Pharmaceutical Sciences*, 96(11):2893–2909, 2007.

[22] D. Galinis-Luciani, L. Nguyen, and M. Yazdanian. Is PAMPA a Useful Tool for Discovery? *Journal of Pharmaceutical Sciences*, 96(11):2886–2892, 2007.

[23] J-M. Pagès, C. E. James, and M. Winterhalter. The porin and the permeating antibiotic: a selective diffusion barrier in Gram-negative bacteria. *Nature Reviews Microbiology*, 6(12):893–903, December 2008.

[24] J. M. Diver, L. J. Piddock, and R. Wise. The accumulation of five quinolone antibacterial agents by Escherichia coli. *The Journal of Antimicrobial Chemotherapy*, 25(3):319–333, 1990.

[25] K. Hirai, H. Aoyama, T. Irikura, S. Iyobe, and S. Mitsuhashi. Differences in Susceptibility to Quinolones of Outer Membrane Mutants of Salmonella typhimurium and Escherichia coli. *Antimicrobial Agents and Chemotherapy*, 29 (3):535–538, 1986.

[26] J. S. Chapman and N. H. Georgopapdakou. Routes of quinolone permeation in Escherichia coli. *Antimicrobial Agents and Chemotherapy*, 32(4):438–442, 1988.

[27] S. Kaščáková, L. Maigre, J. Chevalier, M. Réfrégiers, and J. M. Pagès. Antibiotic transport in resistant bacteria: Synchrotron UV fluorescence microscopy to determine antibiotic accumulation with single cell resolution. *PLoS ONE*, 7(6): e38624, 2012.

[28] P. G. Mortimer and L. J. Piddock. A comparison of methods used for measuring the accumulation of quinolones by Enterobacteriaceae, Pseudomonas aeruginosa and Staphylococcus aureus. *The Journal of Antimicrobial Chemotherapy*, 28(5): 639–653, 1991.

[29] J. R. Mansfield, K. W. Gossage, C. C. Hoyt, and R. M. Levenson. Autofluorescence removal, multiplexing, and automated analysis methods for in-vivo fluorescence imaging. *Journal of Biomedical Optics*, 10(4):41207, 2005.

[30] D. C. Hooper. Mechanisms of action and resistance of older and newer fluoroquinolones. *Clinical Infectious Diseases*, 31(Suppl 2):S24–S28, 2000.

[31] D. C. Hooper. Mechanisms of action of antimicrobials: focus on fluoroquinolones. *Clinical Infectious Diseases*, 32(Suppl 1):S9–S15, 2001.

[32] C. M. Oliphant and G. M. Green. Quinolones: A comprehensive review. *American Family Physician*, 65(3):455–464, 2002.

[33] P. Mueller, D. O. Rudin, H. T. Tien, and W. C. Wescott. Reconstitution of cell membrane structure in vitro and its transformation into an excitable system. *Nature*, 194:979–980, 1962.

[34] M. Montal and P. Mueller. Formation of bimolecular membranes from lipid monolayers and a study of their electrical properties. *Proceedings of the National Academy of Sciences of the United States of America*, 69(12):3561–3566, 1972.

[35] B. J. Frisken, C. Asman, and P. J. Patty. Studies of Vesicle Extrusion. *Langmuir*, 16(3):928–933, 2000.

[36] M. I. Angelova and D. S. Dimitrov. Liposome Electro formation. *Faraday Discussions of the Chemical Society*, 81:303–311, 1986.

[37] T. Pott, H. Bouvrais, and P. Méléard. Giant unilamellar vesicle formation under physiologically relevant conditions. *Chemistry and Physics of Lipids*, 154(2):115–119, 2008.

[38] R. Dimova, S. Aranda, N. Bezlyepkina, V. Nikolov, K. A. Riske, and R. Lipowsky. A practical guide to giant vesicles. Probing the membrane nanoregime via optical microscopy. *Journal of Physics: Condensed Matter*, 18(28): S1151–S1176, 2006.

[39] Q. Al-Awqati. One hundred years of membrane permeability: does Overton still rule? *Nature Cell Biology*, 1(8):E201–E202, 1999.

[40] A. Missner and P. Pohl. 110 years of the Meyer-Overton rule: Predicting membrane permeability of gases and other small compounds. *Chemphyschem*, 10(9-10):1405–1414, 2009.

[41] G. M. Whitesides. The origins and the future of microfluidics. *Nature*, 442: 368–373, 2006.

[42] A. P. Tan, J. S. Dudani, A. Arshi, R. J. Lee, H. T. K. Tse, D. R. Gossett, and D. Di Carlo. Continuous-flow cytomorphological staining and analysis. *Lab on a Chip*, 14:522–31, 2014.

[43] M. T. Guo, A. Rotem, J. A. Heyman, and D. A. Weitz. Droplet microfluidics for high-throughput biological assays. *Lab on a Chip*, 12:2146, 2012.

[44] B. Herranz-Blanco, L. R. Arriaga, E. Mäkilä, A. Correia, N. Shrestha, S. Mirza, D. A. Weitz, J. Salonen, J. Hirvonen, and H. A. Santos. Microfluidic assembly of multistage porous silicon-lipid vesicles for controlled drug release. *Lab on a Chip*, 14(6):1083–6, 2014.

[45] F. K. Balagaddé, L. You, C. L. Hansen, F. H. Arnold, and S. R. Quake. Long-term monitoring of bacteria undergoing programmed population control in a microchemostat. *Science*, 309(5731):137–140, 2005.

[46] N. R. Pollock, J. P. Rolland, S. Kumar, P. D. Beattie, S. Jain, F. Noubary, V. L. Wong, R. A. Pohlmann, U. S. Ryan, and G. M. Whitesides. A Paper-Based Multiplexed Transaminase Test for Low-Cost, Point-of-Care Liver Function Testing. *Science Translational Medicine*, 4(152):152ra129–152ra129, 2012.

[47] R. N. Zare and S. Kim. Microfluidic platforms for single-cell analysis. *Annual Review of Biomedical Engineering*, 12:187–201, 2010.

[48] A. R. Wheeler, W. R. Throndset, R. J. Whelan, A. M. Leach, R. N. Zare, Y. H. Liao, K. Farrell, I. D. Manger, and A. Daridon. Microfluidic device for single-cell analysis. *Analytical Chemistry*, 75(14):3581–3586, 2003.

[49] J. L. Wilson, S. Suri, A. Singh, C. A. Rivet, H. Lu, and T. C. McDevitt. Single-Cell Analysis of Embryoid Body Heterogeneity Using Microfluidic Trapping Assay. *Biomedical Microdevices*, 16(1):79–90, 2014.

[50] Y. Alapan, J. A. Little, and U. A. Gurkan. Heterogeneous Red Blood Cell Adhesion and Deformability in Sickle Cell Disease. *Scientific Reports*, pages srep07173:1–8, 2014.

[51] V. Chokkalingam, J. Tel, F. Wimmers, X. Liu, S. Semenov, J. Thiele, C. G. Figdor, and W. T. S. Huck. Probing cellular heterogeneity in cytokine-secreting immune cells using droplet-based microfluidics. *Lab on a Chip*, 13(24):4740–4, 2013.

[52] S. Pagliara, K. Franze, C. R. McClain, G. W. Wylde, C. L. Fisher, R. J. M. Franklin, A. J. Kabla, U. F. Keyser, and K. J. Chalut. Auxetic nuclei in embryonic stem cells exiting pluripotency. *Nature Materials*, 13(6):638–44, 2014.

[53] D. Qin, Y. Xia, and G. M. Whitesides. Soft lithography for micro- and nanoscale patterning. *Nature Protocols*, 5(3):491–502, 2010.

[54] S. Bhattacharya, A. Datta, J. M. Berg, and S. Gangopadhyay. Studies on surface wettability of poly(dimethyl) siloxane (PDMS) and glass under oxygen-plasma treatment and correlation with bond strength. *Journal of Microelectromechanical Systems*, 14(3):590–597, 2005.

[55] M. A. Eddings, M. A. Johnson, and B. K. Gale. Determining the optimal PDMS-PDMS bonding technique for microfluidic devices. *Journal of Micromechanics and Microengineering*, 18:067001, 2008.

[56] T. Robinson, P. Kuhn, K. Eyer, and P. S. Dittrich. Microfluidic trapping of giant unilamellar vesicles to study transport through a membrane pore. *Biomicrofluidics*, 7:044105, 2013.

[57] N. Stuurman, N. Amdodaj, and R. Vale. μManager: Open Source Software for Light Microscope Imaging. *Microscopy Today*, 15:42–43, 2007.

[58] G. M. Whitesides, E. Ostuni, S. Takayama, X. Jiang, and D. E. Ingber. Soft Lithography in Biology and Biochemistry. *Annual Review of Biomedical Engineering*, 3:335–373, 2001.

[59] M. H. Horrocks, L. Rajah, P. Jönsson, M. Kjaergaard, M. Vendruscolo, T. P. J. Knowles, and D. Klenerman. Single-molecule measurements of transient biomolecular complexes through microfluidic dilution. *Analytical Chemistry*, 85:6855–6859, 2013.

[60] C. Chimerel. *Passive transport through biological membranes*. PhD thesis, 2012.

[61] B. Alberts, A. Johnson, J. Lewis, M. Raff, K. Roberts, and P. Walker. *Molecular Biology of the Cell*. Garland Science, 5th edition, 2008. ISBN 987-0815341055.

[62] O. S. Andersen and R. E. Koeppe. Bilayer thickness and membrane protein function: an energetic perspective. *Annual Review of Biophysics and Biomolecular Structure*, 36:107–130, 2007.

[63] A. Finkelstein. Water and nonelectrolyte permeability of lipid bilayer membranes. *The Journal of General Physiology*, 68:127–135, 1976.

[64] Z. Li and D. E. Vance. Phosphatidylcholine and choline homeostasis. *Journal of Lipid Research*, 49(6):1187–1194, 2008.

[65] F. Martínez-Morales, M. Schobert, I. M. López-Lara, and O. Geiger. Pathways for phosphatidylcholine biosynthesis in bacteria. *Microbiology*, 149(12):3461–3471, 2003.

[66] J. H. Exton. Phosphatidylcholine breakdown and signal transduction. *Biochimica et Biophysica Acta - Lipids and Lipid Metabolism*, 1212(1):26–42, 1994.

[67] C. Sohlenkamp, I. M. López-Lara, and O. Geiger. Biosynthesis of phosphatidylcholine in bacteria. *Progress in Lipid Research*, 42(2):115–162, 2003.

[68] T. J. McIntosh. Hydration properties of lamellar and non-lamellar phases of phosphatidylcholine and phospatidylethanolamine. *Chemistry and Physics of Lipids*, 81(2):117–131, 1996.

[69] W. R. Redwood, F. R. Pfeiffer, J. A. Weisbach, and T. E. Thompson. Physical properties of bilayer membranes formed from a synthetic saturated phospholipid in n-decane. *Biochimica et Biophysica Acta*, 233(1):1–6, 1971.

[70] W. C. Hung, F. Y. Chen, and H. W. Huang. Order-disorder transition in bilayers of diphytanoyl phosphatidylcholine. *Biochimica et Biophysica Acta - Biomembranes*, 1467(1):198–206, 2000.

[71] C-H. Hsieh, S-C. Sue, P-C. Lyu, and W-g. Wu. Membrane Packing Geometry of Diphytanoylphosphatidylcholine Is Highly Sensitive to Hydration: Phospholipid Polymorphism Induced by Molecular Rearrangement in the Headgroup Region. *Biophysical Journal*, 73:870–877, 1997.

[72] H. Nikaido and D. G. Thanassi. Penetration of lipophilic agents with multiple protonation sites into bacterial cells: Tetracyclines and Fluoroquinolones as examples. *Antimicrobial Agents and Chemotherapy*, 37(7):1393–1399, 1993.

[73] P. Zhang, H. Li, S. Yao, and W. Wang. Effects of pH and polarity on the excited states of norfloxacin and its 4'-N-acetyl derivative: A steady-state and time-resolved study. *Science China Chemistry*, 57(3):409–416, 2014.

[74] J. Ashby, L. J. V. Piddock, and R. Wise. An investigation of the hydrophobicity of the quinolones. *Journal of Antimicrobial Chemotherapy*, (16):805–808, 1985.

[75] J. C. Mathai, S. Tristram-Nagle, J. F. Nagle, and M. L. Zeidel. Structural determinants of water permeability through the lipid membrane. *The Journal of General Physiology*, 131(1):69–76, 2008.

[76] H. I. Petrache, S. W. Dodd, and M. F. Brown. Area per lipid and acyl length distributions in fluid phosphatidylcholines determined by (2)H NMR spectroscopy. *Biophysical Journal*, 79(6):3172–3192, 2000.

[77] S. Tristram-Nagle, D. J. Kim, N. Akhunzada, N. Kučerka, J. C. Mathai, J. Katsaras, M. Zeidel, and J. F. Nagle. Structure and Water Permeability of Fully Hydrated DiphytanoylPC. *Chemistry and Physics of Lipids*, 163(6):630–637, 2010.

[78] W. Shinoda and M. Mikami. Molecular dynamics study on the effects of chain branching on the physical properties of lipid bilayers: 2. Permeability. *The Journal of Physical Chemistry B*, 108:9346–9356, 2004.

[79] J. K. Dunnick and W. M. O'Leary. Correlation of bacteria lipid composition with antibiotic resistance. *Journal of Bacteriology*, 101(3):892–900, 1970.

[80] I. Chopra and M. Roberts. Tetracycline Antibiotics : Mode of Action , Applications , Molecular Biology , and Epidemiology of Bacterial Resistance. *Microbiology and Molecular Biology Reviews*, 65(2):232–260, 2001.

[81] World Health Organization. WHO Model List of Essential Medicines. Technical report, 2013.

[82] N. E. Rigler, S. P. Bag, D. E. Leyden, J. L. Sudmeier, and C. N. Reilley. Determination of a Protonation Scheme of Tetracycline Using Nuclear Magnetic Resonance. *Analytical Chemistry*, 37:872–875, 1965.

[83] S. Schneider, M. O. Schmitt, G. Brehm, M. Reiher, P. Matousek, and M. Towrie. Fluorescence kinetics of aqueous solutions of tetracycline and its complexes with Mg2+ and Ca2+. *Photochemical and Photobiological Sciences*, 2:1107–1117, 2003.

[84] A. P. Alivisatos. Perspectives on the Physical Chemistry of Semiconductor Nanocrystals. *Journal of Physical Chemistry*, 100(95):13226–13239, 1996.

[85] R. E. Bailey, A. M. Smith, and S. Nie. Quantum dots in biology and medicine. *Physica E*, 25:1–12, 2004.

[86] R. E. Bailey and S. Nie. Alloyed Semiconductor Quantum Dots : Tuning the Optical Properties without Changing the Particle Size. *Journal of the American Chemical Society*, (24):7100–7106, 2003.

[87] X. Zhong, Y. Feng, W. Knoll, and M. Han. Alloyed ZnxCd1-xS Nanocrystals with Highly Narrow Luminescence Spectral Width. *Journal of the American Chemical Society*, 125(44):13559–13563, 2003.

[88] L. Qu and X. Peng. Control of photoluminescence properties of CdSe nanocrystals in growth. *Journal of the American Chemical Society*, 124(9):2049–2055, 2002.

[89] S. Kim, B. Fisher, H. J. Eisler, and M. Bawendi. Type-II quantum dots: CdTe/CdSe(core/shell) and CdSe/ZnTe(core/shell) heterostructures. *Journal of the American Chemical Society*, 125(38):11466–11467, 2003.

[90] M. Bruchez, M. Moronne, P. Gin, S. Weiss, and A. P. Alivisatos. Semiconductor nanocrystals as fluorescent biological labels. *Science*, 281(5385):2013–2016, 1998.

[91] W. C. Chan and S. Nie. Quantum dot bioconjugates for ultrasensitive nonisotopic detection. *Science*, 281(5385):2016–2018, 1998.

[92] X. Wu, H. Liu, J. Liu, K. N. Haley, J. A. Treadway, J. P. Larson, N. Ge, F. Peale, and M. P. Bruchez. Immunofluorescent labeling of cancer marker Her2 and other cellular targets with semiconductor quantum dots. *Nature Biotechnology*, 21(1):41–46, 2003.

[93] M. Han, X. Gao, J. Z. Su, and S. Nie. Quantum-dot-tagged microbeads for multiplexed optical coding of biomolecules. *Nature Biotechnology*, 19(7):631–635, 2001.

[94] X. Michalet, F. F. Pinaud, L. A. Bentolila, J. M. Tsay, S. Doose, J. J. Li, G. Sundaresan, A. M. Wu, S. S. Gambhir, and S. Weiss. Quantum Dots for Live Cells, in Vivo Imaging and Diagnostics. *Science*, 307:538–544, 2005.

[95] B. Ballou, B. C. Lagerholm, L. A. Ernst, M. P. Bruchez, and A. S. Waggoner. Noninvasive Imaging of Quantum Dots in Mice. *Bioconjugate Chemistry*, 15: 79–86, 2004.

[96] L. Järup, M. Berglund, C. G. Elinder, G. Nordberg, and M. Vanter. Health effects of cadmium exposure - a review of the literature and a risk estimate. *Scandinavian Journal of Work, Environment and Health*, 24:1–51, 1998.

[97] N. Chen, Y. He, Y. Su, X. Li, Q. Huang, H. Wang, X. Zhang, R. Tai, and C. Fan. The cytotoxicity of cadmium-based quantum dots. *Biomaterials*, 33(5): 1238–1244, 2012.

[98] Y. Su, Y. He, H. Lu, L. Sai, Q. Li, W. Li, L. Wang, P. Shen, Q. Huang, and C. Fan. The cytotoxicity of cadmium based, aqueous phase - Synthesized, quantum dots and its modulation by surface coating. *Biomaterials*, 30(1):19–25, 2009.

[99] C. E. Bradburne, J. B. Delehanty, K. Boeneman Gemmill, B. C. Mei, H. Mattoussi, K. Susumu, J. B. Blanco-Canosa, P. E. Dawson, and I. L. Medintz. Cytotoxicity of quantum dots used for in vitro cellular labeling: Role of QD surface ligand, delivery modality, cell type, and direct comparison to organic fluorophores. *Bioconjugate Chemistry*, 24(9):1570–1583, 2013.

[100] W-h. Chan and N-h. Shiao. Cytotoxic effect of CdSe quantum dots on mouse embryonic development. *Acta Pharmacologica Sinica*, 29(2):259–266, 2008.

[101] W. Cai, A. R. Hsu, Z-B. Li, and X. Chen. Are quantum dots ready for in vivo imaging in human subjects? *Nanoscale Research Letters*, 2(6):265–281, 2007.

[102] S. A. Klein, S. J. Wilk, T. J. Thornton, and J. D. Posner. Formation of nanopores in suspended lipid bilayers using quantum dots. *Journal of Physics: Conference Series*, 109:012022, 2008.

[103] J. Cama, H. Bajaj, S. Pagliara, T. Maier, Y. Braun, M. Winterhalter, and U. F. Keyser. Quantification of Fluoroquinolone Uptake through the Outer Membrane Channel OmpF of Escherichia coli. *Journal of the American Chemical Society*, 137(43):13836–13843, 2015.

[104] N. Ruiz, D. Kahne, and T. J. Silhavy. Advances in understanding bacterial outer-membrane biogenesis. *Nature Reviews Microbiology*, 4(1):57–66, 2006.

[105] A. H. Delcour. Outer Membrane Permeability and Antibiotic Resistance. *Biochim Biophys Acta.*, 1794(5):808–816, 2009.

[106] C. R. H. Raetz and C. Whitfield. Lipopolysaccharide Endotoxins. *Annual Review of Biochemistry*, 71:635–700, 2002.

[107] R. E. W. Hancock. Role of Porins in Outer Membrane Permeability. *Journal of Bacteriology*, 169(3):929–933, 1987.

[108] H. Nikaido and E. Y. Rosenberg. Effect on Solute Size on Diffusion Rates through the Transmembrane Pores of the Outer Membrane of Escherichia coli. *The Journal of General Physiology*, 77:121–135, 1981.

[109] T. A. Krulwich, G. Sachs, and E. Padan. Molecular aspects of bacterial pH sensing and homeostasis. *Nature Reviews Microbiology*, 9:330–343, 2011.

[110] L. M. G. van Golde, H. Schulman, and E. P. Kennedy. Metabolism of membrane phospholipids and its relation to a novel class of oligosaccharides in Escherichia coli. *Proceedings of the National Academy of Sciences of the United States of America*, 70(5):1368–1372, 1973.

[111] E. P. Kennedy. Osmotic regulation and the biosynthesis of membrane-derived oligosaccharides in Escherichia coli. *Proceedings of the National Academy of Sciences of the United States of America*, 79:1092–1095, 1982.

[112] H. Schulman and E. P. Kennedy. Localization of Membrane-Derived Oligosaccharides in the Outer Envelope of Escherichia coli and Their Occurence in Other Gram-Negative Bacteria. *Journal of Bacteriology*, 137(1):686–688, 1979.

[113] K. Sen, J. Hellman, and H. Nikaido. Porin channels in intact cells of Escherichia coli are not affected by Donnan potentials across the outer membrane. *Journal of Biological Chemistry*, 263(3):1182–1187, 1988.

[114] E. Yamashita, M. V. Zhalnina, S. D. Zakharov, O. Sharma, and W. A. Cramer. Crystal structures of the OmpF porin: function in a colicin translocon. *The EMBO Journal*, 27:2171–2180, 2008.

[115] S. W. Cowan, T. Schirmer, G. Rummel, M. Steiert, R. Ghosh, R. A. Pauptit, J. N. Jansonius, and J. P. Rosenbusch. Crystal structures explain functional properties of two E. coli porins. *Nature*, 358:727–733, 1992.

[116] H. Nikaido. Molecular basis of bacterial outer membrane permeability revisited. *Microbiology and Molecular Biology Reviews*, 67(4):593–656, 2003.

[117] R. Benz. Structure and Function of Porins from Gram-Negative Bacteria. *Annual Reviews in Microbiology*, 42:359–393, 1988.

[118] R. M. Garavito and J. P. Rosenbusch. Three-dimensional crystals of an integral membrane protein: an initial x-ray analysis. *Journal of Cell Biology*, 86:327–329, 1980.

[119] J. P. Rosenbusch. Characterization of the Major Envelope Protein from Escherichia coli : Regular Arrangement on the Peptidoglycan and Unusual Dodecyl-Sulfate Binding. *Journal of Biological Chemistry*, 249:8019–8029, 1974.

[120] L. S. Redgrave, S. B. Sutton, M. A. Webber, and L. J. V. Piddock. Fluoroquinolone resistance: Mechanisms, impact on bacteria, and role in evolutionary success. *Trends in Microbiology*, 22(8):438–445, 2014.

[121] K. Hirai, H. Aoyama, S. Suzue, T. Irikura, S. Iyobe, and S. Mitsuhashi. Isolation and Characterization of Norfloxacin-Resistant Mutants of Escherichia coli K-12. *Antimicrobial Agents and Chemotherapy*, 30(2):248–253, 1986.

[122] S. P. Cohen, L. M. McMurry, D. C. Hooper, J. S. Wolfson, and S. B. Levy. Cross-resistance to fluoroquinolones in multiple-antibiotic-resistant (Mar) Escherichia coli selected by Tetracycline or Chloramphenicol: Decreased drug accumulation associated with membrane changes in addition to OmpF reduction. *Antimicrobial Agents and Chemotherapy*, 33(8):1318–1325, 1989.

[123] R. Kishii and M. Takei. Relationship between the expression of ompF and quinolone resistance in Escherichia coli. *Journal of Infection and Chemotherapy*, 15:361–366, 2009.

[124] M. Sato, K. Machida, E. Arikado, H. Saito, T. Kakegawa, and H. Kobayashi. Expression of outer membrane proteins in Escherichia coli growing at acid pH. *Applied and Environmental Microbiology*, 66(3):943–947, 2000.

[125] A. D. Thomas and I. R. Booth. The regulation of expression of the porin gene ompC by acid pH. *Journal of General Microbiology*, 138:1829–1835, 1992.

[126] J. T. Smith and N. T. Ratcliffe. Einfluss von pH-Wert und Magnesium auf die antibakterielle Aktivitat von Chinolonpraparaten. *Infection*, 14(Suppl. 1):S31–S35, 1986.

[127] L. J. V. Piddock, Y-F. Jin, V. Ricci, and A. E. Asuquo. Quinolone accumulation by Pseudomonas aeruginosa, Staphylococcus aureus and Escherichia coli. *Journal of Antimicrobial Chemotherapy*, 43:61–70, 1999.

[128] J. C. Wilks and J. L. Slonczewski. pH of the cytoplasm and periplasm of Escherichia coli: Rapid measurement by green fluorescent protein fluorimetry. *Journal of Bacteriology*, 189(15):5601–5607, 2007.

[129] R. de Jonge, K. Takumi, W. S. Ritmeester, and F. M. van Leusden. The adaptive response of Escherichia coli O157 in an environment with changing pH. *Journal of Applied Microbiology*, 94:555–560, 2003.

[130] A. H. Delcour. Function and modulation of bacterial porins: Insights from electrophysiology. *FEMS Microbiology Letters*, 151:115–123, 1997.

[131] H. Nikaido, E. Y. Rosenberg, and J. Foulds. Porin channels in Escherichia coli: studies with beta-lactams in intact cells. *Journal of Bacteriology*, 153(1):232–240, 1983.

[132] H. Nikaido and E. Y. Rosenberg. Porin channels in Escherichia coli: studies with liposomes reconstituted from purified proteins. *Journal of Bacteriology*, 153 (1):241–252, 1983.

[133] H. Nikaido, K. Nikaido, and S. Harayama. Identification and characterization of porins in Pseudomonas aeruginosa. *Journal of Biological Chemistry*, 266(2): 770–779, 1991.

[134] G. Sun, S. Pal, A. K. Sarcon, S. Kim, E. Sugawara, H. Nikaido, M. J. Cocco, E. M. Peterson, and L. M. De La Maza. Structural and functional analyses of the major outer membrane protein of Chlamydia trachomatis. *Journal of Bacteriology*, 189(17):6222–6235, 2007.

[135] K. R. Mahendran, E. Hajjar, T. Mach, M. Lovelle, A. Kumar, I. Sousa, E. Spiga, H. Weingart, P. Gameiro, M. Winterhalter, and M. Ceccarelli. Molecular basis of Enrofloxacin translocation through OmpF, an outer membrane channel of Escherichia coli - When binding does not imply translocation. *Journal of Physical Chemistry B*, 114:5170–5179, 2010.

[136] M. Kreir, C. Farre, M. Beckler, M. George, and N. Fertig. Rapid screening of membrane protein activity: electrophysiological analysis of OmpF reconstituted in proteoliposomes. *Lab on a Chip*, 8:587–595, 2008.

[137] E. M. Nestorovich, C. Danelon, M. Winterhalter, and S. M. Bezrukov. Designed to penetrate: time-resolved interaction of single antibiotic molecules with bacterial pores. *Proceedings of the National Academy of Sciences of the United States of America*, 99(15):9789–94, 2002.

[138] S. M. Bezrukov, A. M. Berezhkovskii, and A. Szabo. Diffusion model of solute dynamics in a membrane channel: Mapping onto the two-site model and optimizing the flux. *Journal of Chemical Physics*, 127(2007), 2007.

[139] R. Benz and A. Schmidt. Mechanism of sugar transport through the sugar-spesific LamB channel of Esherichia coli outer membrane. *The Journal of Membrane Biology*, 100:21–29, 1987.

[140] G. Schwarz, C. Danelon, and M. Winterhalter. On translocation through a membrane channel via an internal binding site: kinetics and voltage dependence. *Biophysical Journal*, 84:2990–2998, 2003.

[141] K. Karamdad, R. V. Law, J. M. Seddon, N. J. Brooks, and O. Ces. Preparation and mechanical characterisation of giant unilamellar vesicles by a microfluidic method. *Lab on a Chip*, 15:557–562, 2015.

[142] L. R. Arriaga, S. S. Datta, S. H. Kim, E. Amstad, T. E. Kodger, F. Monroy, and D. A. Weitz. Ultrathin shell double emulsion templated giant unilamellar lipid vesicles with controlled microdomain formation. *Small*, 10(5):950–956, 2014.

[143] H. Gaimster, J. Cama, S. Hernández-Ainsa, U. F. Keyser, and D. K. Summers. The indole pulse: a new perspective on indole signalling in Escherichia coli. *PLoS ONE*, 9(4):e93168, 2014.

[144] J. H. Lee and J. Lee. Indole as an intercellular signal in microbial communities. *FEMS Microbiology Reviews*, 34(4):426–444, 2010.

[145] T. Bansal, R. C. Alaniz, T. K. Wood, and A. Jayaraman. The bacterial signal indole increases epithelial-cell tight-junction resistance and attenuates indicators of inflammation. *Proceedings of the National Academy of Sciences of the United States of America*, 107(1):228–233, 2010.

[146] M. J. Berridge, M. D. Bootman, and P. Lipp. Calcium - a life and death signal. *Nature*, 395(6703):645–8, 1998.

[147] M. J. Berridge, P. Lipp, and M. D. Bootman. The versatility and universality of calcium signalling. *Nature Reviews Molecular Cell Biology*, 1(1):11–21, 2000.

[148] C. Chimerel, E. Emery, D. K. Summers, U. F. Keyser, F. M. Gribble, and F. Reimann. Bacterial Metabolite Indole Modulates Incretin Secretion from Intestinal Enteroendocrine L Cells. *Cell Reports*, 9(4):1202–1208, 2014.

[149] S. Piñero Fernandez, C. Chimerel, U. F. Keyser, and D. K. Summers. Indole transport across Escherichia coli membranes. *Journal of Bacteriology*, 193(8): 1793–1798, 2011.

[150] W. M. A. Newton and E. E. Snell. An inducible tryptophan synthetase in tryptophan auxotrophs of Escherichia coli. *Proceedings of the National Academy of Sciences of the United States of America*, 48:1431–1439, 1962.

[151] E. L. Chant and D. K. Summers. Indole signalling contributes to the stable maintenance of Escherichia coli multicopy plasmids. *Molecular Microbiology*, 63 (1):35–43, 2007.

[152] H. Hirakawa, M. Hayashi-Nishino, A. Yamaguchi, and K. Nishino. Indole enhances acid resistance in Escherichia coli. *Microbial Pathogenesis*, 49(3):90–94, 2010.

[153] H. Hirakawa, Y. Inazumi, T. Masaki, T. Hirata, and A. Yamaguchi. Indole induces the expression of multidrug exporter genes in Escherichia coli. *Molecular Microbiology*, 55:1113–1126, 2005.

[154] R. S. Mueller, S. Beyhan, S. G. Saini, F. H. Yildiz, and D. H. Bartlett. Indole acts as an extracellular cue regulating gene expression in Vibrio cholerae. *Journal of Bacteriology*, 191(11):3504–3516, 2009.

[155] H. H. Lee, M. N. Molla, C. R. Cantor, and J. J. Collins. Bacterial charity work leads to population-wide resistance. *Nature*, 467(7311):82–85, 2010.

[156] C. Huttenhower, D. Gevers, R. Knight, S. Abubucker, J. H. Badger, A. T. Chinwalla, H. H. Creasy, A. M. Earl, M. G. FitzGerald, R. S. Fulton, M. G. Giglio, K. Hallsworth-Pepin, E. A. Lobos, R. Madupu, V. Magrini, J. C. Martin, M. Mitreva, D. M. Muzny, E. J. Sodergren, J. Versalovic, A. M. Wollam, K. C. Worley, J. R. Wortman, S. K. Young, Q. Zeng, K. M. Aagaard, O. O. Abolude, E. Allen-Vercoe, E. J. Alm, L. Alvarado, G. L. Andersen, S. Anderson, E. Appelbaum, H. M. Arachchi, G. Armitage, C. A. Arze, T. Ayvaz, C. C. Baker, L. Begg, T. Belachew, V. Bhonagiri, M. Bihan, M. J. Blaser, T. Bloom, V. Bonazzi, J. Paul Brooks, G. A. Buck, C. J. Buhay, D. A. Busam, J. L. Campbell, S. R. Canon, B. L. Cantarel, P. S. G. Chain, I-M. A. Chen, L. Chen, S. Chhibba, Ken Chu, D. M. Ciulla, J. C. Clemente, S. W. Clifton, S. Conlan, J. Crabtree, M. A. Cutting, N. J. Davidovics, C. C. Davis, T. Z. DeSantis, C. Deal, K. D. Delehaunty, F. E. Dewhirst, E. Deych, Y. Ding, D. J. Dooling, S. P. Dugan, W. Michael Dunne, A. Scott Durkin, R. C. Edgar, R. L. Erlich, C. N. Farmer, R. M. Farrell, K. Faust, M. Feldgarden, V. M. Felix, S. Fisher, A. A. Fodor, L. J. Forney, L. Foster, V. Di Francesco, J. Friedman, D. C. Friedrich, C. C. Fronick, L. L. Fulton, H. Gao, N. Garcia, G. Giannoukos, C. Giblin, M. Y. Giovanni, J. M. Goldberg, J. Goll, A. Gonzalez, A. Griggs, S. Gujja, S. Kinder Haake, B. J. Haas, H. A. Hamilton, E. L. Harris, T. A. Hepburn, B. Herter, D. E. Hoffmann, M. E. Holder, C. Howarth, K. H. Huang, S. M. Huse, J. Izard, J. K. Jansson, H. Jiang, C. Jordan, V. Joshi, J. A. Katancik, W. A. Keitel, S. T. Kelley, C. Kells, N. B. King, D. Knights, H. H. Kong, O. Koren, S. Koren, K. C. Kota, C. L. Kovar, N. C. Kyrpides, P. S. La Rosa, S. L. Lee, K. P. Lemon, N. Lennon, C. M. Lewis, L. Lewis, R. E. Ley, K. Li, K. Liolios, B. Liu, Y. Liu, C-C. Lo, C. A. Lozupone, R. Dwayne Lunsford, T. Madden, A. A. Mahurkar, P. J. Mannon, E. R. Mardis, V. M. Markowitz, K. Mavromatis, J. M. McCorrison, D. McDonald, J. McEwen, A. L. McGuire, P. McInnes, T. Mehta, K. A. Mihindukulasuriya, J. R. Miller, P. J. Minx, I. Newsham, C. Nusbaum, M. O'Laughlin, J. Orvis, I. Pagani, K. Palaniappan, S. M. Patel, M. Pearson, J. Peterson, M. Podar, C. Pohl, K. S. Pollard, M. Pop, M. E. Priest, L. M. Proctor, X. Qin, J. Raes, J. Ravel, J. G. Reid, M. Rho, R. Rhodes, K. P. Riehle, M. C. Rivera, B. Rodriguez-Mueller, Y-H. Rogers, M. C. Ross, C. Russ, R. K. Sanka, P. Sankar, J. Fah Sathirapongsasuti, J. aA. Schloss, P. D. Schloss, T. M. Schmidt,

M. Scholz, L. Schriml, Al. M. Schubert, N. Segata, J. A. Segre, W. D. Shannon, R. R. Sharp, T. J. Sharpton, N. Shenoy, N. U. Sheth, G. A. Simone, I. Singh, C. S. Smillie, J. D. Sobel, D. D. Sommer, P. Spicer, G. G. Sutton, S. M. Sykes, D. G. Tabbaa, M. Thiagarajan, C. M. Tomlinson, M. Torralba, T. J. Treangen, R. M. Truty, T. A. Vishnivetskaya, J. Walker, L. Wang, Z. Wang, D. V. Ward, W. Warren, M. A. Watson, C. Wellington, K. A. Wetterstrand, J. R. White, K. Wilczek-Boney, Y-Q. Wu, K. M. Wylie, T. Wylie, C. Yandava, L. Ye, Y. Ye, S. Yooseph, B. P. Youmans, L. Zhang, Y. Zhou, Y. Zhu, L. Zoloth, J. D. Zucker, B. W. Birren, R. A. Gibbs, S. K. Highlander, B. A. Methé, K. E. Nelson, J. F. Petrosino, G. M. Weinstock, R. K. Wilson, and O. White. Structure, function and diversity of the healthy human microbiome. *Nature*, 486(7402):207–214, 2012.

[157] C. Chimerel, C. M. Field, S. Piñero Fernandez, U. F. Keyser, and D. K. Summers. Indole prevents Escherichia coli cell division by modulating membrane potential. *Biochimica et Biophysica Acta - Biomembranes*, 1818(7): 1590–1594, 2012.

[158] C. Chimerel, A. J. Murray, E. R. Oldewurtel, D. K. Summers, and U. F. Keyser. The effect of bacterial signal indole on the electrical properties of lipid membranes. *Chemphyschem*, 14(2):417–23, 2013.

[159] G. Li and K. D. Young. Indole production by the tryptophanase TnaA in Escherichia coli is determined by the amount of exogenous tryptophan. *Microbiology*, 159(2):402–410, 2013.

[160] S. Lacour and P. Landini. Sigma(S)- Dependent Gene Expression at the Onset of Stationary Phase in Escherichia coli : Function of Sigma(S) -Dependent Genes and Identification of Their Promoter Sequences. *Journal of Bacteriology*, 186(21): 7186–7195, 2004.

[161] J. M. Miller and J. W. Wright. Spot indole test: Evaluation of four reagents. *Journal of Clinical Microbiology*, 15(4):589–592, 1982.

[162] B. Volkmer and M. Heinemann. Condition-Dependent cell volume and concentration of Escherichia coli to facilitate data conversion for systems biology modeling. *PLoS ONE*, 6(7):1–6, 2011.

[163] T. R. Garbe, M. Kobayashi, and H. Yukawa. Indole-inducible proteins in bacteria suggest membrane and oxidant toxicity. *Archives of Microbiology*, 173(1):78–82, 2000.

[164] M. M. Faul and B. E. Huff. Strategy and methodology development for the total synthesis of polyether ionophore antibiotics. *Chemical Reviews*, 100(6): 2407–2473, 2000.

[165] A. M. O'Hara and F. Shanahan. The gut flora as a forgotten organ. *EMBO Reports*, 7(7):688–693, 2006.

[166] W. R. Wikoff, A. T. Anfora, J. Liu, P. G. Schultz, S. A. Lesley, E. C. Peters, and G. Siuzdak. Metabolomics analysis reveals large effects of gut microflora on mammalian blood metabolites. *Proceedings of the National Academy of Sciences of the United States of America*, 106(10):3698–3703, 2009.

[167] J. B. Furness. Types of neurons in the enteric nervous system. *Journal of the Autonomic Nervous System*, 81(1-3):87–96, 2000.

[168] O. Lundgren, J. Svanvik, and L. Jivegard. Enteric Nervous System I. Physiology and Pathophysiology of the Intestinal Tract. *Digestive Diseases and Science*, 34(2): 264–283, 1989.

[169] S. M. Collins and P. Bercik. The Relationship Between Intestinal Microbiota and the Central Nervous System in Normal Gastrointestinal Function and Disease. *Gastroenterology*, 136(6):2003–2014, 2009.

[170] J. M. Yano, K. Yu, G. P. Donaldson, G. G. Shastri, P. Ann, L. Ma, C. R. Nagler, R. F. Ismagilov, S. K. Mazmanian, and E. Y. Hsiao. Indigenous Bacteria from the Gut Microbiota Regulate Host Serotonin Biosynthesis. *Cell*, 161(2):264–276, 2015.

[171] S. Matosevic and B. M. Paegel. Stepwise synthesis of giant unilamellar vesicles on a microfluidic assembly line. *Journal of the American Chemical Society*, 133 (9):2798–2800, 2011.

[172] V. Uivarosi. Metal complexes of quinolone antibiotics and their applications: An update. *Molecules*, 18(9):11153–11197, 2013.

[173] T. A. Schaedler, Z. Tong, and H. W. van Veen. The multidrug transporter LmrP protein mediates selective calcium efflux. *Journal of Biological Chemistry*, 287: 27682–27690, 2012.

[174] N. A. W. Bell, C. R. Engst, M. Ablay, G. Divitini, C. Ducati, T. Liedl, and U. F. Keyser. DNA Origami Nanopores. *Nano Letters*, 12(1):512–7, 2012.

[175] N. A. W. Bell and U. F. Keyser. Nanopores formed by DNA origami: A review. *FEBS Letters*, 588(19):3564–3570, 2014.

[176] J. R. Burns, K. Göpfrich, J. W. Wood, V. V. Thacker, E. Stulz, U. F. Keyser, and S. Howorka. Lipid-bilayer-spanning DNA nanopores with a bifunctional porphyrin anchor. *Angewandte Chemie - International Edition*, 52(46):12069–12072, 2013.

[177] S. A. Stricker. Comparative biology of calcium signaling during fertilization and egg activation in animals. *Developmental Biology*, 211(2):157–176, 1999.

[178] M. Whitaker and R. Patel. Calcium and cell cycle control. *Development*, 108(4): 525–542, 1990.

[179] S. M. Cain and T. P. Snutch. Voltage-gated calcium channels and disease. *BioFactors*, 37(3):197–205, 2011.

[180] A. Takahashi, P. Camacho, J. D. Lechleiter, and B. Herman. Measurement of intracellular calcium. *Physiological Reviews*, 79(4):1089–1125, 1999.

[181] G. Grynkiewicz, M. Poenie, and R. Y. Tsien. A new generation of Ca2+ indicators with greatly improved fluorescence properties. *Journal of Biological Chemistry*, 260(6):3440–3450, 1985.

[182] E. Neher. The use of fura-2 for estimating Ca buffers and Ca fluxes. *Neuropharmacology*, 34(11):1423–1442, 1995.

[183] D. R. Gossett, W. M. Weaver, A. J. MacH, S. C. Hur, H. T. K. Tse, W. Lee, H. Amini, and D. Di Carlo. Label-free cell separation and sorting in microfluidic systems. *Analytical and Bioanalytical Chemistry*, 397(8):3249–3267, 2010.

[184] L. Schmid, D. A. Weitz, and T. Franke. Sorting drops and cells with acoustics: acoustic microfluidic fluorescence-activated cell sorter. *Lab on a Chip*, 14(19): 3710–3718, 2014.

[185] P. Wang, L. Robert, J. Pelletier, W. L. Dang, F. Taddei, A. Wright, and S. Jun. Robust growth of Escherichia coli. *Current Biology*, 20(12):1099–1103, 2010.

[186] S. M. Amato, M. A. Orman, and M. P. Brynildsen. Metabolic control of persister formation in Escherichia coli. *Molecular Cell*, 50(4):475–87, 2013.

[187] K. Lewis. Platforms for antibiotic discovery. *Nature Reviews Drug discovery*, 12 (5):371–87, 2013.

[188] C. C. Dawson, C. Intapa, and M. A. Jabra-Rizk. "Persisters": Survival at the cellular level. *PLoS Pathogens*, 7(7):2–4, 2011.

[189] Editorial. Laying better plans for mice. *Nature Biotechnology*, 31(4):263, 2013.